

AN ABSTRACT OF THE THESIS OF

Todd L. Miles for the degree of Master of Science in Nuclear Engineering presented on December 9, 1991.

Title: Monte Carlo Uncertainty Reliability and Isotope Production Calculations for a Fast Reactor.

Abstract approved:

Redacted for Privacy

Stephen E. Binney

With the advent of more powerful, less expensive computing resources, more and more attention is being given to Monte Carlo techniques in design application. In many circles, stochastic solutions are considered the next best thing to experimental data. Statistical uncertainties in Monte Carlo calculations are typically determined by the first and second moments of the tally. For certain types of calculations, there is concern that the uncertainty estimate is significantly non-conservative. This is typically seen in reactor eigenvalue problems where the uncertainty estimate is aggravated by the generation-to-generation fission source. It has been speculated that optimization of the random walk, through biasing techniques, may increase the non-conservative nature of the uncertainty estimate. A series of calculations are documented here which quantify the reliability of the Monte Carlo Neutron and Photon (MCNP) mean and uncertainty estimates by comparing these estimates to the true mean. These calculations were made with a liquid metal fast reactor model, but every effort was made to isolate the statistical nature of the

uncertainty estimates so that the analysis of the reliability of the MCNP estimates should be relevant for small thermal reactors as well.

Also, preliminary reactor physics calculations for two different special isotope production test assemblies for irradiation in the Fast Flux Test Facility (FFTF) were performed using MCNP and are documented here. The effect of an yttrium-hydride moderator to tailor the neutron flux incident on the targets to maximize isotope production for different designs in different locations within the reactor is discussed. These calculations also demonstrate the useful application of MCNP in design iterations by utilizing many of the codes features.

Monte Carlo
Uncertainty Reliability
and Isotope Production Calculations
for a Fast Reactor

by

Todd L. Miles

A THESIS

submitted to

Oregon State University

in partial fulfillment of
the requirements for the
degree of

Master of Science

Completed December 9, 1991

Commencement June 1992

APPROVED:

Redacted for Privacy

Associate Professor of Nuclear Engineering in Charge of Major

Redacted for Privacy

Head of Department of Nuclear Engineering

Redacted for Privacy

Dean of Graduate School

Date Thesis is Presented December 9, 1991

Typed by Researcher for Todd L. Miles

ACKNOWLEDGEMENT

There are number of people who have been very helpful during the completion of my Master's degree program both at Oregon State and at Richland. Dr. L. L. Carter was extremely helpful, patient, and kind during my time at WHC. Everything that follows in this document is the result of countless hours in Dr. Carter's office. I am grateful for both the financial support and work experience made possible by Dr. J. W. Daughtry of Westinghouse Hanford Company (WHC) during my graduate school years. R. A. Schwartz and D. H. Wootan of WHC were both helpful in the area of fast neutron physics and the use of the MCNP computer code. My parents have always provided the foundation of support and encouragement in my life and their role in my graduate studies was no different. I would especially like to thank Dr. S. E. Binney of Oregon State University for his guidance both in the technical arena and in my career direction choice. I find that it is no small thing to have an advisor whose concern extends past the classroom, one whom you trust personally. For that I feel truly blessed.

TABLE OF CONTENTS

1	INTRODUCTION	1
2	A BRIEF EXPLANATION OF MONTE CARLO METHODS AND MCNP	5
	2.1.0 History of the Monte Carlo Method	5
	2.2.0 Monte Carlo Computational Methods	7
	2.2.1 Particle Tracking	7
	2.2.2 Comparison with Deterministic Methods	9
	2.3.0 Overview of MCNP	10
	2.3.1 Geometry and Materials	10
	2.3.2 Source Modeling	11
	2.3.3 Tallies	12
	2.3.4 Monte Carlo Optimization Techniques	15
	2.3.5 Monte Carlo Uncertainty	16
3	A QUANTITATIVE ANALYSIS OF MCNP UNCERTAINTIES IN REACTOR PHYSICS PROBLEMS	18
	3.1.0 The Problem	18
	3.2.0 Statistics	20
	3.2.1 Calculation of Statistical Uncertainty Estimates	20
	3.2.2 Reliability of Uncertainty Estimates	22
	3.2.2.1 In Extraneous Sources Problems	22
	3.2.2.2 In Eigenvalue Problems	23
	3.2.3 Statistical Analysis and Quantification Strategy	27
	3.3.0 Geometry and Test Problem	32
	3.3.1 Geometry	32
	3.3.2 The Tallies	34
	3.3.3 Test Cases	37
	3.3.3.1 Case I	38
	3.3.3.2 Case II	39
	3.3.3.3 Case III	39
	3.3.3.4 Case IV	41
	3.3.3.5 Case V	41
	3.4.0 Comparisons and Results	43
	3.4.1 Explanation of Tables	43
	3.4.1.1 Case I Results	44
	3.4.1.2 Case II Results	45
	3.4.1.3 Case III Results	46
	3.4.1.4 Case IV Results	46
	3.4.1.5 Case V Results	47
	3.4.2 Correction Factor	49
	3.4.3 Results from Tallies with Poor Precision	50
	3.5.0 Conclusions	53
4	THE MIP-II TEST	57
	4.1.0 Introduction	57
	4.1.1 Isotope Production	57
	4.1.2 MIP-II Computational Objectives	58
	4.1.3 MCNP Computational Precedent	61
	4.2.0 MCNP Computational Model	62
	4.2.1 Geometry and Materials	62

TABLE OF CONTENTS cont.

4.2.2	Biasing	68
4.3.0	Calculational Summary	70
4.3.1	Summary of Runs	70
4.3.2	Calculational Techniques	71
4.3.2.1	Heating Tallies	71
4.3.2.2	Reaction Rate Tallies	72
4.4.0	Results	73
4.4.1	Row 7 Heating Rates	74
4.4.2	Row 7 Reaction Rates	79
4.4.3	Row 6 Heating Rates	84
4.4.4	Row 6 Reaction Rates	88
4.4.5	Macrocell Accuracy Check	98
4.5.0	Conclusions	99
4.5.1	Discussion of Results	100
4.5.2	MIP-II Calculations Application	101
5	NEUTRON MODERATION IN A MOTA CANISTER	102
5.1.0	Introduction	102
5.1.1	The MOTA Canister	102
5.1.2	MOTA Calculational Objective	102
5.2.0	MCNP Calculational Model	105
5.2.1	Geometry and Materials	105
5.2.2	Biasing	106
5.3.0	Calculational Summary	112
5.3.1	Summary of Runs	112
5.3.2	Calculational Techniques	115
5.3.2.1	Heating Tallies	115
5.3.2.2	Reaction Rate Tallies	116
5.4.0	Results	116
5.4.1	Isotope Reaction Rates in the Target Area	117
5.4.2	Effect of $YH_{1.8}$ on Li-6 Experiments	121
5.4.3	Effect of $YH_{1.8}$ on Total and Fast Flux	123
5.4.4	Heat Deposition Rates in Adjacent Fuel	123
5.5.0	Conclusions	129
5.5.1	Summary of Results	129
5.5.2	MOTA Calculations Application	130
	References	131
	APPENDIX A DENOMAKUE Source File Listing	133

LIST OF FIGURES

<u>FIGURE</u>		<u>PAGE</u>
2.1	Particle Tracking Schematic	9
3.1	Plan View of Hexagonal Matrix	25
3.2	Elevation View of Reactor Model	35
3.3	Plan View of Hexagonal Fast Reactor Computational Model at Core Midplane	36
3.4	Lower Bounds of Neutron Weight Windows for Case III	40
4.1	Plan View of MIP-II Test Assembly	60
4.2	Plan View of FFTF Reactor Assembly Matrix	63
4.3	Adjacent Fuel Pin Locations for Target Assembly in 2701	64
4.4	Adjacent Fuel Pin Locations for Target Assembly in 1610	65
4.5	Lower Bounds of Photon Weight Windows in Full Core Model	69
5.1	Plan View of MOTA Test Assembly	104
5.2	Plan View of MOTA Computational Macrocell	107
5.3	Lower bounds of Neutron Weight Windows in Full Core Model	108
5.4	Adjacent Fuel Pin Locations for Fuel Assembly 2304	110
5.5	Adjacent Fuel Pin Locations for Fuel Assembly 3301	111
5.6	Neutron Flux in Canister 4-C Target Area	120

LIST OF TABLES

<u>Table</u>	<u>Page</u>
3.1 Summary of Cases	38
3.2 Summary with Minimal Optimization and 5,000 Neutrons/Generation	45
3.3 Summary with Minimal Optimization and 200 Neutrons/Generation	46
3.4 Summary with Spatial Optimization and 5,000 Neutrons/Generation	47
3.5 Summary with Spatial Optimization and 200 Neutrons/Generation	48
3.6 Summary with Spatial and Energy Optimization and 200 Neutrons/Generation	48
3.7 Effect of Multiplier on Uncertainty Distribution	50
3.8 Summary with Minimal Optimization and 5000 Neutrons/Generation (Small Batch Size)	52
4.1 Potential Radioisotopes	59
4.2 Peak Heating in Adjacent Fuel Pins for Fuel Assemblies 1609 and 1610 - Stainless Steel Filter Pins	75
4.3 Peak Heating in Adjacent Fuel Pins for Fuel Assemblies 1609 and 1610 - Nd ₂ O ₃ Filter Pins	76
4.4 Effect of Nd ₂ O ₃ Filter Pins on Fuel Pin Heating	77
4.5 Projected Isotopic Reaction Rates Nd ₂ O ₃ Filter Pins	80
4.6 Projected Isotopic Reaction Rates Stainless Steel Filter Pins	81
4.7 Effect of Nd ₂ O ₃ Filter Pins on Reaction Rates	82
4.8 Nd ₂ O ₃ Filter Pins Hard Spectrum Reaction Rates	83
4.9 Peak Heating in Fuel Pins for Assemblies 1609, 2501, 1508, and 2601 - Stainless Steel Filter Pins	85
4.10 Peak Heating in Fuel Pins for Assemblies 1609, 2501, 1508, and 2601 - Nd ₂ O ₃ Filter Pins	87

LIST OF TABLES cont.

<u>Table</u>	<u>Page</u>
4.11 Example of Peak Heating in Individual Fuel Pins in an Adjacent Fuel Assembly for a Row 6 Test Assembly Stainless Steel Filter Pins	88
4.12 Example of Peak Heating in Individual Fuel Pins in an Adjacent Fuel Assembly for a Row 6 Test Assembly Nd ₂ O ₃ Filter Pins	89
4.13 Effect of Nd ₂ O ₃ Filter Pins on Heating in a Row 6 Test Assembly	90
4.14 Projected Row 6 Isotopic Reaction Rates Stainless Steel Filter Pins	91
4.15 Projected Row 6 Isotopic Reaction Rates Nd ₂ O ₃ Filter Pins	93
4.16 Effect of Nd ₂ O ₃ Filter Pins on Row 6 Reaction Rates	94
4.17 Stainless Steel Filter Pins Hard Spectrum Reaction Rates - Test Assembly in Row 6	95
4.18 Nd ₂ O ₃ Filter Pins Hard Spectrum Reaction Rates Test Assembly in Row 6	96
4.19 Nd ₂ O ₃ Effect on Hard Spectrum Reaction Rates Row 6 Test Assembly Position	97
4.20 Row 6 and Row 7 Reaction Rate Comparison	97
4.21 ¹⁴⁶ Nd Reaction Rates	98
4.22 Comparison of Macrocell Run - Accuracy Test	99
5.1 Summary of Cases	115
5.2 Isotope Reaction Rates in MOTA Target Area	118
5.3 Effect of YH _{1.8} on Tritium Production Experiments in Adjacent Canisters	121
5.4 Effect of YH _{1.8} on Fast Flux and Total Flux in the MOTA	124
5.5 Fuel Pin Heating in Adjacent Fuel Assemblies	124
5.6 Fuel Pin to Assembly Heating Ratio in Adjacent Fuel Assemblies	125

LIST OF TABLES cont.

<u>Table</u>	<u>Page</u>
5.7 Peak Heating in Individual Pins in Adjacent Fuel Assemblies - Test Assembly in Position 2406 With YH _{1.8}	127
5.8 Peak Heating in Individual Pins in Adjacent Fuel Assemblies - Test Assembly in Position 2406 Without YH _{1.8}	128

**MONTE CARLO UNCERTAINTY RELIABILITY
AND ISOTOPE PRODUCTION CALCULATIONS FOR A FAST REACTOR**

CHAPTER 1

INTRODUCTION

During the summer of 1990, plans were made for the running of two different irradiation tests in the Fast Flux Test Facility (FFTF), located on the Hanford Site in southeastern Washington. The FFTF¹, a 400 MW, sodium cooled, fast neutron flux reactor, is operated by Westinghouse Hanford, under contract with the U.S. Department of Energy. The FFTF was originally designed for the irradiation testing of nuclear reactor fuels and materials for subsequent development and use in the liquid metal fast breeder reactor program. Since that time, FFTF has demonstrated great potential as a facility for the production of medical and commercial isotopes.

The Isotope Production group at WHC proposed two tests at that time. These included the Multi-Isotope Production II test (MIP-II) and the Materials Open Test Assembly (MOTA) test. Each test was located in a different part of the reactor, thus utilizing different flux distributions. Each test assembly was designed with special material and geometric configurations, in particular various yttrium hydride moderator regions, to tailor the flux spectrum to a predetermined need. The purpose of the tests was to determine the feasibility of generating a useful product, such as a radionuclide used in medical applications, in the special test specific assemblies. Before actual implementation of the experiments could be authorized, preliminary neutronics calculations had to be performed. Of primary concern was the effect of the yttrium hydride moderator used in the

experiment. It was necessary to determine the effect that the extra moderator would have on the adjacent fuel pins and other nearby experiments.

The Monte Carlo Neutron Photon (MCNP) code² was used to model the test assemblies for the two experiments and calculate both reaction rates and heating rates. The code was chosen because of the capability to model the complicated three-dimensional test assemblies within the core and perform coupled neutron and photon transport calculations using its extensive continuous energy cross section sets. Monte Carlo codes, especially MCNP, are used extensively in neutronic design applications for shielding, reaction rate, and criticality calculations. In the absence of experimental data, Monte Carlo calculations are often employed in the benchmarking and validation of transport and diffusion codes, as well as problematic design methodologies, because of the stochastic nature of the Monte Carlo solution. However, because of this probabilistic nature, Monte Carlo codes rely heavily upon statistical uncertainties, rather than accuracy determined by experimental verification, to define the precision of the solution.

Design studies utilizing Monte Carlo codes typically use estimates of the statistical uncertainty to determine the total uncertainty. There are theoretical reasons, supported by observations of Monte Carlo output, to believe that Monte Carlo confidence limits in eigenvalue (criticality) problems are sometimes significantly underpredicted. This problem is accentuated when the random walk of the Monte Carlo calculation is optimized by biasing. Obviously, it is

important to understand and quantify the nature and magnitude of this nonconservatism in the uncertainty estimates for typical day-to-day design applications.

This thesis documents the concerns and applications of Monte Carlo calculations in design studies involving criticality problems. The nonconservative nature of the uncertainty estimates was investigated and quantified. Details of the MCNP calculational model used in the neutronics studies for both the proposed MIP-II and MOTA tests are explained, as well as the assumptions that were made. Results of the calculations, including heating rates and reaction rates, are presented in detail.

Chapter 2 provides an overview of Monte Carlo methods, including a summary of the Monte Carlo code MCNP. Included in the overview is a brief history of the Monte Carlo method and a comparison with deterministic techniques. The summary of MCNP covers enough detail and background about many of the specific functions of the code so that any function referred to later will be adequately explained without having to consult the MCNP User's manual² to understand the material. Chapter 3 covers the uncertainty analysis that was performed on the code. Included in the chapter is an explanation of the statistical nature of the code and its calculation of uncertainty estimates. The model that was used in the quantification is described in detail as well as the calculational strategy. The manner in which MCNP calculates uncertainty estimates is explained and derived. A FORTRAN program which reads MCNP output, massages the data, and performs a series of statistical analyses was written. Results from

this program demonstrated the nonconservative nature of the MCNP uncertainty estimates and allowed for the determination of uncertainty multipliers based on the degree of biasing employed in the problem.

Chapter 4 describes the MIP-II preliminary physics calculations that were performed using MCNP. Included is a summary of the goals of the calculations and a description of the test model and methodology. Calculations were performed for both a row 6 and row 7 test assembly location. The calculations are described, and results are summarized for target reaction rates and adjacent fuel pin heating in both the row 6 and row 7 test locations. Chapter 5 describes the MOTA test. It addresses essentially the same range of topics that Chapter 4 does for the MIP-II test. Also included in the results of Chapter 5 is an investigation of the impact of the yttrium-hydride moderator on nearby tritium production tests.

Although these results are broad and far from exhaustive, they do serve to demonstrate the calculational power of MCNP in present day design applications.

CHAPTER 2

A BRIEF EXPLANATION OF MONTE CARLO METHODS AND MCNP

2.1.0 HISTORY OF THE MONTE CARLO METHOD

It is difficult to determine a date for the genesis of the Monte Carlo method, although as a tool for the solution of transport problems, Monte Carlo methods were developed during the World War II effort at Los Alamos. Previously known simply as statistical sampling, the mathematical technique was worked on at a feverish pitch during the war years. The work to perfect the numerical technique was performed concurrent with the development of the first electronic computer - the ENIAC. Principal developers in the emergence of Monte Carlo as a useful tool at this time were Enrico Fermi, Stanislaw Ulam and Max von Nuemann³. Monte Carlo methods are by nature probabilistic. As such, they are driven by the generation of random numbers. As will be explained later, in order to obtain useful results from Monte Carlo, large quantities of random numbers must be generated, on the order of millions. In its early stage, before the advent of more powerful computational devices, statistical sampling was awkward, and calculations were rudimentary at best. Rumors have it that the sight of a room full of scientist's wives at Los Alamos, spending their days generating numbers to support their husband's computations, was what spawned and provided the impetus for the development of electronic computing systems.³

Due to the inadequacies of the computing systems at the time, use of statistical sampling during the war effort was limited to neutron

multiplication and fission problems. Because of the length, magnitude, and tediousness of the calculations, sampling techniques as a design tool had fallen out of favor with design engineers. However, when the results of the ENIAC were reviewed, it became apparent that sampling techniques should be resuscitated, improved, and implemented. It was then that the imaginations of scientists such as Fermi and Ulam were recaptured and the Monte Carlo method was given birth.

Fermi had apparently invented something akin to the Monte Carlo method during the 1930's while working on neutron moderation problems in Rome. He later revealed that many of his amazing predictions of experimental results came not only through great insight, but also because of statistical sampling calculations he performed in his head when suffering from an insomnia bout.³ After hearing the results of the ENIAC project, Fermi designed an analog device to aid neutron transport studies aptly named the FERMIAC. The FERMIAC ran neutron histories in two dimensions and provided some much needed insight into the Monte Carlo method.

The growth of Monte Carlo methods progressed at a rapid pace. By 1949, a national symposium was held devoted entirely to the Monte Carlo method. In 1952, the MANIAC-I computer became operational, and a study of nuclear cascades based on nuclear collisions was performed. Advances continued, and MCN (the Monte Carlo Neutron transport code) was introduced in 1967. Version 1.0 of MCNP was written in 1977.

The impact of Monte Carlo methods extends past the area of neutron transport. The emergence of experimental mathematics was undoubtedly a result of the electronic computer and Monte Carlo has played a

strong, if not major, role in the genesis and development of the discipline. Because of this, mathematics now shares, with all other sciences, the equal duplicity of experiment and theory.

2.2.0 MONTE CARLO CALCULATIONAL METHODS

In contrast to other methods of numerical analysis, Monte Carlo is characterized by the use of random sampling to simulate a problem, physical or mathematical, and construct its solution. Construct is a key word in that an exact solution is not derived or calculated, but individual events, governed by probability distributions, are simulated sequentially until enough events are statistically sampled to describe the entire problem. This can best be understood in the case of particle transport, where the physical process may be modeled without even considering the transport equation. Individual particles are followed from a source, throughout their lives to termination. Probability distributions are sampled from transport data which dictate the outcome of events during the course of the particle's life. These events cover everything from distance to next collision and type of interaction to energy and angle of particle motion following the event.

2.2.1 Particle Tracking

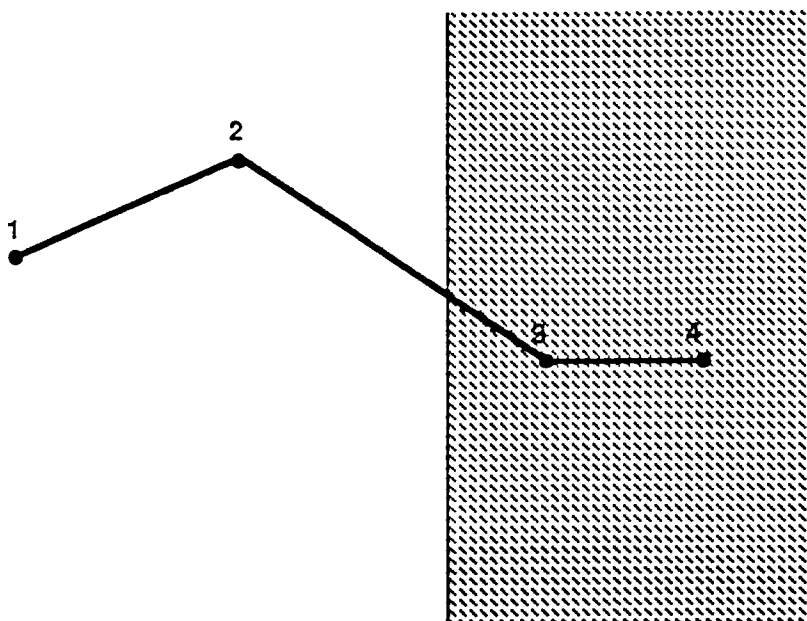
In a Monte Carlo calculation, the "history" of a neutron's life is characterized by a series of decisions based on statistical probabilities. These probability distributions are a function of both geometry and physics. At each decision point, the pertinent probability distributions are statistically sampled with the use of

random numbers. The statistical sampling process can best be illustrated with an example.

A particle is started in a region of fissionable material. The energy and direction of the particle flight is statistically determined by sampling from distributions characterizing the physics within the material. Random numbers are generated to determine the distance to the next interaction, if it occurs at all within the present region. When an interaction does take place, probability distributions, representative of the incoming energy, are sampled to determine the type of interaction. If scattering takes place, a new energy and flight direction are selected from distributions based on physical data. In Figure 2.1, a neutron is started at point 1. The energy and flight direction are statistically sampled. The distance to next interaction is statistically determined. This carries the particle to point 2. At the interaction point, random numbers determine the type of interaction. If fission was determined to happen, that point would be banked and a particle would be started from that position during the next generation of neutrons. If scattering is determined to take place, a new energy and direction are sampled. Random numbers are again used to determine a new point of interaction. In the example shown in Figure 2.1, a distance to next interaction was calculated which causes the particle to cross into a different region before the interaction. At the region boundary, a new distance to the next interaction is sampled based on the physics of the different material in the region. At the collision point

(point 3), the process continues until the particle is terminated by absorption when sampling from interaction types at point 4.

FIGURE 2.1
PARTICLE TRACKING SCHEMATIC



2.2.2 Comparison With Deterministic Methods

Deterministic methods, in comparison to Monte Carlo, solve the transport equation for an average particle. In doing so, deterministic methods, such as discrete ordinates, will provide extensive information for the average particle behavior within the entire phase space. Monte Carlo provides only the information requested in the form of tallies, which can be limited to a very small portion of the energy/phase space. As stated earlier, Monte Carlo does not solve an equation for transport problems. The discrete ordinates method solves the integro-differential transport equation and many maintain that Monte Carlo solves the integral equation. This is true only to the extent that just as there are no space or time derivatives in the integral equation, Monte Carlo tracks particles

between events rather than in the space and time phase. A more detailed discussion of the simulation of the mathematical models by the Monte Carlo method can be found in the book by Carter and Cashwell.⁴ In this publication, the authors provide an excellent comparison between Monte Carlo and numerical methods, including an analysis of how the integral form of the transport equation can be used to provide additional insight into the Monte Carlo sampling process.

2.3.0 OVERVIEW OF MCNP

MCNP is a general purpose, continuous energy, generalized geometry, time dependent Monte Carlo code for neutron and photon transport. MCNP was developed by the Applied Physics Division at Los Alamos National Laboratory. Although a thorough discussion of the theory and features of MCNP is presented in the MCNP manual², the special features and theory pertinent to this work are briefly highlighted here.

2.3.1 Geometry and Materials

MCNP is, for the most part, nongeneralized and user directed problem specific. There are no simple geometries, materials, or sources from which the user must choose to best represent or fit the problem. The user can go into as much detail as necessary on geometry and materials with computer time and available cross sections being the only restrictions. Geometrical bodies, in MCNP, are bounded by first, second, and fourth degree surfaces that are defined by the user in the Cartesian coordinate system. These bodies can then be combined

to form cells by the binary Boolean operations of complement, intersection, and union. Materials are defined by element and either weight or atom percent.

2.3.2 Source Modeling

For the purpose of modeling a transport problem, an accurate representation of the source is needed. MCNP provides two means of neutron and photon source specification. The first is a specific source description where the user picks one of five standard sources, such as a point source or a plane wave, and then tailors the source to fit the user's needs by describing location, energy, direction, etc. For most core physics applications, where the "source" is neutron multiplication and propagation throughout the reactor, the standard sources are impractical. In these instances, the KCODE option can be utilized. The KCODE option simulates a fission source on a generation- to- generation basis. The user supplies an initial estimate of the multiplication constant and the spatial distribution. This distribution is used as the neutron source for the first cycle. During each cycle, a specified number of source particles are individually followed until death. This could result via capture, escape from the system, etc. All captures by fissile nuclides are treated as fission events, and the location of the fission is "banked" until the completion of the cycle. All progeny of the fissions are then used to construct the neutron distribution for the next cycle. It may take a number of cycles, depending on the geometry, for the "source" to be uniformly distributed throughout the entire system and accurately model a true fission source.

An option frequently utilized in MCNP calculations which are iterative in nature is the Surface Source Write card (SSW). This card will write a KCODE source volume to the surface source file, WSSA. The user specifies cells or surfaces on the card and the individual neutrons that cross the surfaces of the bounded volume are recorded. The WSSA file can be used as the source for subsequent problems. This is practical in MCNP problems where iterations are made with tallies in specific areas. By using a WSSA file for the source, the user will know that the same flux distribution is used during each iteration.

2.3.3 Tallies

Output and solutions to MCNP calculations are given in the form of tallies, and each tally is requested by the user. As the code tracks particles, each time a particle crosses the boundary of a cell for which the user has requested specific information, the code records the crossing of that boundary. At the end of the run, all the "tally marks" are added up, and normalized by the number of source particles which were run in the problem. There are a variety of tally types available. Within the scope of this thesis, the two primary tallies utilized were flux tallies and heating tallies. The flux tally behaves much like the example above. Heating tallies are done by recording the number of collisions that occur within a cell. Each collision results in a randomly sampled reaction of some kind, and each reaction is multiplied by the sum of its excitation energy and Q-value. The products of all the tallies and energies are summed up and normalized by the number of source particles.

In the MCNP input deck, tallies are ordered with an F* card, where the star is a number where the last digit (1 through 8) designates the type of tally to be performed. An F4 or F14 tally will calculate particle flux averaged over a cell in units of particles/cm³. An F6 or F36 tally will calculate energy deposition averaged over a cell in units of MeV/g of material. There are a variety of other command cards that allow the user to change the scope and parameters of the designated tally. The command cards that were utilized in the analysis covered in this paper are the FM* card, the E* card, and the SD* card.

The FM* card is the tally multiplier card, where the star is the same number used to designate the tally in the F* card. The FM* card can involve many parameters, but within the scope of this paper, it included only three. The first parameter designates the constant multiplier. The results of the tally will be multiplied by this number and then printed to the output file. The second and third parameters are used if infinite dilute reaction rate information is wanted. The second parameter designates the material of interest. The third parameter designates the reaction, such as an (n, γ) or (n,p) reaction.

The E* card uses the same numbering scheme as described above. The card simply includes a list of energy limits which identify a series of energy bins into which the tallies are separated. The E* card allows for multigroup fluxes and reaction rates to be calculated.

The SD* card is a tally segmenting card. Many of the tallies are normalized by both the number of neutron histories and the volume or

area of the cell. The SD* card allows the user to set or change the volumes and areas by which the code normalizes the tallies. In the analysis presented in Chapters 4 and 5, the SD* card was used to set the volumes or areas of the tally cells to unity so an absolute reaction rate was calculated.

The features briefly outlined above are illustrated with the following example:

```
FC54   Mo-98   n, gamma
F54:n  (2410 2405) (2416 2412) (2429 2418) t
FM54   3.51E+19 75 102
E54    7.58E-09 1.23E-03 1.69E+01
SD54   1 1 1 1
```

The FC card is a comment card. The tally is designated by the F54:n card which calls for neutron flux tallies in four different cell groups. Tallies are calculated in cells 2410 and 2405, cells 2416 and 2412, cells 2429 and 2418, and the total of the six individual cells. The FM54 card calls for each tally result to be multiplied by 3.51E+19. The second parameter calls for the infinitely dilute cross sections of material 75 (defined in the input file as Mo-98) to be used, and the third parameter calls for reaction number 102 (an (n, γ) reaction) to be calculated. The E54 card calls for the reaction rate tallies to be separated into four energy bins. These include a total (n, γ) reaction rate and reaction rates between the energies of zero and 7.58E-09 MeV, 7.58E-09 and 1.23E-03 MeV, etc. Each of the reaction rate tallies is normalized by a volume of 1.0 cm³, which in effect will yield an absolute reaction rate in units of reactions/s.

2.3.4 Monte Carlo Optimization Techniques

To optimize Monte Carlo calculations, the particles can be biased into geometric regions and energies of interest and away from regions and energies where information is not needed. In doing so, the majority of the calculational time is spent in regions of interest and valuable time is not wasted running particles where calculations need not be made. To maintain accuracy, MCNP uses a weighting function to ensure that by biasing, the physics of the model is still valid.

If a problem were run with absolutely no biasing, then each particle run in MCNP would represent one real physical particle. In the case of biasing, a number of MCNP particles may be run to represent one physical particle. If W MCNP particles are run to simulate one particle from a source, then each MCNP particle would have a weight of $1/W$. Although each MCNP particle would have a different random walk, when the results of the problem are added together, with the results of each individual tally being multiplied by the weight of the contributing particle, the true number of real particles is preserved through statistical averages. When biasing techniques are employed to more extensively sample a part of the problem of higher interest, weighting serves to maintain the accurate representation of the physical model.

There are two main techniques of biasing utilized in MCNP. These are the use of importances and weight windows. Importances are simply a measure of the value that each cell has relative to all others. If a particle with weight W travels from a cell with importance I into a cell with importance J , either geometry splitting or Russian roulette

takes place. If J/I is greater than 1.0, the particle is split into N particles where $N = J/I$, each with weight W/N . If J/I is less than 1.0, Russian roulette is played and the particle is terminated with probability $1 - J/I$. If the particle survives, then it is assigned a weight of $W*I/J$.

Weight window techniques are a little more complicated than the use of importances. Basically, the user specifies an upper and a lower weight bound. The ratio of upper to lower bounds is always constant. If a particle is below the lower weight bound of the cell it enters, then Russian roulette is played on that particle. If it survives then the weight of the particle is increased to a value within the window. If the particle's weight is above the upper bound, then the particle is split until all split particle weights are within the window.

2.3.5 Monte Carlo Uncertainty

Being a stochastic calculational device, statistics are of prime importance in Monte Carlo problems, for the statistics define the worth and reliability of the tally. Chapter 3 of this paper is dedicated to determining the accuracy of the MCNP calculated statistics. The statistical uncertainty that accompanies each tally result is a measure of the precision of the calculation. It is important to differentiate between precision and accuracy. The precision of a calculation is the uncertainty in a tally mean caused by statistical fluctuations in the magnitude of all individual contributing tallies. In theory, these contributing tallies should be normally distributed about the tally mean. Obviously, the more particles which are run, the higher the precision of the calculation.

Accuracy is a measure of the difference between the tally mean and the true answer. The user bears much of the responsibility for the accuracy of the solution, for the accuracy is determined through the geometrical and physical model which the user specifies. Regardless of how precise a solution is, if the physics and geometry of the problem are poorly specified, the accuracy will be off.

A great deal of detail and attention is given to error analysis in Chapter 3. It is important to understand that Monte Carlo methods do not solve for the "true" answer mentioned above, but they merely estimate a solution through a series of random walks. Since each individual tally should be normally distributed about the mean, the variance of the population can be calculated to provide an estimate of the precision of the calculation. The process of Monte Carlo uncertainty determination is detailed in Chapter 3.

CHAPTER 3
A QUANTITATIVE ANALYSIS OF MCNP UNCERTAINTIES
IN REACTOR PHYSICS PROBLEMS

3.1.0 THE PROBLEM

Design studies, utilizing Monte Carlo codes, usually include estimates of the statistical uncertainty in a determination of the total uncertainty in the parameters of interest. This statistical uncertainty is typically obtained using the first and second moments of the tally mean in the Monte Carlo calculation. Because of this, there is a statistical variation in the estimate of the uncertainty. There are theoretical reasons, supported by observations of Monte Carlo output of special test problems, to believe that this leads to a nonconservative estimate of the uncertainty and that the Monte Carlo confidence limits are sometimes significantly underpredicted. Clearly, it is important to understand the nature and reliability of this estimate.

It has long been observed that the statistical uncertainty will decrease approximately inversely proportional to the square of the number of source neutrons, as the theoretical standard deviation should behave. However, in some instances, the uncertainty will suddenly jump due to the contributions of the progeny of some individual source neutron. Because of this, the MCNP manual² cautions the user in the application and interpretation of the uncertainty limits. The user is advised to use tallies only if the relative uncertainty is less than at least 10 percent, and the standard

deviation decreases smoothly with an increasing number of source neutrons. The latter indicator can be monitored by virtue of the figure-of-merit, which is calculated and dumped to the user in the code output.

In the case of MCNP eigenvalue problems, there are two known reasons for the nonconservative estimate of uncertainties in the tally results. The estimate of the tally is inherently nonconservative due to the generation-to-generation nature of the random walk simulation. The algorithm used by MCNP assumes that the fission source particles are not correlated on a generation-to-generation basis, whereas in reality, there is a very definite correlation between a source neutron and its progeny. This correlation may introduce a significant underestimation of the variance when neglected in the code.⁵ There is also a small bias in the generation-to-generation simulation caused by the fission source where the expected values do not converge to the true values as the number of source neutrons approaches infinity.^{4,6} In principle, this problem can be solved by using a sufficiently large number of neutrons per generation. In practice, this approach can be undesirable because a large number of generations is usually required for satisfactory convergence to the eigenfunction, and the associated computer time is often costly.

Comparisons of various physics design calculations at FFTF have indicated that the trends discussed above were occurring in the MCNP computations. It was observed in some instances that the neutron environment in one cell was calculated to be statistically different from another cell in a nearly symmetrical azimuthal location. There

were also cases where a comparison of MCNP calculations revealed that two tallies that should have been the same differed by more than two standard deviations. Most of these observations were made in long complicated runs where it was impossible to accurately assess the reasons for the discrepancy. Version 4 of MCNP currently allows for the optimization of the fission source neutron's random walk in both space and time. It is possible that strong optimization of the random walk may accentuate the nonconservative estimate of the confidence limits. Clearly, it is important to understand the role that optimization plays and to quantify the nonconservatism in the uncertainty estimates, as a function of biasing method utilized in the MCNP calculation.

3.2.0 STATISTICS

3.2.1 Calculation of Statistical Uncertainty Estimates

The tally mean of an individual sample is calculated in MCNP by:

3.1)

$$\langle F \rangle = \frac{1}{n} \sum_{k=1}^n T_k$$

where:

$\langle F \rangle$ = The tally mean

n = The number of histories run

T_k = The contribution from the k^{th} source neutron and its progeny. Note that the progeny only includes the current generation for eigenvalue problems.

The second moment of the tally mean is given by:

3.2)

$$\langle F^2 \rangle = \frac{1}{n} \sum_{k=1}^n T_k^2$$

It follows that the relative standard deviation is calculated by MCNP as:

3.3)

$$D = \frac{1}{\langle F \rangle} \sqrt{\frac{\langle F^2 \rangle - \langle F \rangle^2}{n}}$$

Statistical theory would have an $(n-1)$ term in Equation 3.2 in place of the n term in the divisor, but for practical MCNP application, the number of source particles run in a problem is so large that the results are equivalent if either term is used.

Since $\langle F \rangle$ and $\langle F^2 \rangle$ are averaged over a total of n source neutrons, they will theoretically approach constant values as n approaches infinity, if the contribution from each tally source neutron is finite. Because of this, the standard deviation will decrease inversely proportional to the square root of the number of source neutrons. This would seem to make it possible to predict the number of histories that need to be run in order to obtain results within a desired confidence limit. However, in practice this is not possible, because the possibility always exists that the contribution from a large single tally will lead to a substantial increase in the Monte Carlo estimate of both the mean and standard deviation.

3.2.2 Reliability of Uncertainty Estimates

3.2.2.1 Reliability of Uncertainty Estimates in Extraneous Source Problems

An example of a potentially unreliable uncertainty prediction involves a point detector estimator,⁴ where the point detector is located in a void close to a material region. In the Monte Carlo code,² a point detector is a deterministic estimate of the flux at a point in space and is based on source and collision events throughout the random walk of the particle. Because there is a $1/R^2$ term in the denominator of the general flux expression, collisions occurring in an immediately adjacent material will cause the theoretical tally score and variance to approach infinity. However, this is impossible, because the point detector is located in a void region. Until a large number of collisions have occurred, the results are suspect, making long computer intensive calculations necessary. The MCNP manual even urges caution in the use of the potentially anomalous statistics which the detector scheme will provide. It is theoretically possible to reduce the computation time by use of an appropriate biasing technique. Optimization, if used correctly, can both decrease the variance and increase the reliability of its estimate.

Very often in this type of problem the observation is made that the mean and second moment of the individual tallies will tend to be low. That is, a large enough ensemble of J statistically independent calculations with n source neutrons per calculation will lead to the correct mean, obtained by averaging over the entire ensemble. In some cases, however, most of the contributing J calculations will yield

individual estimates which are lower than the true mean, with just a few of the estimates over the mean, but high enough to drive the average up near the "true mean." Sometimes this results from over-optimization of the random walks in portions of phase space.

3.2.2.2 Reliability of Uncertainty Estimates in Eigenvalue Problems

In addition to the reliability questions surrounding the uncertainty in extraneous source problems, the generation-to-generation nature of the eigenvalue calculations introduces other problems. It is well known that there is an actual bias in most Monte Carlo eigenfunction problems,^{6,7} with the eigenvalue shape bias being inversely proportional to the number of neutrons per generation. In practical application, the attempt to resolve this problem is made by running a large number of neutrons per generation. However, since that number will always be finite, it is impossible to completely eliminate the entire bias.

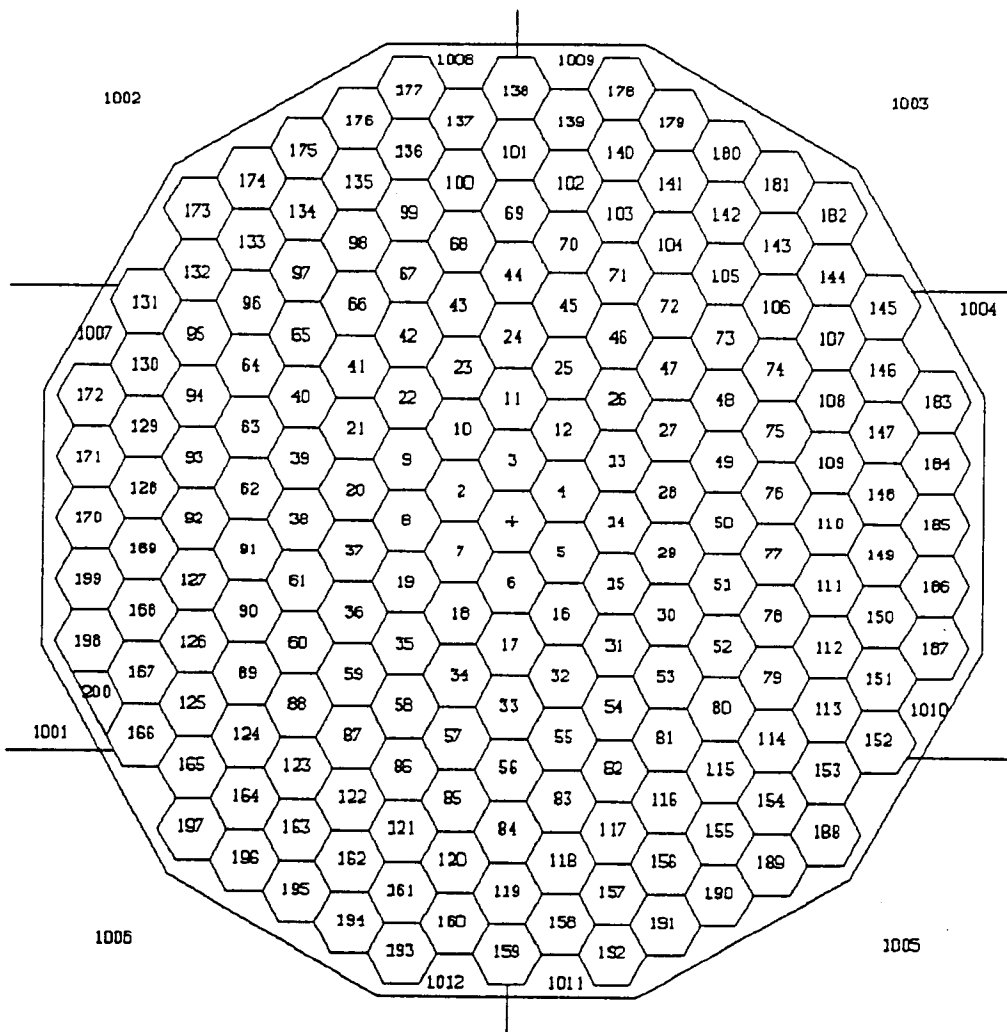
Increasing the number of neutrons per generation in the Monte Carlo calculation improves stability for a reactor with the property that at least one dimension is a very large number of mean free paths. This has been demonstrated in simple MCNP calculations involving a long thin cylinder of homogenized water and fissionable material with the ²³⁵U concentration adjusted to give an effective multiplication constant near unity. The cylinder was long enough that it typically required a large number of neutrons per generation for neutrons starting at one end of the cylinder to produce source neutrons at the opposite end. If a small number of neutrons per generation were used, the observation was made that the source tended to statistically

gather at various axial locations. Tallies integrated over each of the axial two halves would often differ by more than the statistical uncertainty dictated was possible, considering that there was axial symmetry.

Because of this, it is obvious that either a new simulation algorithm for the code is required or a large number of neutrons per generation must be used. For reasons already discussed, the use of a large number of neutrons per generation can be undesirable, as the calculations tend to be very computer-intensive. Such time investment is often not possible.

Even relatively small reactors with substantial leakage exhibit generation-to-generation source phenomena that are of concern. Wave-like patterns have been observed as a function of the azimuthal angle in the calculation of fission powers of individual fuel assemblies located in row 6 (Cells 61 to 90 of Figure 3.1), the outermost fuel row, next to the reflector of the liquid-metal-cooled FFTF reactor. These wave-like patterns were observed to move around in the azimuthal direction as more generations were simulated. Since design calculations often involve a small portion of the core, absolute reaction rates within this small portion depend upon a reliable neutron source. Hence, this type of observation is of concern. It is interesting that such wave-like patterns would be observed, since a fission source in the center of the reactor will lead to nearly the eigenfunction shape in only five generations. Studies with MCNP have shown that only five generations are required to obtain approximate convergence to the fundamental mode for a high leakage reactor after

FIGURE 3.1
PLAN VIEW OF HEXAGONAL MATRIX



starting with a delta function source at the center of the core. Hence, fission source correlations should be small.

Another related area of concern is the generation-to-generation correlation between source neutrons and the impact of this correlation on the estimation of uncertainties. MCNP uses the first and second moment of the tallies, as given by Equations 3.1 and 3.2, to calculate the estimate of the relative standard deviation. These equations do not take into account the correlation between source neutrons and progeny. The code also uses this same algorithm to estimate uncertainties in the eigenvalue (KCODE) calculations, where the number of source neutrons is the total number of generation-to-generation fission source neutrons after discarding the first few generations to ensure convergence to the fundamental mode.

Fortunately, the user of MCNP usually has a good idea of the maximum tally that should result from the problem calculation, or whether the type of problem that is being run should have stability problems. As mentioned before, the code provides some insight into this, as the user should look for standard deviations that are less than 5 percent and a relatively constant figure-of-merit.

If the estimate of the uncertainty is determined to be reliable, the next step is to assign confidence limits to the results. If a sufficiently large number of histories have been sampled, the tally distribution should be normally distributed.⁴ This implies that the following confidence limits can be assigned based on the standard normal distribution function: The mean is accurate to plus or minus 1.645 times the standard deviation with 90 percent confidence; to plus

or minus 1.96 times the standard deviation with 95 percent confidence; and to plus or minus 2.326 times the standard deviation with 98 percent confidence. Various statistical tests have been made to check the assumption that the tally results are normally distributed about the true value.⁸

3.2.3 Statistical Analysis and Quantification Strategy

The strategy employed in the attempt to quantify the magnitude of the nonconservatism in the uncertainty estimates centered upon the comparison of individual tallies to the "true" answer, where the "true" answer is the solution that the code would arrive at if there were not any inherent biases. A number of carefully controlled problems, each with a different degree or type of optimization technique, were analyzed. The individual tallies were then compared to the "true," expected value. If the MCNP results are in fact normally distributed and the uncertainty estimates accurate, then 90 percent of the tallies should fall within plus or minus 1.645 times their standard deviation of the "true" value, etc. If the percentage is less than a normal distribution would predict, then the conclusion can be reached that the uncertainty estimates are in fact nonconservative. If enough tallies are utilized in the comparison to ensure statistically significant results, then the magnitude of the nonconservatism can be determined.

MCNP will output tally results and relative uncertainties every M cycles, where M is a user-specified integer. However, the number of source neutrons used in the normalization of the tallies and uncertainty estimates is not constant for every batch of tallies

included in the output every M cycles. The tallies represent the mean and relative standard deviation averaged over the cumulative number of source neutrons. If N is the number of source neutrons per generation, then after M cycles (following proper convergence to a uniform source distribution), the first batch of tallies will be normalized by N*M source neutrons. After another M generations are run, tally results are dumped to the output file which are normalized by 2*N*M source neutrons, and so on.

However, these quantities cannot be compared to each other while maintaining statistical accuracy, because this would introduce additional correlations. The tally samples would be for differing numbers of source neutrons, rendering the results of statistical comparison questionable. To find the tally averaged over the same quantity of source neutrons, for example every NM neutrons, it is necessary to weight the MCNP output according to the cumulative number of source histories and find the difference. The treatment of the tallies is straightforward. The corresponding first and second moments for one cycle of M generations, based on NM source neutrons can be determined as:

3.4)

$$\langle F \rangle_{\bullet i} = \frac{\langle F \rangle_i C_i - \langle F \rangle_{i-1} C_{i-1}}{C_i - C_{i-1}}$$

3.5)

$$\langle F^2 \rangle_{\bullet i} = \frac{\langle F^2 \rangle_i C_i - \langle F^2 \rangle_{i-1} C_{i-1}}{C_i - C_{i-1}}$$

where:

i = Number of batches with M generations per batch

$C_i = iNM$ = cumulative number of source neutrons with N the number of source neutrons per generation (note that $C_0 = 0$).

The subscript i denotes the cumulative sum up through and including batch i , while the subscript θi denotes the contribution from only batch i . With this notation, the denominators in the above equations could have been written $C_{\theta i}$, where $C_i - C_{i-1} = C_{\theta i}$.

The MCNP estimate of the standard deviation can be determined in batch notation by inserting the results of Equations 3.4 and 3.5 into Equation 3.3:

3.6)

$$D_{\bullet i} = \frac{1}{\langle F \rangle_{\bullet i}} \sqrt{\frac{\langle F^2 \rangle_{\bullet i} - \langle F \rangle_{\bullet i}^2}{C_{\bullet i}}}$$

In collapsing the M generations per cycle, it is assumed that these batches are largely uncorrelated. It is possible, however, that as M increases to values greater than 1.0, the generation-to-generation source correlation, described in Section 3.1, may be introduced into the overall error estimation. Note that as M increases, the standard deviation decreases, becoming statistically more reliable. This was an important consideration in the selection of a value for M , as will be described later.

The reliability of the uncertainty in MCNP calculations based upon the relative standard deviation estimate given by Equation 3.6 could be quantified if the tally results of a large number of individual batches were obtained and the true means were known. Of course, it is impossible to calculate the true mean of a Monte Carlo problem, but it can be determined with a high degree of precision and accuracy if a large number of histories is run and minimal biasing takes place. In

doing so, the precision would be high, and the biasing effects on the estimate of the mean caused by over-optimization of the random walk, as described previously, would be minimized.

As was described above, the quantification applied here tests the theory that the tallies are normally distributed with standard deviations given by Equation 3.6. Standard tables of normal distributions are available which show what fraction of samples should fall beyond the specified confidence limits. The real concern involves samples that fall on the tails of the distribution. Consequently, those samples that fall outside the 90 percent, 95 percent, and 98 percent confidence levels, which correspond to 1.645, 1.96, and 2.326 standard deviations, were investigated.

Because the estimate of the standard deviation is calculated from the first and second moments, it too has a statistical uncertainty. The intent here is to use the tallies in the reliability tests only if the samples are large enough so that the statistical uncertainty in the standard deviation is small. The MCNP manual² describes the quality of any tally whose relative error is 50 percent as being "garbage," while relative errors of 10 to 20 percent are "questionable." In this study, the batch size utilized was typically large enough that most of the standard deviations utilized were less than 10 percent and never more than 20 percent. Hence, the results should be applicable to design studies with relative standard deviations in the 5 to 10 percent range.

Unfortunately, the requirement that most of the relative standard deviations be in the 10 percent or less range requires a fairly large

number of neutrons per batch. This conflicts with the desire to have a very large number of batches in order to observe tallies out on the tails of the distribution. To increase the number of samples, a problem was chosen with a high degree of symmetry so that many tallies with the same expected value (due to symmetry) could be obtained during each neutron history.

A program was written in FORTRAN (DENOMAKUE - DEtermination of NONconservative MAgnitude of Kcode Uncertainty Estimates. See Appendix A for listing.) to read the MCNP output file and obtain the first and second moments for each print dump after the user-specified number of generations. After extracting all the information from the entire output file, the program sorts the sample data and calculates the first and second moment and standard deviation for each individual batch according to Equations 3.4, 3.5, and 3.6. The user has the option of selecting the batch size. There is a tradeoff in selecting the batch size, however. For larger batch sizes, the relative standard deviation of each statistical sample will be decreased, but the number of samples is reduced, causing a reduction in the certainty of the conclusions. For small batch sizes, there are a large number of samples, but the relative standard deviations of each is so large that it is difficult to use the results in any meaningful statistical analysis. In this study, the batch size was selected so that nearly all of the samples were considered reliable. Then each of the individual batch means was compared to the "true" mean, and the difference, in number of standard deviations, was determined. The

data were then tabulated within the confidence level bins and written to tables.

The effort to quantify the nonconservatism of the uncertainty estimates was very computer intensive. Five different cases (described in detail in Section 3.3.3) each employing a different degree or technique of optimization were run. In order to conduct a comparison of tallies and their uncertainties that results in statistically significant results, a large number of individual tallies needed to be made for each. Timing studies done on a SUN^a Model 4/260 workstation indicated that the workstation ran MCNP at approximately 10 percent the cpu rate of the CRAY^b X-MP/18. The use of the workstation during the night and weekends resulted in the equivalent of over 100 effective CRAY computational hours invested into this problem. Therefore, the utilization of the workstation and a problem specifically designed to produce information which was applicable to the resolution of this problem enabled the valuable quantification of the uncertainty limit behavior reported here.

3.3.0 GEOMETRY AND TEST PROBLEM

3.3.1 Geometry

The design of the calculational model utilized in the study had a two-fold purpose. First, the geometry was similar to that of the FFTF core, so that the results of the study could be directly applied to physics design efforts involving the FFTF. Second, the geometry was

^a Trademark of SUN Microsystems, Inc.

^b Trademark of CRAY Research, Inc.

designed to have a high degree of uniformity and symmetry. As was explained earlier, symmetry was used as much as possible to maximize the number of tallies for the purpose of comparison. Uniform fuel densities and reflector densities were included to enhance the uncertainty study. The MCNP calculational model, which will be described in more detail in Chapter 4, had the following features:

- 1) A uniform hexagonal matrix of assemblies was modeled consisting of eight full rows and a partial ninth row as shown in Figure 3.1.
- 2) A uniform fuel loading in rows 1 through 6 was used. This was done by smearing the materials in the hexagonal matrix; i.e., homogenizing the fuel assemblies by the appropriate volume fraction of enriched UO_2 fuel, stainless steel, and sodium corresponding to the stainless steel clad fuel pins surrounded by the sodium coolant and contained within an outside assembly duct of stainless steel. The ^{235}U enrichment in the fuel was adjusted to obtain a multiplication factor of approximately unity for the calculational model. All assemblies within rows 1 through 6 had identical compositions and were treated as fuel; i.e., there were no control or safety rods included in this idealized study of statistical uncertainties in order to take maximum advantage of azimuthal symmetries.
- 3) A homogenized steel-sodium reflector material in rows 7 through 9 was modeled.
- 4) Five axial zones were included in this calculational model with

the central zone being the fuel zone. Immediately above and below the central fuel zone were lower and upper axial reflectors consisting of a homogenized mixture of stainless steel, inconel, and sodium. Above and below the axial reflectors was a homogenous mixture of stainless steel and sodium. This was utilized to represent the lower sodium inlet nozzle in the lower region and the gas plenum in the upper region. (See Figure 3.2.)

3.3.2 The Tallies

Fission power tallies were made in each of the row 6 assemblies. Row 6 is composed of 30 cells, but there are only three distinct cell types due to the intentional symmetrical loading of the calculational model. These common assembly types are shown in Figure 3.3 with the letters C, O, and I designating Corner, Inner-flat, and Outer-flat locations. Symmetry would predict that for each of these cell types, all the constituent cells would have equivalent fission powers.

The effect of the symmetry is twofold. First, symmetry made it possible to obtain more accurate mean values of the tallies as a basis for the comparison. Accurate mean values were necessary to statistically compare each individual tally to the corresponding mean value of its cell type. The accurate mean value of a cell type was obtained from a long MCNP calculation (the base case) with a large number of neutrons per generation. The individual row 6 tallies from this base case were then separated according to their location (corner, outer-flat, and inner-flat). The tallies for each cell type were then averaged together to represent the "true" value.

FIGURE 3.2
ELEVATION VIEW OF REACTOR MODEL

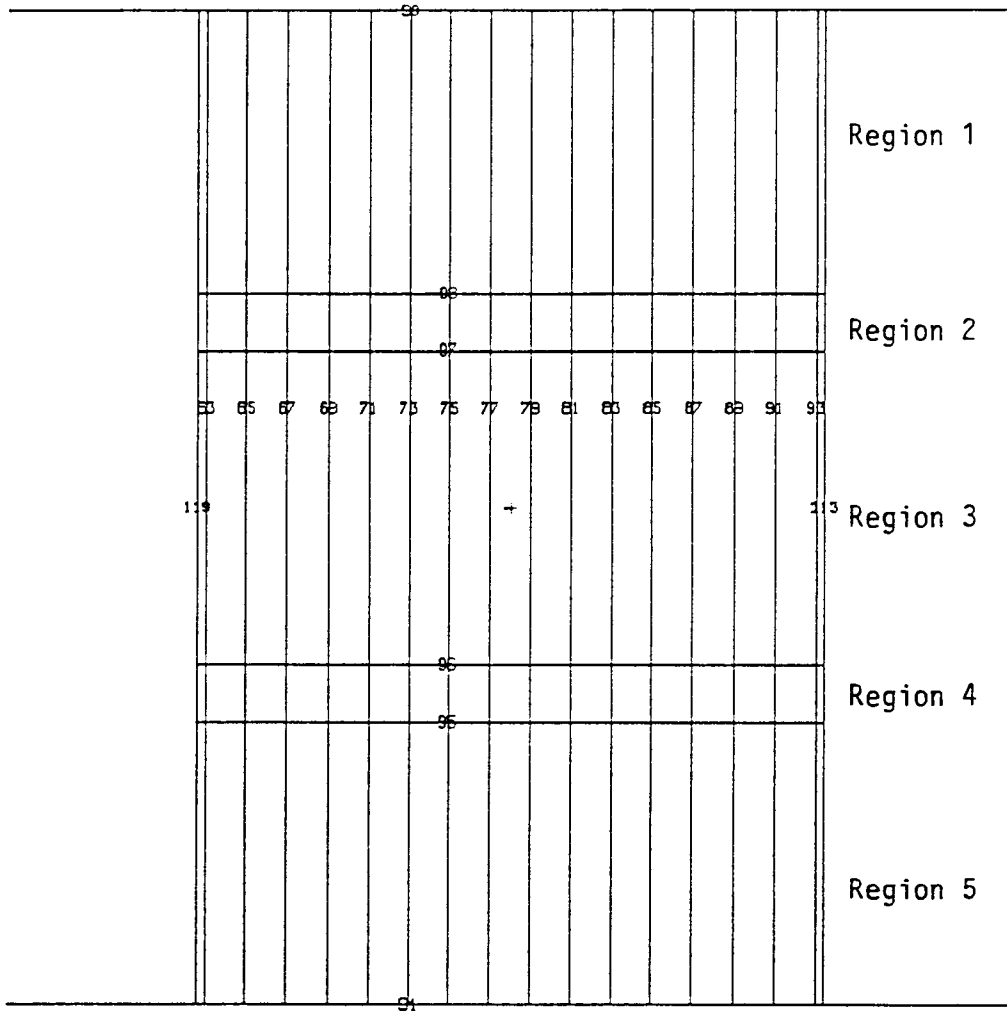
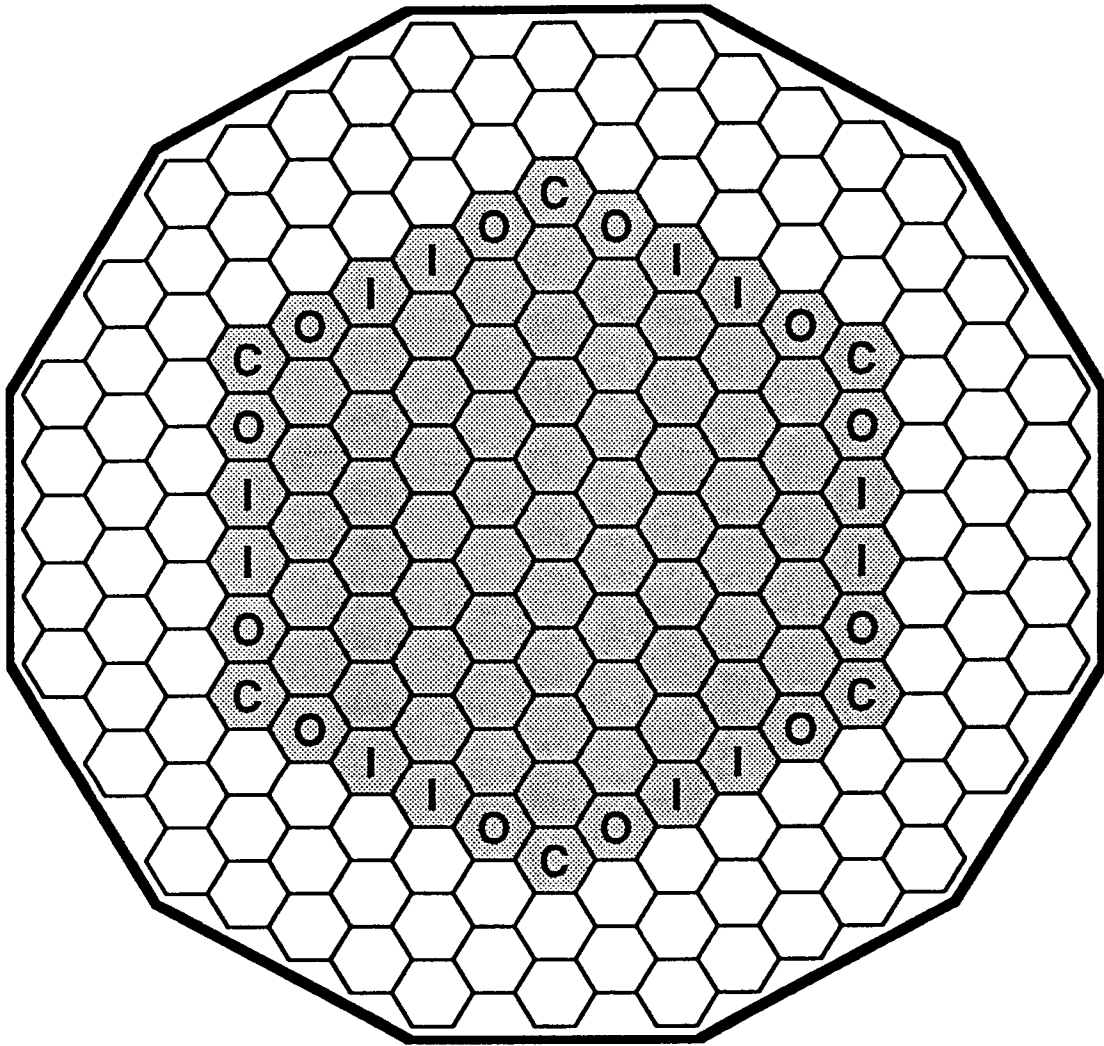


FIGURE 3.3
PLAN VIEW OF HEXAGONAL FAST REACTOR CALCULATIONAL MODEL
AT CORE MIDPLANE



Second, symmetry provided a larger number of data points to compare to the actual values. This made it possible to compare the tally results for more than one cell to the actual value. For example, rather than being able to compare only the results of one corner cell to the actual corner cell value, symmetry made it possible to compare the results from all six corner cells to the "true" corner value. The result was that for each set of source neutron histories, there were 6 statistical tally sample comparisons for the corner cells, and 12 apiece for the inner-flat and outer-flat cells, rather than just one apiece resulting from a batch of source neutrons.

3.3.3 Test Cases

Five different test calculations were made. The five cases were chosen to quantify both the bias due to the number of neutrons per generation, and the magnitude of the nonconservatism in the MCNP estimate of the uncertainties due to both neutron spatial and energy biasing.

For all five cases, tallies were not recorded until 50,000 neutron histories had been made. The SRCTP file records and stores the cycle-to-cycle neutron source distribution. By discarding the first 50,000 neutron histories, the SRCTP file was allowed to converge to the fundamental eigenfunction distribution before any tallies were recorded. This assured that the results would not be biased by a non-uniform starting source distribution.

The five test cases are described below and are summarized in Table 3.1.

TABLE 3.1 Summary of Cases				
CASE	SPATIAL OPTIMIZATION	ENERGY OPTIMIZATION	NEUTRON PER GENERATION	NEUTRONS PER BATCH
I	Weak	No	5000	2,000,000
II	Weak	No	200	800,000
III	Yes	No	5000	500,000
IV	Yes	No	200	150,000
V	Yes	Yes	5000	500,000

3.3.3.1 Case I (The Base Case) - Weak Spatial Optimization and 5,000 n/generation

This calculation obtained an accurate value for the means of the three tallies (corner, outer-flat, and inner-flat), which were subsequently treated as the "true" means for all of the reliability comparisons for all five cases. A reasonably large number (5000) of neutrons per generation (n/generation) was utilized, along with only very weak optimization using importances. Each cell in the fuel region (rows 1 through 6 in axial Region III of Figure 3.1) was given an importance of 1.0, the reflector region (Regions I, II, IV, and V in Figure 3.2, in addition to rows 7 through 9 of Region III in Figure 3.1) cells an importance of 0.5, and the rest of the universe an importance of 0.0. Using a somewhat smaller importance beyond the core reduced the computer time expended in this less interesting portion of the phase space.

In all five of the cases, the problem was started with an initial fission point in the center of the reactor. The first 15 cycles were

discarded to ensure an even source distribution before tallying. Upon convergence of the source to the fundamental mode, tallies were dumped to the output print file every 10 cycles. 8,125,000 total source neutron histories were sampled in this base case. This resulted in one standard deviation uncertainties in the "true" means of about 0.77 percent for the outer-flat and inner-flat tallies and 1.07 percent for the corner tallies.

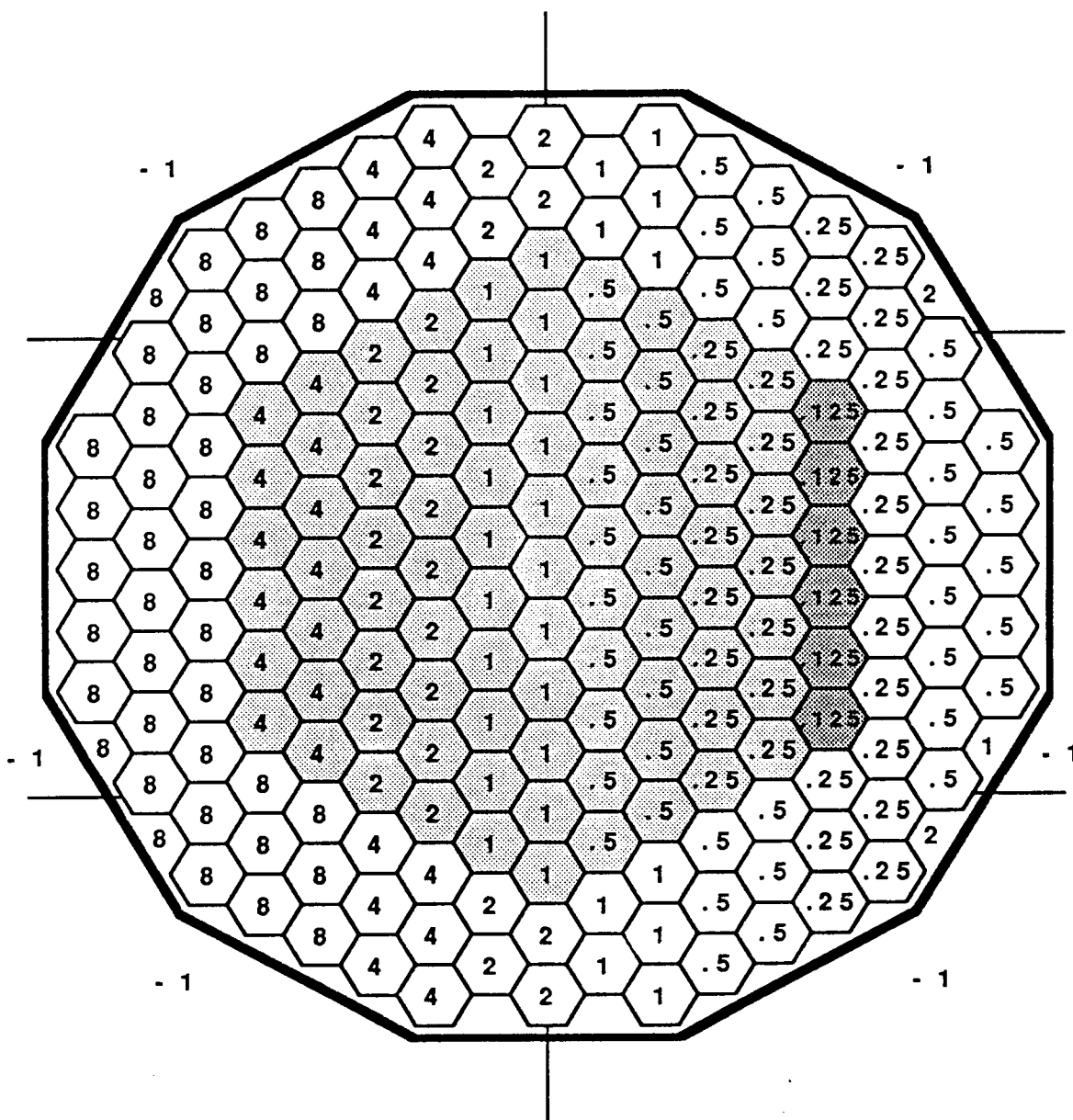
3.3.3.2 Case II Weak Spatial Optimization and 200 n/generation

The Case II calculation was identical to Case I except the number of neutrons per generation was reduced from 5,000 to 200 in an attempt to quantify the bias due to the number of neutrons per generation. Tallies were dumped to the output print file every 250 cycles. 2,602,250 total source neutrons were utilized for Case II. In Cases II through V, the first 50,000 neutron histories were discarded before tallying to allow for convergence to the fundamental mode.

3.3.3.3 Case III Spatial Weight Window Optimization and 5000 n/generation

The Case III calculation was used to quantify the impact of relatively strong spatial optimization of the random walks via weight windows on the reliability of the predicted uncertainties. The weight windows for Case III were decreased proceeding from the left to the right of the core, as shown in Figure 3.4 at core midplane. The weight windows decreased by a factor of two every other row of assemblies. Only the tallies in the six cells along the right hand flat of row 6 were utilized in the statistical study, since the optimization technique is tailored for the tallies in these cells.

FIGURE 3.4
LOWER BOUNDS OF NEUTRON WEIGHT WINDOWS FOR CASE III



This corresponds to the six row 6 cells with weight windows of 0.125, highlighted in Figure 3.4. This resulted in only two corner cells, two outer-flat cells, and two inner-flat cells being utilized in the statistical analysis. Figure 3.4 shows the lower bounds of the windows for the low-energy weight window group below 7 MeV. The windows for the high-energy weight window group above 7 MeV were the same as for the lower-energy weight window group for this case so no high-energy optimization of the random walks takes place. Cycles of 5,000 n/generation were run, with tallies made every 10 cycles. A total of 5,245,000 source neutrons were utilized for Case III.

3.3.3.4 Case IV Spatial Weight Window Optimization with 200 n/generation

The Case IV calculation was identical to Case III, except the number of neutrons per generation was reduced from 5,000 to 200. Tallies were made every 250 cycles. Only 562,250 source neutrons were utilized for Case IV. Because of the very low number of neutron histories, the statistical accuracy of Case IV is very low, and results should be viewed with that in mind.

3.3.3.5 Case V Both Space and Energy Weight Window Optimization with 5,000 n/generation

The Case V calculation was made to explore the combined effect of both space and energy optimization of the random walks, using some of the enhanced features of the Hanford Site version of MCNP for the energy optimization. A number of upgrades have been made to the Hanford Site version of MCNP-3B. One of the upgrades involves improved physics, and the remainder are centered around improved

optimization methods for a variety of problem types. Some of these improvements are now incorporated in Version 4.2 of MCNP. There were two optimization upgrades that were utilized and pertinent to the scope of this study. The first involves the generation-to-generation fission source. In a KCODE problem, the generation-to-generation fission source gives constant weight to each of the source progeny. However, giving constant weight to source neutrons leads to inconsistencies in optimization, particularly when weight windows or importances are being used to preferentially sample from various regions of the geometry. After one generation of neutron random walks has been optimized, the fission source samples progeny uniformly throughout the geometry. Thus, the fission source for one generation is not being optimized consistently with its prior generation. The variable source weight enhancement allows the user to generate new source points with a frequency consistent with the optimization employed in the neutron's random walk. The other enhancement utilized in this study allows the user to optimize the selection of the fission source energy to reduce variances in high energy threshold reaction tallies.

The Case V weight windows in the low-energy group remained the same as Case III. In the higher-energy group, the weight windows were decreased by a factor of 10 relative to the low-energy window groups, in all five regions. Therefore, there is significant optimization of the random walk, including the preferential sampling of the fission source both spatially and to higher energies. Tallies were made every 10 cycles, and 2,000,000 source neutrons were utilized for Case V.

3.4.0 COMPARISONS AND RESULTS

3.4.1 Explanation of Tables

Results of all five cases follow in both qualitative and quantitative format. The tables are arranged by case. These tables give the fraction of samples (from individual samples) that fall within the various limits of the designated confidence interval. If MCNP delivered normally distributed results, with its stated standard deviation, 90 percent of the values would fall within 1.645 standard deviations, etc. Also included in the tables is a column for the maximum number of standard deviations that separated any sample from the "true" mean. The "true" means were also obtained from the same base case calculation that generated Table 3.2. The relative standard deviation for these "true" means is about 1.0 percent for the corners and 0.7 percent for the inner-flat and outer-flat tallies. For each case, the tallies were analyzed with differing amounts of source neutrons contributing to each tally. The tables only include results when 100 percent, or as near as possible, of the individual tallies were reliable (a relative uncertainty of less than 10 percent). As was stated above, when the tallies are reliable and with the assumption that the generation-to-generation correlation is negligible, 90 percent of the values should be within 1.645 standard deviations of the "true" value, i.e., the MCNP output values will be normally distributed.

The footnote at the bottom of each table indicates the typical relative standard deviations for individual samples. Sample sizes were chosen large enough so that most of the individual samples would

have one standard deviation relative errors less than 10 percent. Therefore, the tables only include results when 100 percent, or as near as possible, of the individual tallies were reliable (a one standard deviation relative error less than 10 percent). Section 3.4.3 discusses the results of Case I when a much smaller sample size is used, with large individual relative standard deviations, to demonstrate the folly of believing the MCNP uncertainties when the relative standard deviations are above 20 percent.

3.4.1.1 Case I Results

The results are summarized in Table 3.2 for the base case with minimal optimization of the random walks. There was one sample 4.56 standard deviations away from the "true" mean. This, coupled with the four samples out of the 120 total samples which fell beyond the 98 percent confidence limits, would indicate that perhaps more samples lie in the far wings of the distribution than one would expect for a normal distribution. However, for the 90 percent confidence interval, 12 out of 120 samples would be expected outside the limits, and the study resulted in 14 outside the limits. This does not seem statistically unreasonable.

TABLE 3.2 Summary with Minimal Optimization and 5,000 Neutrons/Generation (Base Case -- also used for "true" means)					
	Random Samples	Fraction Within Limits			Max. Number of SD
		<1.645 SD 90% CI	<1.96 SD 95% CI	<2.326 SD 98% CI	
Corner	24	0.8750	0.9583	1.0000	2.13
Outer	48	0.8958	0.9167	0.9375	4.56
Inner	48	0.8750	0.9375	0.9792	2.34
Total	120	0.8833	0.9333	0.9667	

All individual samples had an MCNP one standard deviation relative error of less than 10% with nearly half being less than 5%.

3.4.1.2 Case II Results

The summary in Table 3.3 shows the results of Case II, which was the same calculation as Case I except the number of neutrons per generation was reduced from 5,000 to 200. In this study, six of the 60 tallies fell outside the 90 percent confidence limits which a normal distribution would predict exactly. However, these same six tallies also fell outside the 95 percent confidence limits. Fifty-seven, rather than the predicted 58, out of the 60 tallies fell within the 98 percent confidence interval. There was one tally 3.09 standard deviations away, but this is not nearly as far as the tally at 4.56 standard deviations away seen in the base case.

TABLE 3.3 Summary with Minimal Optimization and 200 Neutrons/Generation (Case 2)					
	Random Samples	Fraction Within Limits			Max. Number of SD
		<1.645 SD 90% CI	<1.96 SD 95% CI	<2.326 SD 98% CI	
Corner	12	0.9167	0.9167	0.9167	2.67
Outer	24	0.9167	0.9167	1.0000	2.32
Inner	24	0.8750	0.8750	0.9167	3.09
Total	60	0.9000	0.9000	0.9500	
Approximately 85% of the samples had an MCNP one standard deviation relative error of less than 10%.					

3.4.1.3 Case III Results

Table 3.4 shows the results of rather strong optimization of the random walks and 5,000 neutrons per generation. The table seems to indicate that optimization of the random walks causes significantly more samples to fall in the tails of the distribution than would be expected. A normally distributed distribution would predict that 54 of the 60 samples would fall within the 90 percent confidence interval, but the study showed that only 48 of the samples were contained in that interval. The magnitude of the outliers does not appear to be any worse than Cases I or II, with the maximum outlier being 3.21 standard deviations away from the "true" answer.

3.4.1.4 Case IV Results

Table 3.5 shows the results of the same weight window optimization as Case III, but with 200 neutrons per generation. This case involves a small number of samples, but the behavior of the results does

TABLE 3.4 Summary with Spatial Optimization and 5000 Neutrons/Generation (Case 3)					
	Random Samples	Fraction Within Limits			Max. Number of SD
		<1.645 SD 90% CI	<1.96 SD 95% CI	<2.326 SD 98% CI	
Corner	20	0.9000	1.0000	1.0000	1.73
Outer	20	0.7500	0.7500	0.8500	3.21
Inner	20	0.7500	0.8500	0.8500	2.88
Total	60	0.8000	0.8667	0.9000	

All individual samples had an MCNP one standard deviation relative error of less than 10% with about one-fifth being less than 5%.

indicate that the results are a little worse than for Case III, particularly in the larger confidence intervals. This seems to be caused by the magnitude and percentage of the outliers, with one of the samples a full 4.51 standard deviations away from the "true" mean.

3.4.1.5 Case V Results

The summary in Table 3.6 for strong optimization of the random walk in both space and energy indicates that the estimate of the uncertainty is quite nonconservative. Unfortunately, for Cases III, IV, and V the weight window optimization only allows tallies to be taken from six cells, which would require very long calculations in order to obtain a large number of samples. The table does show that only 83 percent of the samples fall within the 90 percent confidence interval. It is also interesting to note that all three tally types (corner, outer-flat, and inner-flat) each had one sample that was beyond the limits of the 98 percent confidence interval. This would

TABLE 3.5 Summary with Spatial Optimization and 200 Neutrons/Generation (Case 4)					
	Random Samples	Fraction Within Limits			Max. Number of SD
		<1.645 SD 90% CI	<1.96 SD 95% CI	<2.326 SD 98% CI	
Corner	6	0.8333	0.8333	0.8333	3.31
Outer	8	1.0000	1.0000	1.0000	1.37
Inner	6	0.6667	0.6667	0.8333	4.51
Total	18	0.8333	0.8333	0.8889	
Approximately 70% of the samples had an MCNP one standard deviation relative error of less than 10%.					

seem to indicate some sort of correlation to the source distribution, especially since there was only one other sample altogether between the 90 and 98 percent confidence limits.

TABLE 3.6 Summary with Spatial and Energy Optimization and 200 Neutrons/Generation (Case 5)					
	Random Samples	Fraction Within Limits			Max. Number of SD
		<1.645 SD 90% CI	<1.96 SD 95% CI	<2.326 SD 98% CI	
Corner	8	0.7500	0.8750	0.8750	3.79
Outer	8	0.8750	0.8750	0.8750	2.66
Inner	8	0.8750	0.8750	0.8750	2.34
Total	24	0.8333	0.8750	0.8750	
All individual samples had an MCNP one standard deviation relative error of less than 10% with nearly half being less than 5%.					

3.4.2 Correction Factor

One easily implemented method to reduce the nonconservatism in the uncertainties would be to simply multiply each of the relative standard deviations by a factor that is somewhat greater than 1.0. Presumably this correction factor would be tailored to the type of model and optimization method utilized. This approach was tried for each of the cases using 5,000 neutrons per generation (Cases I, III, and IV). The results are summarized in Table 3.7. DENOMAKUE was revised to require the user to input a correction factor. This correction factor was multiplied against each of the sample relative standard deviations. If no correction was needed, the proper correction factor would be 1.0. The multipliers shown in Table VI were empirically chosen to reduce the number of samples that appear outside the confidence limits and to bring the distribution into conformity with a normal distribution, i.e., to reduce the number of samples outside the 90 percent confidence limits to 10 percent of the total sample size.

Case I required very little adjustment to fit a normal distribution reasonably well. There was concern about the outlier that appears 4.56 standard deviations away. In a normal distribution, an outlier of that magnitude should only appear one time in 10,000, and there were only 120 samples used in the Case I calculation. A multiplier of about 1.1 was more than sufficient for the degree of optimization used in the Case I problem. For the Case III and V problems, a substantially higher correction factor was needed. Applying the empirical multipliers shown in Table 3.6, which are the calculations

TABLE 3.7			
Effect of Multiplier on Uncertainty Distribution			
CASE I - Only Weak Optimization, Multiplier = 1.1			
Percentage in Confidence Interval		Maximum Outliers	
% < 1.645 SD (90% CI)	92.5	Corner	1.93
% < 1.960 SD (95% CI)	95.8	Outer	4.14
% < 2.326 SD (98% CI)	99.2	Inner	2.13
CASE III - Spatial Optimization, Multiplier = 1.4			
Percentage in Confidence Interval		Maximum Outliers	
% < 1.645 SD (90% CI)	90.0	Corner	1.23
% < 1.960 SD (95% CI)	95.0	Outer	2.29
% < 2.326 SD (98% CI)	100.0	Inner	2.06
CASE IV - Spatial and Energy Optimization, Multiplier = 1.5			
Percentage in Confidence Interval		Maximum Outliers	
% < 1.645 SD (90% CI)	93.3	Corner	2.52
% < 1.960 SD (95% CI)	96.7	Outer	1.76
% < 2.326 SD (98% CI)	96.7	Inner	1.56

with strong optimization, leads to much better fits for the samples with the largest problems and still retains those beyond 90 percent reasonably well. However, this does require a multiplier of about 1.5 for the problem in this study.

3.4.3 Results from tallies with poor precision

The results that are summarized in Tables 3.2 through 3.6 utilized samples that were generally considered reliable. It was described earlier how the statistical analysis code DENOMAKUE allowed the user to choose the number of source neutrons which would contribute to each individual sample. A concerted effort was made to choose a number large enough that all the contributing samples would be reliable,

while still allowing enough samples to allow statistically relevant conclusions. Therefore, the relative standard deviation in each contributing sample was always below 20 percent, and the majority of the time below 10 percent. The five cases summarized in Tables 3.2 through 3.6 utilized 2,000,000; 800,000, 500,000, 150,000, and 500,000 source neutrons per sample, respectively. Case I was reanalyzed with only 50,000 source neutrons per sample to demonstrate the danger of using results from tallies when the MCNP estimate of the uncertainty is large. These results are summarized in Table 3.8.

The summary in Table 3.8 shows far more samples fall outside the confidence limits than would be expected in a normal distribution. Many of the samples are more than 100 standard deviations away from the "true" mean. This is certainly due to the fact that the uncertainties in the estimate of the standard deviation is so large.

The summary at the bottom of Table 3.8 gives the fraction of the samples whose relative standard deviations are below the given limits. Notice that over 60 to 70 percent of the samples have relative standard deviations over 20 percent. Recall from the Chapter 2 discussion that tallies with estimates between 10 and 20 percent are considered unreliable, while it is well documented that tallies with uncertainties greater than 20 percent are notoriously unreliable.^{1,2} The large standard deviation is invariably due to the small number of samples that contribute to each tally mean. Because of statistical fluctuations in the random walks of the small number of neutrons that contribute to a tally mean, some of the samples will have grossly underestimated contributions. This causes a low estimate of both the

TABLE 3.8 Summary with Minimal Optimization and 5000 Neutrons/Generation (Small Batch Size)					
	Random Samples	Fraction Within Limits			Max. Number of SD
		<1.645 SD 90% CI	<1.96 SD 95% CI	<2.326 SD 98% CI	
Corner	966	0.7598	0.7950	0.8385	184.82
Outer	1932	0.7500	0.8002	0.8297	103.33
Inner	1932	0.7376	0.7821	0.8287	189.75
Total	4830	0.7470	0.7919	0.8311	
	Fraction Below Given Relative Error				
	<0.05	<0.10	<0.20	<0.50	<1.00
Corner	0.0176	0.0642	0.3075	0.9648	1.0000
Outer	0.0233	0.0828	0.3670	0.9777	1.0000
Inner	0.0285	0.1030	0.4053	0.9726	1.0000

first and second moment of the tally. Because of this low estimate of the standard deviation, many more of the samples will fall out in the tails of the distribution when compared to the "true" mean.

The "fission power" tallies shown in Table 3.8 have rather large uncertainties for batch sizes of 50,000 source neutrons per sample. The reason for this is that they are not true fission power tallies, but are tallies proportional to the square of the macroscopic fission cross section rather than proportional to just the macroscopic fission cross section as a fission power tally should be. The calculations were all made, and the information was summarized in the tables, before it was discovered that the fm7 tally card in the MCNP input file referenced the fuel number and a "19" ENDF/B-V material reaction number. This "19" response function is a fission cross section, but

tally 7 in MCNP automatically specifies a fission reaction rate. This inadvertently resulted in a tally involving the square of the fission cross section rather than just the fission cross section.

For this study of the unreliability of uncertainty estimates, this type of tally (square of the fission cross section) has the advantage that it represents a worst case scenario due to the response function and energy structure. Because of this, the conclusions reached could be seen as conservative. There is the very great disadvantage, however, that because of the large relative uncertainties in each tally, a large number of source neutrons had to contribute to each sample, thus reducing the number of samples that could be used in the comparison study. This tally has been referred to as a fission power tally in the summary of the test problems, but it is a more complicated function than a fission power tally.

3.5.0 CONCLUSIONS

During physics design studies for the liquid-metal-cooled FFTF reactor, there have been indications that the uncertainties obtained from MCNP calculations are sometimes quite nonconservative. It was further theorized that the nonconservatism may be accentuated by optimization of the random walks to decrease the uncertainties in the tallies of interest. This seems to be consistent with various studies in literature. These sources indicate that the generation-to-generation source correlation may be the major contributor to the nonconservatism in the uncertainty estimates. Furthermore, some of these studies have identified a bias in eigenvalue (KCODE) problems,

due to the finite number of neutrons which can be utilized in a given generation. Commonly, this problem is resolved by increasing the number of neutrons per generation, but while sometimes being impractical, the nonconservatism may be accentuated by strongly optimizing the random walks of the fission neutrons.

The purpose of this study was to explore the reliability of the uncertainty estimates in MCNP calculations and to quantify the magnitude of their nonconservative nature. These quantifications were made for problems involving a variety of optimization techniques, from a near analog calculation to a problem involving optimization in both the spatial and energy phase. Although the geometry was treated ideally to efficiently maximize the amount of information obtained, the results should be indicative of those expected in liquid metal reactors and small-to-moderate-sized thermal systems.

Due to the nature of Monte Carlo calculations and the large number of samples required, attempts to quantify the reliability of uncertainty estimates are very computer intensive. A SUN workstation, that executed Monte Carlo problems at nearly 10 percent of the CPU rate of a CRAY super computer, was utilized in batch mode at night and during the weekends to make the calculations. By making these calculations over a period of months on the workstation, an equivalent of over 100 effective CRAY hours of computer time was invested in this study.

Symmetry was highly utilized in the model for these calculations. This afforded a number of advantages in the attempt to quantify the nonconservatism in the uncertainties. By averaging the results of the

fission power tallies for a number of cells, it was possible to determine the "true" mean from a near analog case with minimal optimization of the random walks. It was also possible to combine the results from all samples into three groups based on their location. This greatly increased the number of samples available for each comparison.

The number of samples that fell within various confidence limits was determined using the "true" mean from above and the MCNP estimate of the mean and relative standard deviation. The confidence limits were determined by the number of samples and their standard deviation, based on a normal distribution. The results indicate that when minimal optimization of the random walks was employed, the number of samples that fell beyond the 90 percent confidence limits is not far from the 10 percent of the total samples number that is expected. However, there tended to be more than expected that fell outside the 98 percent confidence limits. For the five case calculations in this study, about one out of every 150 samples was more than four standard deviations from the "true" mean. A normal distribution would predict that less than one in 10,000 samples would fall this far out in the tails.

For stronger optimization of the fission source neutron random walks, the study indicates that the percentage of samples that fall in the tails of the distribution is increased with an enhanced degree of optimization. There appears to be no significant bias involved with using 200 neutrons per generation in the analog (minimal optimization) case. However, there appeared to be some bias involved with using 200

neutrons per generation when strong optimization techniques were employed, but this was inconclusive due to the small number of samples involved.

To summarize, with minimal optimization of the random walks, the number of samples that fall outside the confidence limits is reasonably consistent with the number predicted by a normal distribution when using MCNP relative standard deviation estimates. However, there appears to be substantially more samples that fall far out in the tails of the distribution than would be expected. There was no significant bias observed using 200 neutrons per generation rather than 5,000 for a case involving minimal biasing.

When a high degree of optimization is employed using both space and energy weight windows, there are more samples that fall outside the confidence limits than a normal distribution would predict, and there appears to be strong source correlations. Multiplying the sample relative standard deviations by an empirical correction factor of 1.5 considerably improved the number of samples out in the tails, bringing the distribution into near conformity with the predicted normal distribution. There was insufficient data to determine whether a correction factor of 1.5 will always be a conservative value, based on the problem. However, this could be the prudent choice for design studies involving strong optimization of the random walks, particularly when it involves optimization of the fission source.

CHAPTER 4

THE MIP-II TEST

4.1.0 INTRODUCTION

During the summer of 1990, the Isotope Production group at Westinghouse Hanford proposed the running of two different tests in the Fast Flux Test Facility. The first of the tests, described in this chapter, is MIP-II. (The MIP-I test was performed in May 1989.) The second isotope production test covered in this paper, which will be described in detail in Chapter 5, involved the MOTA. In this chapter, background on the goals of the MIP-II test, a description of the MCNP calculational model utilized, a discussion of the MCNP calculational techniques employed, and a brief interpretation of the results of the MCNP calculations are provided. The purpose of Chapters 4 and 5 is to describe a variety of MCNP calculational tools and to demonstrate how the interpretation of the Monte Carlo results is used in design applications.

4.1.1 Isotope Production

Radioisotopes and radiation are in widespread use throughout the world. As the utilization of special radioisotopes increases daily, they have become an important player, if not a primary fixture, in the world of science, agriculture, medicine, and industry. Within these arenas, applications of the radioisotopes are diverse, ranging from non-destructive testing and sterilization in industry to food preservation and processing in agriculture.⁹ In the past, medical uses of radioisotopes were essentially limited to diagnostic procedures, such as ^{99}Mo - $^{99\text{m}}\text{Tc}$. While $^{99\text{m}}\text{Tc}$ treatment continues to be

the most widely used radioisotope in the medical field, recent developments have shown that radioisotopes have tremendous potential as radiopharmaceuticals, which can be used in therapeutic treatment of several major diseases. A radioisotope is selected for application depending on half-life, energy, and type of radiation. Studies have been performed which analyze the potential for production of specific radioisotopes in various reactor systems, in particular the FFTF.¹⁰ It was these studies which led to the MIP-II and MOTA isotope production tests. Candidate isotopes were selected for potential production. Production calculations using MCNP, described in Chapters 4 and 5, were then performed for each of the nuclides targeted. The radioisotope, utilization, and approximate market value when available are summarized in Table 4.1.

4.1.2 MIP-II Calculational Objectives

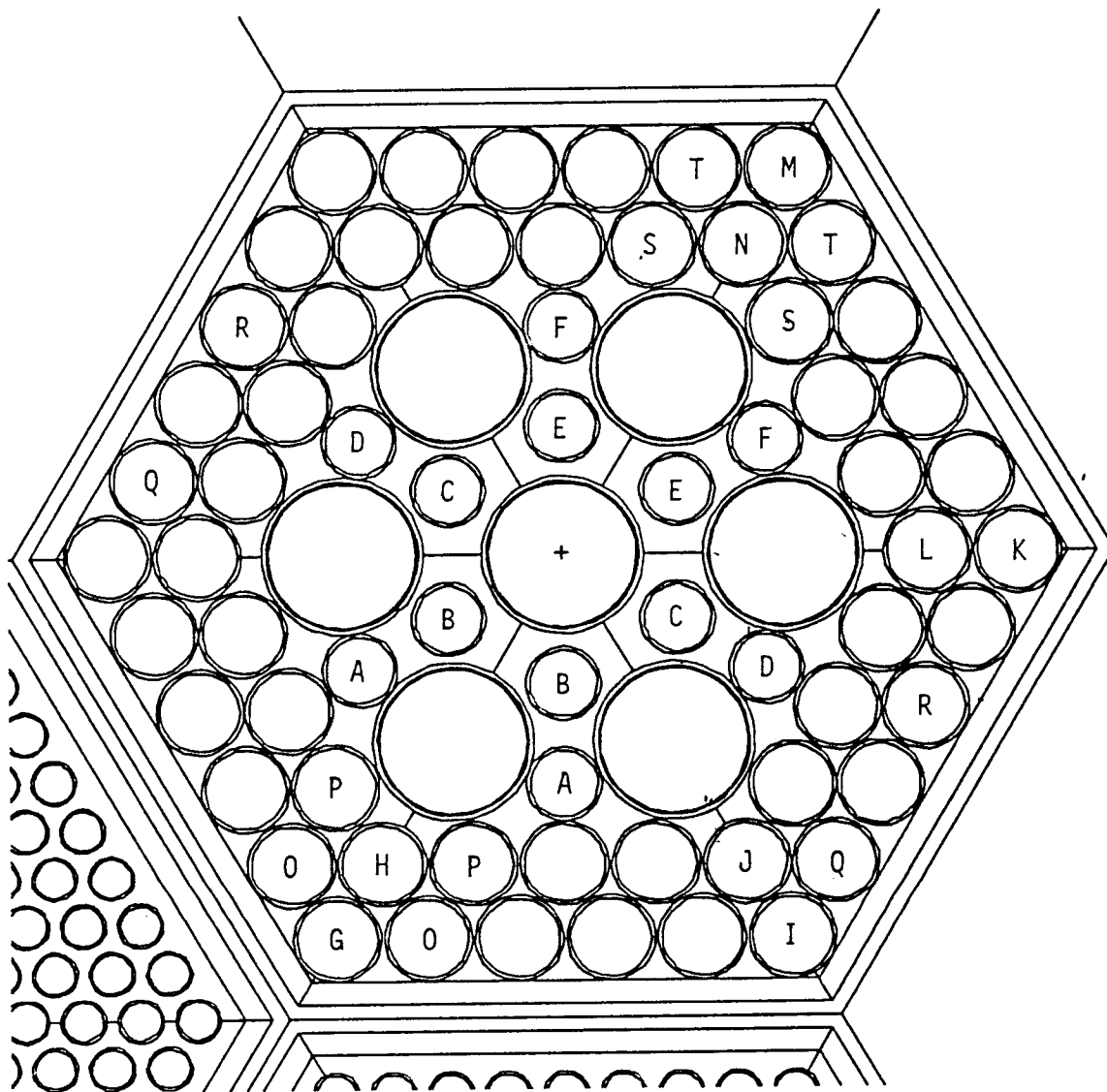
Based on the demand and potential for isotope production described above, a special test assembly was designed to investigate the feasibility of isotope production in the FFTF. A conceptual design of the assembly was made, which had the configuration shown in Figure 4.1. The six large pins in the center of the design were composed of a yttrium-hydride moderator, while the smaller pins were either target or filter pins. The geometry and materials will be described in detail in a later section, but note that there are 13 target pins specified in the configuration that have unique positions. Detailed preliminary neutronic calculations were made for this assembly located both in row 6 and row 7 of the FFTF.

TABLE 4.1 Potential Radioisotopes		
Radioisotope	Application	Market Value*
C-14	Medical-Labeled Compounds	\$11,000/g ¹¹
P-32	Leukemia Treatment	\$3,000,000,000/g ¹¹
Fe-55	Medical, Defense	quotation from IDO ¹²
Ni-63	Defense	
Zn-67	Rare Stable Isotope	
Se-75	Brain Imaging Analyses	quotation from IDO ¹²
Mo-99m	Tc-99m generator for organ imaging	\$59/g
Ag-108	Defense	
Sm-145	Undetermined	
Eu-152	Medical	quotation from IDO ¹²
Eu-155	Osteoporosis Detection	
Gd-153	Osteoporosis Detection	\$17,000,000/g
Re-186	Bone Cancer Pain Relief	
W-187	Undetermined	
* Pure Gold Value = \$16/g		

Of primary concern was the effect of the yttrium-hydride moderator pins on reaction rates and heating in adjacent fuel assemblies. From calculations on these design criteria, a final decision could be made on the specific location of the test assembly (row 6 or row 7) and the final location within the assembly and material loading of both the target and filter pins.

The purpose of the initial physics calculations was to determine return neutron impact on surrounding fuel pins, acceptable pin

FIGURE 4.1
PLAN VIEW OF MIP-II TEST ASSEMBLY



configuration, and reaction rates for a row 6 and row 7 location. Infinitely dilute reaction rates were determined for 24 different isotopes. Since there are a number of target locations spread around the test assembly, the spatial dependence, within the assembly, could be determined. It was also necessary to determine the heating rates in adjacent rows of fuel. Heating rates are always a major concern when introducing new materials into the system. Often, operational limits are placed upon the individual fuel pins. The introduction of the yttrium-hydride moderator into the system would drive these heating rates up as an increase in thermal neutrons incident upon the fuel, returning from the yttrium-hydride pins, would increase the fission rate within the fuel rods. Row 6 linear peaking factors generally vary from 6 to 10 kW/ft.

4.1.3 MCNP Calculational Precedent

The Multi-Isotope Production test assembly was irradiated for the purpose of investigating the potential for using the FFTF as a facility for the production of ^{238}Pu for space applications. A special test assembly was designed for this test in order to maximize the plutonium production and accommodate the targets and dosimeter sets. The test, particularly from an analytical standpoint, was a great success, as the calculational results that MCNP predicted were in very close agreement with actual experimental data.¹³ In large part because of the Monte Carlo calculated success associated with the MIP test, MCNP was the primary calculational tool used in the preliminary physics calculations for the MIP-II test.

4.2.0 MCNP CALCULATIONAL MODEL

4.2.1 Geometry and Materials

The same full core hexagonal matrix model with five axial zones was used that was briefly described and utilized in Chapter 3. The five axial zones (see Figure 3.2) represent the fuel region, upper and lower axial reflectors, and zones representing the lower sodium inlet nozzle and the gas plenum. A cross sectional view of the reactor matrix is shown in Figure 4.2, which also includes the location identifiers of each fuel assembly. The entire reactor model has a flat-to-flat distance of 181.14 cm. Each individual fuel assembly has a flat-to-flat distance of 12.067 cm. As was indicated earlier, calculations were necessary for both a row 6 test and a row 7 test. The row 7 location was preliminarily chosen to be in assembly 1712. For the row 6 calculation, the MIP-II assembly was moved to location 1610.

For each of the calculations a heterogeneous macrocell was utilized. This macrocell extended the full length of the core and included the MIP-II assembly and six assemblies surrounding it. The fuel and target assemblies within the macrocell were modeled in heterogeneous detail. All assemblies outside the macrocell were treated homogeneously. For the row 7 macrocell, there were only two fuel assemblies detailed (see Figure 4.3). These correspond to locations 1609 and 1610. Assemblies 1711, 1813, 1814, and 2701 are reflector assemblies and were treated homogeneously. For the row 6 macrocell, there were four fuel assemblies detailed (see Figure 4.4). These correspond to locations 1609, 1508, 2501, and 2601. Assemblies

FIGURE 4.2
PLAN VIEW OF FFTF REACTOR ASSEMBLY MATRIX

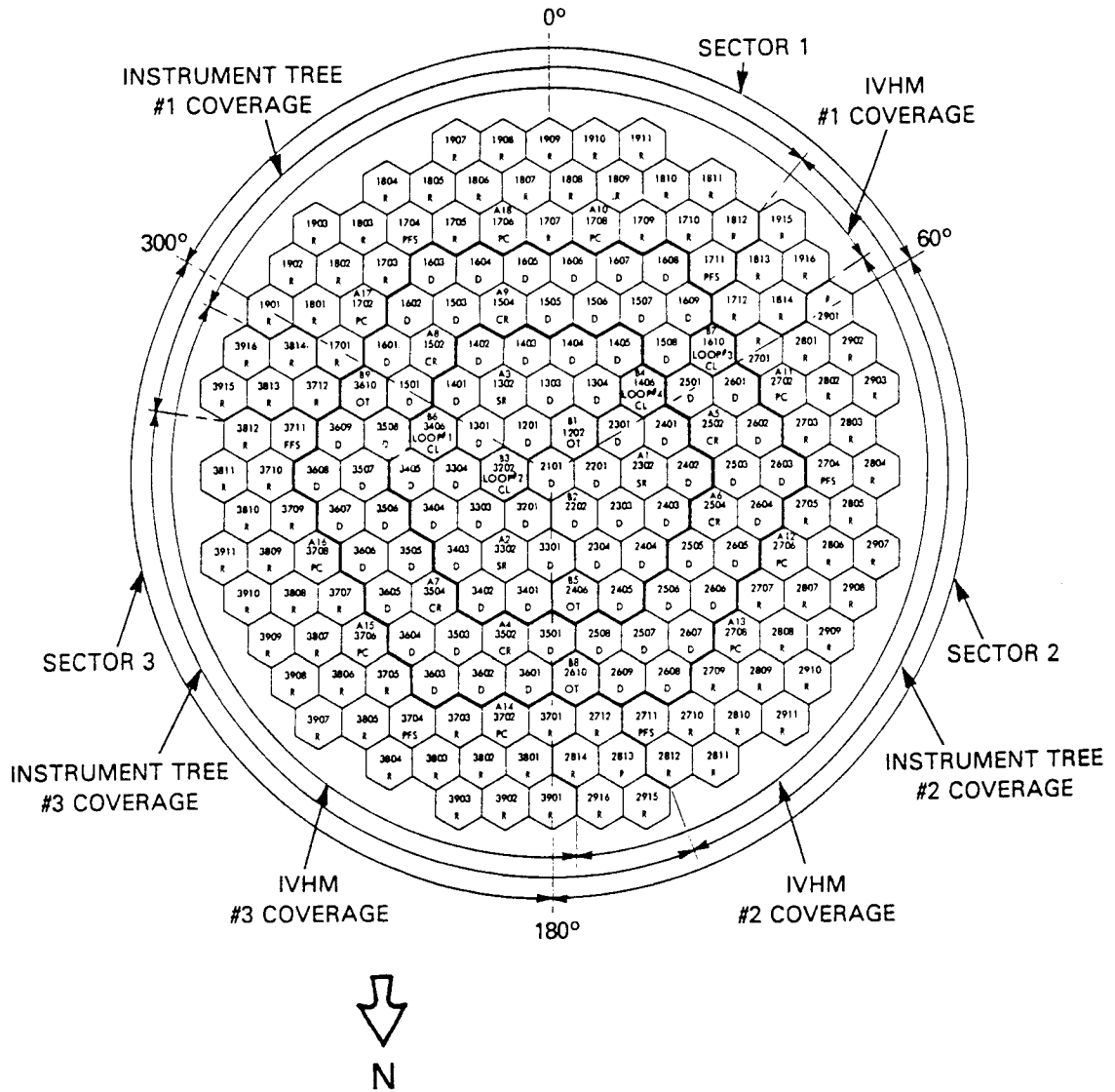


FIGURE 4.3
ADJACENT FUEL PIN LOCATIONS FOR TARGET ASSEMBLY IN 2701

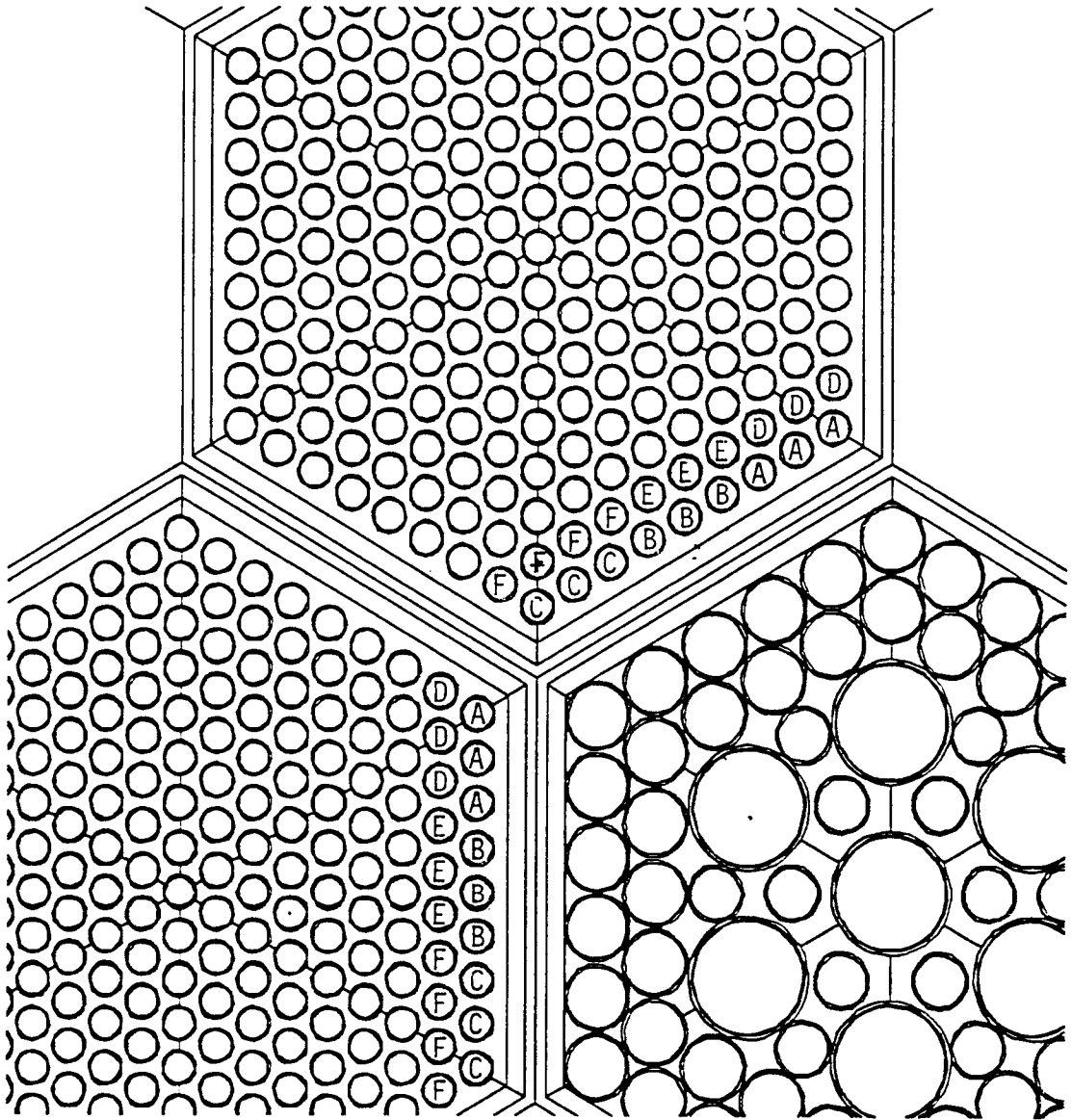
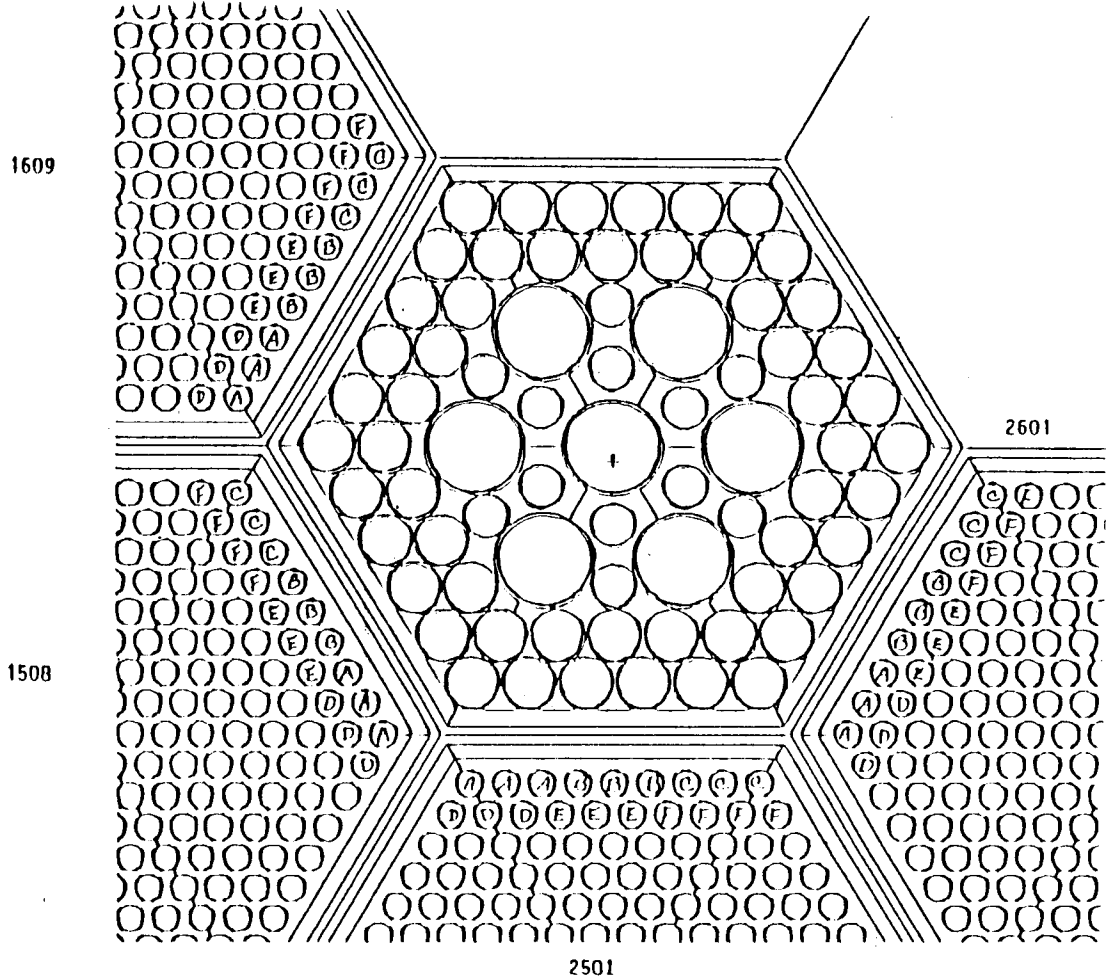


FIGURE 4.4
ADJACENT FUEL PIN LOCATIONS FOR TARGET ASSEMBLY IN 1610



1712 and 2701 are reflector assemblies and were likewise treated homogeneously.

The macrocell was used to give heterogeneous detail in the assemblies near the MIP-II assembly. The typical mean free path of a neutron inside a fast reactor is on the order of about 5 to 15 cm.¹⁴ Therefore, the impact upon the test assembly of neutrons born or scattered from assemblies two or three assemblies (24 to 36 cm) away would likely not be affected by either homogeneous or heterogeneous detail within those distant assemblies. Considerable computer savings are introduced by homogenizing the assemblies which are distant from the location of interest, while still allowing for accurate representation of the reactor core and its flux distribution. The number of neutrons which are sampled in the problem is not necessarily decreased by homogenizing the other assemblies, but each neutron will spend less time in a smeared assembly versus a fully detailed assembly. If there are fewer cells to encounter, there are fewer random numbers and distribution functions that need to be analyzed. It was also necessary to heterogeneously model each fuel assembly adjacent to the MIP-II assembly to calculate the heating rates in the individual fuel pins nearest the test assembly. Most important, the macrocell allowed for the sampling of the same exact source incident upon the region of interest. It is invaluable to maintain as much constancy as possible when performing design iterations. The neutron current incident upon the outer boundaries of the macrocell was written out to a file using the Surface Source Write option described in Section 2.3.2. The same source was subsequently used on each

iteration of the various design parameters within the test assembly. The iterations are described in detail in Section 4.3.0.

Within the test assembly itself are three distinct types of pins. The first are the yttrium-hydride moderator pins (the seven largest pins in Figure 4.1). These pins run the length of the active core and have a hydrogen-to-yttrium-atom ratio of 1.8. The moderator has an outer diameter of 1.92 cm surrounded by a stainless steel sleeve 0.0635 cm thick. The assembly also includes 12 target pins. The target pin has an outer diameter of 0.953 cm surrounded by a 0.051 cm thick stainless steel sleeve. For the MCNP calculations, the target was filled with stainless steel but reaction rates for a variety of materials were sampled as described in Section 2.3.3. There are 54 filter pins forming two rows surrounding the moderator and target pins. The filter pins have an outer diameter of 1.12 cm and are solid stainless steel. In later calculations, the stainless steel was replaced by an Nd_2O_3 pin with an outer diameter of 1.02 cm surrounded by a stainless steel sleeve of thickness 0.051 cm. This was done to "filter" the neutron flux to soften it before entering the target pins in order to maximize reaction rates and to minimize the impact of neutrons returning from the $\text{YH}_{1.8}$ moderator to the fuel pins.

In each fuel assembly, there are 217 fuel pins. Each fuel pin has an outer diameter of 0.51 cm with a stainless steel clad 0.038 cm thick. The fuel pins are 92.28 cm long. The fuel is a PuO_2 - UO_2 mix, with compositions varying depending on loading and burnup.

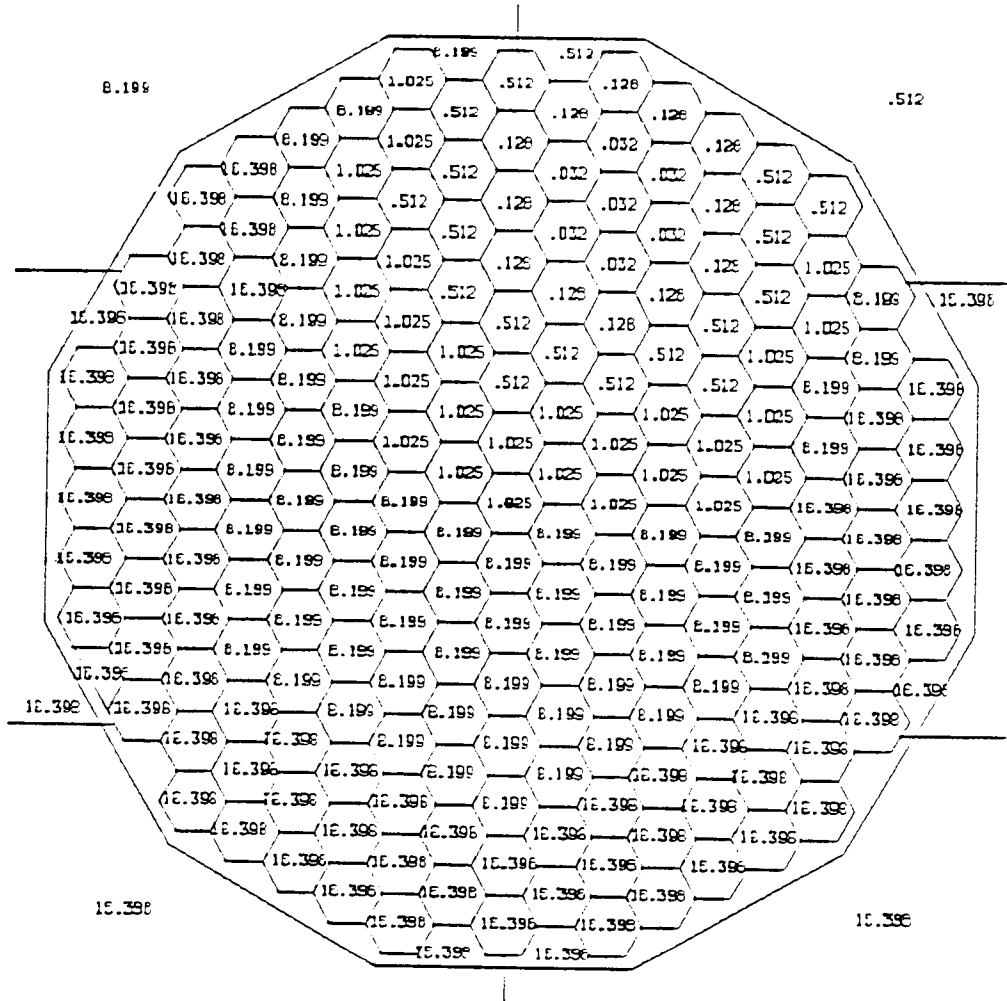
4.2.2 Biasing

Because the volume of the macrocell was so small compared to the full core model, it was essential that the Monte Carlo random walk be optimized to increase the number of random walks in the region of interest. As was discussed in Section 2.3.4, biasing techniques can be employed that will drive the majority of neutrons and/or photons into a specific area without sacrificing accurate physics representation.

Weight windows were employed to increase the frequency of random walks in the vicinity of the MIP-II test assembly and macrocell. Because some of the reaction rates of interest were photon driven, both neutron and photon biasing was employed. Figure 4.5 shows the upper limits of the photon weight windows for each assembly in the active core for the full core run. Because neutron effects were much more critical than those of photons, the upper limits of the neutron weight windows were exactly one-half the upper limits of the photon weight windows for each corresponding assembly in the model. The purpose of the biasing was to drive the neutrons toward the macrocell so as to spend the majority of the computing time performing calculations for neutron and photon behavior in that region.

Once the full core calculation was performed and the incident neutron current on the macrocell was recorded with the SSW card, a series of calculations were made involving only the macrocell. Because information was required from a variety of locations in the macrocell, very little optimization was used for these subsequent calculations. For both the row 6 and row 7 calculations, the cells

FIGURE 4.5
LOWER BOUNDS OF PHOTON WEIGHT WINDOWS IN FULL CORE MODEL



which composed the fuel assemblies and MIP-II test assembly were assigned an upper neutron weight window limit of 0.016. Reflector assembly cells, within the macrocell, were given an upper limit of either 0.032 or 0.064, depending on the distance from the MIP-II test assembly. All other cells in the core were given a value of -1.0 to kill any neutrons which entered them. In that way, all of the calculation time was spent in the macrocell, and the only neutron source was that which was read from the source file written with the SSW card. This helped ensure a better basis for comparing the various iterations.

4.3.0 CALCULATION SUMMARY

4.3.1 Summary of Runs

For each of the test location scenarios (row 6 and row 7), calculations were made for two different cases. The first case utilized stainless steel as the material in the filter pins. Upon examination of the results from this material configuration, it was noticed that the radial heat peaking factors were high. In an effort to reduce the radial peaking factors, the stainless steel inside the filter pins was replaced by Nd_2O_3 . The Nd_2O_3 had the two-fold benefit of both reducing the radial peaking factors by filtering out many of the thermal neutrons returning from the yttrium-hydride moderator before they could reach the fuel assemblies and also producing a useful isotope when the neodymium absorbed the thermal neutrons. The problem of the radial peaking factors is quantified and discussed in detail in Section 4.4.0.

A total of six MCNP calculations were made, three for the row 7 configuration and three for the row 6 configuration. These are described as follows:

1. The whole core was modeled with the test assembly in row 7 to generate the macrocell source. The problem ran for 180 CRAY minutes where 70,000 neutrons were run, generating a total of 48,123 neutrons recorded on the WSSA file to be run in subsequent row 7 problems.

2. The macrocell calculation with stainless steel filter pins was performed. The test assembly in row 7 was surrounded by two fuel pin assemblies and four reflector assemblies in a hexagonal matrix.

3. The row 7 macrocell with Nd_2O_3 filter pins was modeled.

4. The whole core calculation with the test assembly in row 6 to generate the macrocell source was performed. The problem was run for 270 minutes on the CRAY, where 103,495 neutrons were run, generating a total of 99,082 neutrons recorded on the WSSA file to be run in subsequent row 6 problems.

5. The macrocell with stainless steel filter pins was modeled. The test assembly in row 6 was surrounded by four fuel pin assemblies and two reflector assemblies in a hexagonal matrix.

6. The row 6 macrocell calculation with Nd_2O_3 filter pins was run.

All of these calculations produced a large volume of information which is tabulated and discussed in Section 4.4.0.

4.3.2 Computational Techniques

4.3.2.1 Heating Tallies

The fuel pin heating calculations were performed with the use of the MCNP F6 tally card. As was briefly discussed in Section 2.3.3,

heating calculations are performed by summing the products of the collision tallies with the randomly sampled energy deposition. Results of F6 tallies are output in units of MeV/g normalized by the number of source particles run in the problem. The units of the energy deposition tally can easily be converted with the use of the tally multiplier (FM) card. The tally multiplier card simply multiplies each of the tally results by a constant designated by the user.

The conversion from MeV/g/source neutron to kW/foot is straightforward. By utilizing the SD card for the F6 tally, all masses of the tally cells can be set to unity. This will cause tally results to be output essentially in units of MeV/source neutron. At 400 MW,

$$\begin{aligned} \text{FM} &= 1.602\text{E-}13 \text{ J/MeV} * 1 \text{ W-s/J} * 3.51\text{E}19 \text{ source n's/s} * \text{kW}/1000 \text{ W} \\ &= 5623.02 \text{ kW-source neutrons/MeV} \end{aligned}$$

With this multiplier, heating results will have the units of kW/cm³.

4.3.2.2 Reaction Rate Tallies

MCNP F4 tallies, with an FM reaction designator, are output with the units of reactions/cm³-source neutron-barn density, where the density is the atom density of the target in units of atoms/barn-cm. By using the proper multiplier on the FM card, the tally units can be converted to reactions/cm³-barn density-s. In this case, the proper multiplier is the number of source neutrons/s. For a fission source, this is represented by $v\Sigma_f\phi$ multiplied by the volume of the fuel.

This number is found by the following equation:

$$\begin{aligned} \# \text{ neutrons/s} &= v * \text{fissions/s} \\ &= v * \# \text{ MW} / (\# \text{ MeV/fission} * 1.6022\text{e-}19 \text{ MW/MeV-s}) \end{aligned}$$

For the UPuO_2 fuel at 400 MW, this is $3.51\text{E}19$ fission neutrons/ $\text{cm}^3\text{-s}$. With this number, the tally result will be a reaction rate in units of reactions/ $\text{cm}^3\text{-s-barn density}$. By multiplying this result by the atomic density of the target material, an infinitely dilute reaction rate, specific to the target, is calculated.

4.4.0 RESULTS

The primary purpose of the preliminary MIP-II calculations was two-fold. First, it was necessary to determine the impact of the neutrons returning from the yttrium-hydride moderator on adjacent fuel assemblies. If the increased thermal neutron current would drive fuel pin heating upward, radically increasing the linear power peaking and radial power peaking factors, then a change in the test assembly materials and/or configuration would be necessary. The row 7 calculations were performed first because in the event that the fuel pin heating factors were driven to high in the row 7 test assembly, row 6 calculations would not be necessary.

Second, a thorough investigation of potential candidates for radionuclide production was performed. Calculations were performed for a long list of reaction rates in every possible location within the test assembly. It is important to note that the reaction rates given, except for the neodymium reactions in the filter pins, assume an infinitely dilute target, with no flux perturbation due to self-shielding by the target nuclide. This factor will reduce the magnitude of the reaction rates. Also note that the power level at which these heating and reaction rates were calculated was 400 MW.

Although the FFTF is licensed at 400 MW, the operating power during the irradiation tests was planned to be 291 MW. With infinitely dilute reaction rates, the magnitude of the rate will decrease linearly with power level and can be calculated with a simple linear interpolation.

With the compilation of the above information, design modifications could be made to the test assembly and decisions could be made on test assembly location and materials which would maximize efficiency and production of the radionuclides.

4.4.1 Row 7 Heating Rates

Table 4.2 shows the heating rates for individual pins in the first two rows adjacent to the row 7 test assembly. The row 7 test assembly is located in assembly 1712 (see Figure 4.2). The two adjacent fuel assemblies are in locations 1609 and 1610. Figure 4.3 shows the locations of the pins specified in Tables 4.2 to 4.4. Each position specified in the table is comprised of three to four pins, averaged in the interest of better statistics for the tally averages. The average pin heating (kW) is then divided by the length of the rod (ft). The peak heating reported in the third column of Table 4.2 shows the hot spot in the pin as a function of the axial temperature distribution and can be estimated conservatively by multiplying the average heating rate by a factor of 1.22.

The numbers from the third column of Table 4.2 show that the peak heating in the row of pins adjacent to the test assembly in assemblies

TABLE 4.2					
Peak Heating in Adjacent Fuel Pins for Fuel Assemblies 1609 and 1610					
Stainless Steel Filter Pins					
(Test Assembly in Row 7, Position 1712)					
(All calculations at 400 MW unless specified otherwise)					
ASSEMBLY 1609					
POS	UNCERT.	PIN HEAT (kW/ft)	PEAK HEAT (kW/ft)	PEAK HEAT (291 MW)	RAD. PEAK FACTOR
A	0.043	11.305	13.792	10.034	1.503
B	0.039	10.712	13.069	9.058	1.424
C	0.039	10.442	12.739	9.268	1.388
D	0.040	8.296	10.121	7.363	1.103
E	0.029	8.486	10.353	7.532	1.128
F	0.027	8.684	10.594	7.707	1.154
ASSEMBLY 1610					
POS	UNCERT	PIN HEAT (kW/ft)	PEAK HEAT (kW/ft)	PEAK HEAT (291 MW)	RAD. PEAK FACTOR
A	0.036	10.014	12.218	8.889	1.302
B	0.038	10.843	13.228	9.623	1.409
C	0.041	10.080	12.219	8.889	1.310
D	0.027	8.377	10.219	7.434	1.089
E	0.028	8.338	10.173	7.401	1.090
F	0.027	8.318	10.148	7.383	1.081
Each position is the average of the three (or four in the case of position F) pins, including the clad, which are designated by the position title.					

1609 and 1610 is too high. The linear heating factor reaches a maximum of 13.79 kW/ft in the A-group pins in assembly 1609. These numbers represent axial peak heating rates when the reactor is

TABLE 4.3					
Peak Heating in Adjacent Fuel Pins for Fuel Assemblies 1609 and 1610					
Nd ₂ O ₃ Filter Pins					
(Test Assembly in Row 7, Position 1712)					
(All calculations at 400 MW unless specified otherwise)					
ASSEMBLY 1609					
POS	UNCERT.	PIN HEAT (kW/ft)	PEAK HEAT (kW/ft)	PEAK HEAT (291 MW)	RAD. PEAK FACTOR
A	0.041	9.526	11.622	8.455	1.293
B	0.035	9.907	11.098	8.074	1.235
C	0.033	8.868	10.819	7.870	1.204
D	0.028	7.806	9.523	6.928	1.059
E	0.027	7.674	9.362	6.811	1.042
F	0.023	7.905	9.644	7.016	1.073
ASSEMBLY 1610					
POS	UNCERT	PIN HEAT (kW/ft)	PEAK HEAT (kW/ft)	PEAK HEAT (291 MW)	RAD. PEAK FACTOR
A	0.032	8.992	10.970	7.981	1.189
B	0.034	8.994	10.973	7.938	1.189
C	0.035	9.093	11.093	8.070	1.202
D	0.025	7.966	9.719	7.070	1.053
E	0.024	7.798	9.514	6.921	1.031
F	0.025	7.765	9.423	6.892	1.027
Each position is the average of the three (or four in the case of position F) pins, including the clad, which are designated by the position title.					

operating at 400 MW. The test was scheduled to run with the reactor at a power level of 291 MW. The fourth column of Table 4.2 shows the axial peak heating for an operating power level of 291 MW. At this

TABLE 4.4				
Effect of Nd_2O_3 Filter Pins on Fuel Pin Heating				
Test Assembly in Row 7 (Position 1712)				
ASSEMBLY 1609				
POS	PIN HEATING WITH SS	PIN HEATING WITH Nd_2O_3	Nd_2O_3 /SS RATIO	RAD. PEAK RATIO DIFF.
A	10.034	8.455	0.843	0.860
B	9.058	8.074	0.891	0.867
C	9.268	7.870	0.849	0.867
D	7.363	6.928	0.941	0.960
E	7.532	6.811	0.904	0.924
F	7.707	7.016	0.910	0.930
ASSEMBLY 1610				
POS	PIN HEATING WITH SS	PIN HEATING WITH Nd_2O_3	PEAK HEAT RATIO	RAD. PEAK RATIO DIFF.
A	8.889	7.981	0.898	0.913
B	9.623	7.938	0.825	0.844
C	8.947	8.070	0.902	0.918
D	7.434	7.070	0.951	0.967
E	7.401	6.921	0.935	0.946
F	7.383	6.892	0.933	0.950
Each position is the average of the three (or four in the case of position F) pins, including the clad, which are designated by the position title.				

power level, the axial peak heating is not radically different from normal operating conditions. The radial peaking factor is a measure of the temperature distribution throughout the entire fuel assembly. It is calculated by dividing the average heating rate in the specified pin group by the average heating rate over the entire assembly. The

radial peaking factor reaches a maximum of 1.503 in the A-group pins of assembly 1609. Although there are generally no operating limits relating to radial peaking factors, common peaking factors for irradiation tests are on the order of 1.2. The yttrium-hydride moderator induces radial hot spots significantly higher than this.

In an effort to reduce the radial peaking factor to numbers consistent with previous tests, the stainless steel filter pins were replaced with Nd_2O_3 . The thermal neutron cross section of the neodymium is not high but will absorb more of the neutrons returning from the moderator than the stainless steel, thus reducing the hot spots in the fuel assembly nearest the test assembly.

Table 4.3 shows results for the same calculations previously discussed when the stainless steel filter pins are replaced with Nd_2O_3 . With the Nd_2O_3 filter pins, the axial peak heating factors are all below 8.5 kW/ft at a reactor operating level of 291 MW. The radial peaking factors have a maximum of 1.29 in the A-group pins of assembly 1609 which is much more consistent with the radial peaking factors normally associated with irradiation tests.

Table 4.4 provides a direct comparison of the two heating factors between stainless steel filter pins and the Nd_2O_3 filter pins. It can be seen that the Nd_2O_3 filter pins reduce the axial peaking factor in the A-group pins of assembly 1609 by almost 16 percent. The radial peaking factor in the hottest fuel pins is reduced 14 percent with the Nd_2O_3 filter pins.

4.4.2 Row 7 Reaction Rates

The infinitely dilute reaction rates that were calculated with the stainless steel filter pins are listed in Table 4.5. The location for each target is shown on Figure 4.1. In many cases, there are two target locations that were averaged because of symmetry to improve statistics. The reaction rates reported in Tables 4.5 through 4.9 are all infinitely dilute and assume a target material atom density of 1.0 atoms per barn-cm. Because the reaction rates are infinitely dilute, they will not be perturbed by varying the target density. Corrections to the reaction rates can be made simply with a multiplier based on relative target atom density. It is important to note that these numbers were calculated for a reactor power level of 400 MW. For an operating power of 291 MW, the reaction rates would be decreased 27.25 percent.

Unless otherwise indicated, the majority of the reaction rates have relative uncertainties less than 5.0 percent. Table 4.6 lists the reaction rates in Table 4.5 when the stainless steel filter pins are replaced by the Nd_2O_3 filter pins. The effect of the Nd_2O_3 on the reaction rates is given in Table 4.7. For the majority of the reactions, the Nd_2O_3 shields the targets from the thermal neutrons, driving the reaction rates down. The more thermal the reaction, the greater the decrease in rate magnitude. The hard spectrum (n,p) reaction rates actually increased with the Nd_2O_3 filter pins.

TABLE 4.5
Projected Isotopic Reaction Rates
Nd₂O₃ Filter Pins
Test Assembly in Row 7 (Position 1712)

Reaction	A	B	C	D	E	F	Total
Zn-67 (n,p)	2.728E11*	1.437E11*	1.283E11*	8.719E10**	8.818E10**	3.212E10**	1.241E11
Re-185 (n,γ)	1.090E17*	1.444E17*	1.507E17*	1.402E17*	1.487E17*	1.395E17*	1.384E17
W-186 (n,γ)	3.678E16*	5.443E16*	3.965E16*	3.754E16*	6.070E16*	3.261E16*	4.362E16
W-187 (n,γ)	1.586E17	1.607E17	1.834E17	1.594E17	1.851E17	1.702E17	1.695E17
W-188 (n,γ)	2.968E16	3.784E16	3.402E16	3.181E16	4.087E16	2.998E16	2.903E16
Mo-98 (n,γ)	7.440E14**	7.338E14*	7.091E14**	1.110E15**	6.962E14*	5.023E14*	7.483E14*
Mo-99 (n,γ)	2.551E15	2.698E15	2.680E15	2.517E15	2.531E15	2.382E15	2.580E15
S-32 (n,p)	1.282E13	8.376E12	6.797E12	5.943E12	5.103E12	3.148E12	7.032E12
S-33 (n,p)	1.777E13	1.334E13	1.141E13	1.502E13	9.577E12	7.248E12	1.164E13
Gd-152 (n,γ)	3.773E16*	3.564E16*	4.328E16*	3.668E16*	3.288E16	3.804E16*	3.737E16
N-14 (n,p)	2.026E14	2.436E14	2.487E14	1.882E14	2.594E14	2.031E14	2.245E14
Ni-62 (n,γ)	1.474E15	1.828E15	1.893E15	1.399E15	1.974E15	1.551E15	1.666E15
Fe-54 (n,γ)	6.204E14	7.332E14	7.718E14	6.001E14	7.885E14	6.482E14	6.837E14
S-34 (n,γ)	5.288E13	6.165E13	6.351E13	5.155E13	6.388E13	5.429E13	5.795E13
Ag-107 (n,γ)	1.156E16	1.544E16	1.532E16	1.058E16	1.523E16	1.099E16	1.319E16
Ag-108 (n,γ)	1.476E16	1.855E16	1.756E16	1.416E16	1.737E16	1.485E16	1.587E16
Eu-151 (n,γ)	9.041E17	1.102E18	1.211E18	8.421E17	1.219E18	9.637E17	1.041E18
Eu-152 (n,γ)	2.903E17	3.713E17	3.784E17	3.014E17	3.791E17	3.115E17	3.387E17
Eu-154 (n,γ)	1.980E17	2.578E17	2.535E17	2.061E17	2.668E17	2.155E16	2.330E17
Se-74 (n,γ)	4.625E16*	2.308E16*	4.795E16*	4.352E16*	5.552E16*	5.089E16*	4.603E16
Sm-144 (n,γ)	3.461E15	3.817E15	3.897E15	3.306E15	3.456E15	3.302E15	3.507E15
Sm-149 (n,γ)	6.209E16	8.231E16	8.802E16	6.036E16	9.339E16	6.752E16	7.528E16
U-235 (n,fp)	6.111E16	7.344E16	7.528E16	5.898E16	7.829E16	6.245E16	6.793E16
Tc-99 (n,γ)	2.303E16*	2.648E16*	2.607E16*	2.322E16*	2.682E16*	3.558E16*	2.720E16

All values have units of reactions/cm³-s of material

* = uncertainties between 10% and 20%

** = uncertainties over 20%

The total column represents an average rate over all target areas.

TABLE 4.6
Projected Isotopic Reaction Rates
Stainless Steel Filter Pins
Test Assembly in Row 7 (Position 1712)

Reaction	A	B	C	D	E	F	Total
Zn-67 (n,p)	2.073E11*	1.601E11*	1.591E11*	1.810E11*	1.243E11*	70192E10**	1.473E11
Ra-185 (n, γ)	7.147E16*	1.039E17*	1.048E17*	7.287E16	1.180E17*	8.166E17*	9.340E16
W-186 (n, γ)	2.480E16*	2.584E16*	3.976E16*	3.296E16*	4.891E16*	5.078E16*	3.717E16
W-187 (n, γ)	1.330E17	1.594E17	1.622E17	1.474E17	1.815E17	1.469E17	1.517E17
W-188 (n, γ)	2.693E16	2.915E16	3.553E16	3.053E16	3.552E16	3.152E16	2.703E16
Mo-98 (n, γ)	5.119E14**	1.075E15*	7.118E14*	9.358E14**	4.438E14*	2.809E14*	6.800E14*
Mo-99 (n, γ)	2.278E15	2.650E15	2.582E15	2.312E15	2.345E15	2.200E15	2.394E15
S-32 (n,p)	1.104E13	9.100E12	7.484E12	7.475E12	5.948E12	4.688E12	7.583E12
S-33 (n,p)	1.573E13	1.385E13	1.120E13	1.174E13	9.941E12	8.447E12	1.178E13
Gd-152 (n, γ)	2.241E16*	3.585E16*	3.388E16*	3.158E16*	3.490E16*	3.390E16*	3.208E16
N-14 (n,p)	1.310E14	1.785E14	1.790E14	1.407E14	1.783E14	1.293E14	1.581E14
Ni-62 (n, γ)	9.078E15	1.323E15	1.339E15	1.026E15	1.341E15	9.587E14	1.148E15
Fe-54 (n, γ)	4.188E14	5.485E14	5.702E14	4.566E14	5.609E14	4.363E14	4.982E14
S-34 (n, γ)	3.849E13	5.052E13	5.118E13	4.239E13	4.952E13	4.058E13	4.544E13
Ag-107 (n, γ)	1.098E16	1.256E16	1.242E16	1.258E16	1.142E16	9.908E15	1.165E16
Ag-108 (n, γ)	1.152E16	1.443E16	1.452E16	1.279E16	1.417E16	1.213E16	1.328E16
Eu-151 (n, γ)	5.654E17	7.698E17	8.821E16	8.727E17	8.055E17	5.848E17	7.134E17
Eu-152 (n, γ)	2.120E17	2.805E17	2.775E17	2.252E17	2.935E17	2.352E17	2.540E17
Eu-154 (n, γ)	1.417E17	1.826E17	1.981E17	1.519E17	1.992E17*	1.576E16	1.732E17
Se-74 (n, γ)	4.758E16*	4.871E16*	5.406E16*	4.494E16*	4.986E16*	3.851E16*	4.728E16
Sm-144 (n, γ)	2.964E15	3.584E15	3.449E15	3.121E15	3.286E15	2.831E15	3.222E15
Sm-149 (n, γ)	3.416E16	5.682E16	5.734E16	4.039E16	5.819E16	3.583E16	4.712E16
U-235 (n,f)	3.876E16	5.519E16	5.508E16	4.324E16	5.571E16	4.051E16	3.966E16
Tc-99 (n, γ)	2.569E16*	2.251E16*	2.519E16*	2.051E16*	2.051E16*	3.143E16*	2.298E16

All values have units of reactions/cm³-s of material

* = uncertainties between 10% and 20%

** = uncertainties over 20%

The total column represents an average rate over all target areas.

REACTION	WITH SS	WITH Nd ₂ O ₃	Nd ₂ O ₃ /SS
N-14 (n,p)	2.245E14	1.561E14	0.695
S-32 (n,p)	7.032E12	7.583E12	1.078
S-33 (n,p)	1.164E13	1.178E13	1.012
S-34 (n,γ)	5.795E13	4.544E13	0.784
Fe-54 (n,γ)	6.937E14	4.982E14	0.718
Ni-62 (n,γ)	1.686E15	1.149E15	0.681
Se-74 (n,γ)	4.603E16	4.728E16	1.027
Mo-98 (n,γ)	7.493E14	6.600E14	0.881
Mo-99 (n,γ)	2.560E15	2.394E15	0.935
Tc-99 (n,γ)	2.720E16	2.289E16	0.842
Ag-107 (n,γ)	1.319E16	1.165E16	0.883
Ag-108 (n,γ)	1.587E16	1.326E16	0.836
Sm-144 (n,γ)	3.507E15	3.222E15	0.919
Sm-149 (n,γ)	7.528E18	4.712E18	0.626
Eu-151 (n,γ)	1.041E18	7.134E17	0.710
Eu-152 (n,γ)	3.387E17	2.540E17	0.750
Eu-154 (n,γ)	2.330E17	1.732E17	0.743
Gd-152 (n,γ)	3.737E16	3.208E16	0.858
Re-185 (n,γ)	1.384E17	9.340E16	0.675
W-186 (n,γ)	4.362E16	3.717E16	0.852
W-187 (n,γ)	1.695E17	1.517E17	0.895
W-188 (n,γ)	2.903E16	2.703E16	0.931
U-235 (n,fp)	3.793E16	3.966E16	0.584

TABLE 4.8					
Nd ₂ O ₃ Filter Pins Hard Spectrum Reaction Rates					
Test Assembly in Row 7 (Position 1712)					
POS	Zn-67 (n,p)	S-32 (n,p)	S-33 (n,p)	N-14 (n,p)	U-235 (n,fp)
G	3.376E11* (0.1070)	1.945E13 (0.0452)	2.453E13 (0.0353)	5.902E13 (0.0251)	1.428E16 (0.0356)
H	3.186E11 (0.1381)	1.631E13 (0.0516)	2.129E13 (0.0390)	7.559E13 (0.0276)	2.021E13 (0.0315)
I	2.972E11 (0.1030)	1.399E13 (0.0402)	1.841E13 (0.0290)	5.466E13 (0.0203)	1.467E16 (0.0246)
J	2.439E11 (0.0991)	1.187E13 (0.0421)	1.626E13 (0.0302)	7.438E13 (0.0213)	2.212E16 (0.0246)
K	1.001E11 (0.1576)	5.020E12 (0.0633)	8.484E12 (0.0370)	4.699E13 (0.0230)	1.680E16 (0.0263)
L	1.168E11 (0.1352)	5.469E12 (0.0579)	9.105E12 (0.0350)	6.896E13 (0.0228)	2.299E16 (0.0237)
M	5.576E10 (0.1982)	3.270E12 (0.0909)	6.361E12 (0.0470)	4.588E13 (0.0331)	1.717E16 (0.0351)
N	6.469E10 (0.2000)	3.722E12 (0.0884)	7.016E12 (0.0470)	6.493E13 (0.0306)	2.236E16 (0.0367)

All reactions rates are infinitely dilute and are averaged over the length of the core (3 ft). The reaction units are reactions/cm³.

* Uncertainty estimates are included below in parenthesis. Read as 3.376e11 ± 10.70%

With the Nd₂O₃ filter pins, the epithermal and fast neutrons from the fissioning in the fuel pins are essentially unperturbed. To investigate the potential for utilizing this portion of the neutron energy spectrum, hard spectrum reaction rates were calculated for various positions within the test assembly filter pin locations. These reaction rates are listed in Table 4.8 with the positions corresponding to those in Figure 4.1.

4.4.3 Row 6 Heating Rates

Heating and reaction rate calculations were made for the test assembly when in row 6. Table 4.9 shows the heating rates for individual fuel pins in the first two rows of the four fuel assemblies adjacent to the row 6 test assembly. The row 6 test assembly is located in assembly 1610 of Figure 4.2. The four adjacent fuel assemblies are in assembly locations 1609, 1508, 2501, and 2601 of the same figure. Figure 4.4 shows the locations of all the pins addressed in Tables 4.9 to 4.13. In Tables 4.9 to 4.11, the specified position is comprised of three to four pins, averaged in the interest of better statistics. Determination of the heating rates and the axial and radial peaking factors were likewise calculated the same as was described previously.

The peak heating numbers show that when the reactor is operating at 400 MW, the peak heating rates are too high in almost every pin location. This reaches a maximum in assembly 1508 where the peak heating rate exceeds 18.8 kW/ft in the B-location. At the normal operating level of 291 MW, the peak heating is reduced, but still is too high in assembly 1508, where the B-location pins have a peak heating rate calculated to be 13.7 kW/ft. It was reported earlier that peaking factors, based on previous tests, should be near 1.2. The radial peaking factors throughout the specified pin locations range from 1.1 to 1.7. It is interesting to note that the radial peaking factors are lower in the fuel assemblies with the higher linear peak heating rates. The highest linear peaking factors were found in the pin locations which were nearest the reflector

TABLE 4.9					
Peak Heating in Fuel Pins for Assemblies 1609, 2501, 1508, and 2601					
Stainless Steel Filter Pins					
(All calculations at 400 MW unless specified otherwise.)					
Assembly 1609					
POS	UNCERT.	PIN HEAT (KW/FT)	PEAK HEAT (KW/FT)	PEAK HEAT (291 MW)	RAD PEAK FACTOR
A	0.043	11.559	14.102	10.259	1.1566
B	0.039	11.757	14.344	10.435	1.583
C	0.039	11.340	13.835	10.065	1.527
D	0.040	9.072	11.068	8.052	1.222
E	0.029	9.148	11.161	8.119	1.232
F	0.027	9.244	11.278	8.205	1.245
Assembly 2501					
POS	UNCERT.	PIN HEAT. (KW/FT)	PEAK HEAT. (KW/FT)	PEAK HEAT. (291 MW)	RAD PEAK FACTOR
A	0.036	12.905	15.744	11.454	1.407
B	0.038	13.498	16.468	11.980	1.472
C	0.041	13.100	15.982	11.627	1.428
D	0.027	10.236	12.488	9.085	1.116
E	0.028	10.758	13.125	9.548	1.173
F	0.027	10.557	12.880	9.370	1.151
Assembly 1508					
POS	UNCERT.	PIN HEAT. (KW/FT)	PEAK HEAT. (KW/FT)	PEAK HEAT. (291 MW)	RAD PEAK FACTOR
A	0.044	14.470	17.653	12.843	1.347
B	0.054	15.462	18.864	13.723	1.439
C	0.053	14.568	17.773	12.930	1.356
D	0.037	12.306	15.013	10.922	1.145
E	0.033	13.166	16.063	11.685	1.225
F	0.040	12.253	14.949	10.875	1.140
Assembly 2601					
POS	UNCERT.	PIN HEAT. (KW/FT)	PEAK HEAT. (KW/FT)	PEAK HEAT. (291 MW)	RAD PEAK FACTOR
A	0.073	11.859	14.468	10.525	1.703
B	0.079	11.514	14.047	10.219	1.653
C	0.076	11.416	13.928	10.132	1.639
D	0.056	9.347	11.403	8.296	1.342
E	0.054	9.137	11.147	8.110	1.312
F	0.059	8.754	10.680	7.770	1.257

assemblies. The radial peaking factors from the row 7 test assembly calculations reached a maximum of 1.5, significantly lower by comparison. This is to be expected because the nearer to the center of the core the test assembly is, the more impactful the yttrium-hydride moderator is going to be on the reactor flux shape and distribution.

Heating rate calculations were then performed with Nd_2O_3 filter pins replacing the stainless steel filter pins. Table 4.10 lists the results of these calculations. The peak heating of the fuel pins was reduced significantly, but the A- and B-location pins of assembly 1508 were still too high to safely irradiate the test assembly in the reactor. The radial peaking factors are still high with a maximum of 1.60 in the A-location pins of assembly 2601.

Because the heating rates in many of the pin locations were judged to be too high, more information was needed to address the problem. Heating tallies were made for each individual fuel pin in the two rows nearest the test assembly of each fuel assembly specified earlier. The results of these calculations are presented in Tables 4.11 and 4.12. Table 4.11 details the heating calculations summarized in Table 4.9, while Table 4.12 details the calculations summarized in Table 4.10.

The effect of the Nd_2O_3 is summarized in Table 4.13. It can be seen that the Nd_2O_3 filter pins caused a 5 to 20 percent reduction in peak heating rates. The effect upon the radial peaking factors was much the same. It is interesting to note that the impact of the Nd_2O_3 is greater in the row 7 test assembly than in the row 6 test assembly,

TABLE 4.10					
Peak Heating in Fuel Pins for Assemblies 1609, 2501, 1508, and 2601					
Nd ₂ O ₃ Filter Pins					
(All calculations at 400 MW unless specified otherwise.)					
Assembly 1609					
POS	UNCERT.	PIN HEAT (KW/FT)	PEAK HEAT (KW/FT)	PEAK HEAT (291 MW)	RAD PEAK FACTOR
A	0.058	10.478	12.783	9.300	1.395
B	0.067	10.373	12.655	9.207	1.381
C	0.060	10.951	13.360	9.720	1.458
D	0.040	9.048	11.039	8.031	1.204
E	0.039	8.973	10.947	7.964	1.194
F	0.044	8.755	10.681	7.771	1.165
Assembly 2501					
POS	UNCERT.	PIN HEAT. (KW/FT)	PEAK HEAT. (KW/FT)	PEAK HEAT. (291 MW)	RAD PEAK FACTOR
A	0.055	11.393	13.899	10.112	1.270
B	0.061	10.995	13.414	9.759	1.226
C	0.062	10.576	12.903	9.387	1.179
D	0.039	9.584	11.692	8.506	1.068
E	0.042	9.620	11.736	8.538	1.072
F	0.045	9.480	11.566	8.414	1.057
Assembly 1508					
POS	UNCERT.	PIN HEAT. (KW/FT)	PEAK HEAT. (KW/FT)	PEAK HEAT. (291 MW)	RAD PEAK FACTOR
A	0.044	13.906	16.965	12.342	1.280
B	0.054	14.102	17.204	12.516	1.298
C	0.053	13.654	16.658	12.119	1.257
D	0.037	12.337	15.051	10.950	1.135
E	0.033	12.542	15.279	11.116	1.153
F	0.040	12.164	14.840	10.796	1.119
Assembly 2601					
POS	UNCERT.	PIN HEAT. (KW/FT)	PEAK HEAT. (KW/FT)	PEAK HEAT. (291 MW)	RAD PEAK FACTOR
A	0.073	9.899	12.077	8.786	1.606
B	0.079	9.716	11.854	8.623	1.577
C	0.076	9.161	11.176	8.131	1.487
D	0.056	8.139	9.930	7.224	1.321
E	0.054	8.414	10.265	7.468	1.365
F	0.059	8.071	9.847	7.163	1.310

TABLE 4.11					
Example of Peak Heating in Individual Fuel Pins in an Adjacent Fuel Assembly for a Row 6 Test Assembly Stainless Steel Filter Pins (All calculations at 400 MW unless specified otherwise.)					
ASSEMBLY 1508					
POS	UNCERT	PIN HEAT. (KW/FT)	PEAK HEAT. (KW/FT)	PEAK HEAT. (291 MW)	PIN/ASSEM. RATIO
1	0.044	13.290	16.214	11.796	1.237
2	0.052	14.151	17.264	12.560	1.317
3	0.062	15.968	19.481	14.172	1.486
4	0.054	15.192	18.534	13.483	1.414
5	0.072	16.169	19.726	14.351	1.505
6	0.054	15.025	18.331	13.336	1.398
7	0.053	14.327	17.479	12.716	1.333
8	0.065	16.063	19.597	14.257	1.495
9	0.056	13.313	16.242	11.816	1.239
10	0.037	12.319	15.029	10.934	1.147
11	0.041	12.262	14.960	10.883	1.141
12	0.041	12.338	15.052	10.950	1.148
13	0.033	12.359	15.078	10.959	1.150
14	0.044	14.019	17.101	12.441	1.305
15	0.054	13.123	16.010	11.647	1.221
16	0.052	13.972	17.050	12.404	1.301
17	0.040	11.846	14.452	10.514	1.103
18	0.043	11.982	14.618	10.635	1.115
19	0.044	11.208	13.674	9.948	1.043

where the neutron flux is so much stronger that the same number of filter pins are unable to compensate.

4.4.4 Row 6 Reaction Rates

The infinitely dilute reaction rates that were calculated with the stainless steel filter pins are listed in Table 4.14. The location for each target specified in the table is shown on Figure 4.1. As was discussed in the Section 4.2 for the row 7 reaction rates, in many cases there are two target locations that are averaged, if symmetry allows, in the interest of better statistics. The reaction rates

TABLE 4.12					
Example of Peak Heating in Individual Fuel Pins in an Adjacent Fuel Assembly for a Row 6 Test Assembly Nd ₂ O ₃ Filter Pins (All calculations at 400 MW unless specified otherwise.)					
ASSEMBLY 1508					
POS	UNCERT	PIN HEAT. (KW/FT)	PEAK HEAT. (KW/FT)	PEAK HEAT. (291 MW)	PIN/ASSEM. RATIO
1	0.044	14.105	17.208	12.519	1.298
2	0.052	13.282	16.204	11.788	1.222
3	0.062	14.331	17.484	12.720	1.319
4	0.054	14.184	17.304	12.589	1.305
5	0.072	13.941	17.008	12.373	1.283
6	0.054	14.182	17.302	12.587	1.305
7	0.053	14.034	17.121	12.456	1.292
8	0.065	14.178	17.297	12.584	1.305
9	0.056	12.751	15.556	11.317	1.174
10	0.037	12.401	15.129	11.006	1.141
11	0.041	11.750	14.335	10.429	1.081
12	0.041	12.861	15.690	11.414	1.184
13	0.033	12.559	15.332	11.147	1.156
14	0.044	12.509	15.261	11.102	1.151
15	0.054	12.558	15.321	11.146	1.156
16	0.052	12.252	14.947	10.874	1.128
17	0.040	12.550	15.311	11.139	1.155
18	0.043	12.118	14.784	10.755	1.115
19	0.044	11.737	14.319	10.417	1.080

listed are at 400 MW and cover the same nuclides that were analyzed in the row 7 test. The statistics for these reaction rate tallies are all very good with almost every uncertainty less than 5.0 percent. Only in the case of the Mo-98 (n, γ) reaction are the numbers unreliable with standard deviations over 20 percent. They are reported in the table for the purpose of broad comparison.

Table 4.15 lists the same reaction rates that are given in Table 4.14 when the stainless steel filter pins are replaced by the Nd₂O₃ pins. The effect of the Nd₂O₃ on the reaction rates is given in Table 4.16. As in the row 7 calculations, the effect of the Nd₂O₃ is to

TABLE 4.13						
Effect of Nd_2O_3 Filter Pins on Heating in a Row 6 Test Assembly (All Calculations at 291 MW.)						
Assembly 1609						
POS	LIN. PEAK SS	LIN. PEAK Nd_2O_3	Nd_2O_3 /SS RATIO	RAD. PEAK SS	RAD. PEAK Nd_2O_3	Nd_2O_3 /SS RATIO
A	9.664	9.300	0.962	1.556	1.395	0.90
B	10.435	9.207	0.882	1.583	1.381	0.87
C	10.065	9.137	0.908	1.527	1.371	0.90
D	8.052	8.037	0.998	1.224	1.205	0.98
E	7.935	7.964	1.001	1.232	1.195	0.97
F	8.205	7.771	0.947	1.245	1.166	0.94
Assembly 2501						
POS	LIN. PEAK SS	LIN. PEAK Nd_2O_3	Nd_2O_3 /SS RATIO	RAD. PEAK SS	RAD. PEAK Nd_2O_3	Nd_2O_3 /SS RATIO
A	11.447	10.112	0.883	1.406	1.270	0.90
B	11.981	9.758	0.814	1.472	1.225	0.83
C	11.627	9.387	0.807	1.128	1.179	0.83
D	9.085	8.506	0.936	1.116	1.068	0.96
E	9.548	8.538	0.894	1.173	1.072	0.92
F	9.370	8.414	0.898	1.151	1.057	0.92
Assembly 1508						
POS	LIN. PEAK SS	LIN. PEAK Nd_2O_3	Nd_2O_3 /SS RATIO	RAD. PEAK SS	RAD. PEAK Nd_2O_3	Nd_2O_3 /SS RATIO
A	12.843	12.342	0.961	1.347	1.280	0.95
B	13.723	12.516	0.912	1.439	1.298	0.90
C	12.930	12.119	0.937	1.356	1.257	0.93
D	10.922	10.950	1.003	1.145	1.135	0.99
E	11.686	11.132	0.953	1.225	1.154	0.94
F	10.875	10.796	0.953	1.141	1.120	0.98
Assembly 2601						
POS	LIN. PEAK SS	LIN. PEAK Nd_2O_3	Nd_2O_3 /SS RATIO	RAD. PEAK SS	RAD. PEAK Nd_2O_3	Nd_2O_3 /SS RATIO
A	10.525	8.576	0.815	1.703	1.479	0.87
B	10.219	8.623	0.844	1.653	1.451	0.88
C	10.132	8.131	0.803	1.640	1.368	0.83
D	8.296	7.223	0.871	1.342	1.215	0.91
E	8.109	7.467	0.921	1.312	1.256	0.96
F	7.770	6.941	0.893	1.257	1.168	0.93

TABLE 4.14
Projected Row 6 Isotopic Reaction Rates
Stainless Steel Filter Pins

Reaction	A	B	C	D	E	F	Total
Zn-67 (n,p)	3.289E11*	2.692E11*	1.896E11*	2.491E11*	1.476E11**	2.053E11*	2.316E11
Fe-185 (n, γ)	1.309E17*	1.541E17	1.491E17	1.448E17*	1.674E17*	1.178E17	1.453E17
W-186 (n, γ)	7.201E16*	6.812E16*	5.330E16*	5.883E16*	5.797E16*	4.649E16*	6.029E16
W-187 (n, γ)	2.068E17	2.403E17	2.577E17	2.037E17	2.499E17	2.332E17	2.320E17
W-188 (n, Σ)	4.407E16	4.637E16	5.220E16	4.140E16	4.341E16	4.353E16	4.516E16
Mo-98 (n, γ)	1.058E15**	1.202E15**	9.718E14**	1.089E15**	1.074E15**	7.759E14**	1.029E15*
Mo-99 (n, γ)	3.408E15	3.749E15	3.645E15	3.387E15	3.631E15	3.479E15	3.549E15
S-32 (n,p)	1.783E13	1.473E13	1.162E13	1.486E13	9.999E12	9.718E12	1.314E13
S-33 (n,p)	2.464E13	2.153E13	1.815E13	2.118E13	1.623E13	1.566E13	1.957E13
Gd-152 (n, γ)	4.069E16*	5.065E16	5.163E16	4.238E16*	4.983E16	4.790E16	4.718E16
N-14 (n,p)	2.696E14	3.463E14	3.548E14	2.820E14	3.598E14	2.907E14	3.172E14
Ni-62 (n, γ)	1.933E15	2.573E15	2.656E15	2.046E15	2.721E15	2.178E15	2.351E15
Fe-54 (n, γ)	7.211E14	9.045E14	9.166E14	7.473E14	9.351E14	8.106E14	8.392E14
S-34 (n, γ)	6.891E13	8.458E13	8.551E13	7.051E13	8.660E13	7.544E13	7.860E13
Ag-107 (n, γ)	1.609E16	1.847E16	1.907E16	1.637E16	1.950E16	1.655E16	1.787E16
Ag-108 (n, γ)	1.990E16	2.314E16	2.352E16	1.981E16	2.304E16	2.021E16	2.156E16
Eu-151 (n, γ)	1.066E17	1.478E18	1.679E18	1.269E18	1.681E18	1.399E18	4.432E18
Eu-152 (n, γ)	4.169E17	5.501E17	5.387E17	4.275E17	5.663E17	4.679E17	4.946E17
Eu-154 (n, γ)	2.761E17	3.774E17	3.575E17	2.852E17	2.932E17	3.105E16	3.333E17
Se-74 (n, γ)	5.969E16*	7.945E16*	7.967E16*	5.624E16*	8.770E16*	7.188E16*	7.241E16
Sm-144 (n, γ)	4.720E15	5.322E15	5.151E15	4.717E15	5.184E15	5.044E15	5.023E15
Sm-149 (n, γ)	8.079E18	1.057E19	1.041E19	8.248E18	1.045E19	8.571E18	9.388E18
U-235 (n,f β)	8.073E16	1.066E17	1.094E17	8.422E16	1.107E17	9.115E16	9.713E16
Tc-99 (n, γ)	3.268E16*	3.787E16*	4.101E16*	3.201E16*	3.367E16*	3.820E16*	3.590E16

All values have units of reactions/cm³-s of material

* = uncertainties between 10% and 20%

** = uncertainties over 20%

The total column represents an average rate over all target areas

drive the reaction rates down. This is particularly true in the thermal spectrum rates. Table 4.17 and 4.18 list the results of hard

spectrum reaction rate calculations, with and without the Nd_2O_3 filter pins, respectively. A U-235 fission reaction rate was also calculated for comparative purposes. A variety of positions, identified in Figure 4.1, were used. It can be seen that the Nd_2O_3 serves to drive the hard spectrum reaction rates up in all (n,p) reactions except for N-14. The U-235 fission rate, a primarily thermal reaction, is decreased. A comparison of the effects of the Nd_2O_3 is summarized in Table 4.19.

Table 4.20 shows a summary of the comparison for the total reaction rates between the row 7 test assembly and the row 6 test assembly. As would be expected, the reaction rates decrease in the row 7 location. This decrease ranges from 5 percent for the Re-185 (n, γ) reaction to 47 percent in the S-32 (n,p) reaction.

As was noted earlier, the filter pins have a two-fold purpose of not only softening the impact of the neutrons returning from the moderator to the fuel pins, but to also produce a useful product. To determine the potential for isotope production in the filter pins, a series of tallies were made in the Nd_2O_3 filter pins to find Nd-146 (n, γ) reaction rates. The results of these calculations are summarized in Table 4.21. The locations identified in the table are shown in Figure 4.1. Since the neodymium was present in the target material, this calculation is not infinitely dilute but does account for self shielding.

TABLE 4.15
Projected Row 6 Isotopic Reaction Rates
Nd₂O₃ Filter Pins

Reaction	A	B	C	D	E	F	Total
Zn-67 (n,p)	3.828E11*	2.854E11*	2.912E11*	2.591E11*	2.163E11*	2.408E11*	2.792E11
Re-185 (n,γ)	9.083E16*	1.585E17	1.312E17	1.200E17*	1.413E17*	1.091E17*	1.248E17
W-186 (n,γ)	2.141E16*	4.278E16*	4.922E16*	4.858E16*	6.771E16*	5.451E16*	4.737E16
W-187 (n,γ)	1.750E17	2.138E17	2.014E17	1.747E17	2.299E17	1.886E17	1.972E17
W-188 (n,γ)	2.992E16	3.931E16	4.097E16	3.910E16	5.003E16	4.287E16	4.038E16
Mo-98 (n,γ)	1.194E15**	1.347E15*	8.379E14*	6.780E14*	6.792E14*	1.039E15**	9.622E14
Mo-99 (n,γ)	3.373E15	3.722E15	3.702E15	3.240E15	3.608E15	3.330E15	3.496E15
S-32 (n,p)	1.836E13	1.587E13	1.447E13	1.560E13	1.280E13	1.220E12	1.485E13
S-33 (n,p)	2.500E13	2.227E13	2.055E13	2.163E13	1.859E13	1.761E13	2.084E13
Gd-152 (n,γ)	4.088E16*	4.768E16	4.253E16	3.543E16	4.901E16*	4.532E16	4.348E16
N-14 (n,p)	1.831E14	2.487E14	2.354E14	1.753E14	2.436E14	1.651E14	2.082E14
Ni-62 (n,γ)	1.260E15	1.795E15	1.721E15	1.236E15	1.805E15	1.189E15	1.501E15
Fe-54 (n,γ)	5.495E14	7.503E14	7.258E14	5.545E14	7.702E14	5.496E14	6.500E14
S-34 (n,γ)	5.393E13	6.837E13	6.754E14	5.343E13	6.974E13	5.439E13	3.123E13
Ag-107 (n,γ)	1.239E16	1.682E16	1.539E16	1.209E16	1.667E16	1.306E16	1.440E16
Ag-108 (n,γ)	1.512E16	1.870E16	1.816E16	1.552E16	1.987E16	1.167E16	1.651E16
Eu-151 (n,γ)	7.464E17	1.087E18	1.037E18	7.418E17	1.097E18	7.504E17	9.100E17
Eu-152 (n,γ)	2.849E17	3.895E17	3.781E17	2.928E17	3.948E17	2.891E17	3.382E17
Eu-154 (n,γ)	1.967E17	2.679E17	2.487E17	2.052E17	2.692E17	1.979E17	2.309E17
Se-74 (n,γ)	5.746E16*	5.410E16*	5.942E16*	4.592E16*	9.749E16*	7.121E16*	6.427E16
Sm-144 (n,γ)	4.167E15	4.746E15	4.838E15	4.078E15	4.803E15	4.406E15	4.507E15
Sm-149 (n,γ)	4.825E16	7.485E16	7.469E16	5.058E16	7.897E16	4.184E16	6.170E16
U-235 (n,fp)	5.388E16	7.374E16	7.154E16	5.348E16	7.421E16	5.189E16	6.312E16
Tc-99 (n,γ)	2.891E16**	3.694E16*	3.649E16*	5.848E16*	3.612E16	3.221E16*	3.319E16
B-10 (n,α)	3.147E17	4.576E17	4.386E17	3.107E17	4.830E17	2.974E17	3.803E17

All values have units of reactions/cm³-s of material

* = uncertainties between 10% and 20%

** = uncertainties over 20%

The total column represents an average rate over all target areas

TABLE 4.16
Effect of Nd₂O₃ Filter Pins
on Row 6 Reaction Rates

REACTION	WITH SS	WITH Nd ₂ O ₃	Nd ₂ O ₃ /SS
N-14 (n,p)	3.712E14	2.082E14	0.656
S-32 (n,p)	1.314E13	1.485E13	1.130
S-33 (n,p)	1.957E13	2.094E13	1.070
S-34 (n,γ)	7.860E13	6.123E13	0.799
Fe-54 (n,γ)	8.392E14	6.500E14	0.755
Ni-62 (n,γ)	2.351E15	1.501E15	0.638
Se-74 (n,γ)	7.241E16	6.427E16	1.127
Mo-98 (n,γ)	1.029E15	9.622E14	0.935
Mo-99 (n,γ)	3.549E15	3.496E15	0.985
Tc-99 (n,γ)	3.590E16	3.319E16	0.925
Ag-107 (n,γ)	1.767E16	1.440E16	0.815
Ag-108 (n,γ)	2.156E16	1.651E16	0.766
Sm-144 (n,γ)	5.023E15	4.507E15	0.897
Sm-149 (n,γ)	9.388E18	6.170E18	0.657
Eu-151 (n,γ)	1.432E18	9.100E17	0.635
Eu-152 (n,γ)	4.946E17	3.382E17	0.684
Eu-154 (n,γ)	3.333E17	2.309E17	0.693
Gd-152 (n,γ)	4.718E16	4.348E16	0.922
Re-185 (n,γ)	1.453E17	1.248E17	0.859
W-186 (n,γ)	6.029E16	4.737E16	0.786
W-187 (n,γ)	2.320E17	1.972E17	0.850
W-188 (n,γ)	4.516E16	4.036E16	0.894
U-235 (n,fp)	9.713E16	6.312E16	0.650
All uncertainties are less than 7%.			

TABLE 4.17					
Stainless Steel Filter Pins Hard Spectrum Reaction Rates					
Test Assembly in Row 6 (Position 1610)					
POS	Zn-67 (n,p)	S-32 (n,p)	S-33 (n,p)	N-14 (n,p)	U-235 (n,fp)
G	3.376E11* (0.1070)	1.945E13 (0.0452)	2.453E13 (0.0353)	5.902E13 (0.0251)	1.428E16 (0.0356)
H	3.186E11 (0.1381)	1.631E13 (0.0516)	2.129E13 (0.0390)	7.559E13 (0.0276)	2.021E13 (0.0315)
I	2.972E11 (0.1030)	1.399E13 (0.0402)	1.841E13 (0.0290)	5.466E13 (0.0203)	1.467E16 (0.0246)
J	2.439E11 (0.0991)	1.187E13 (0.0421)	1.626E13 (0.0302)	7.438E13 (0.0213)	2.212E16 (0.0246)
K	1.001E11 (0.1576)	5.020E12 (0.0633)	8.484E12 (0.0370)	4.699E13 (0.0230)	1.680E16 (0.0263)
L	1.168E11 (0.1352)	5.469E12 (0.0579)	9.105E12 (0.0350)	6.896E13 (0.0228)	2.299E16 (0.0237)
M	5.576E10 (0.1982)	3.270E12 (0.0909)	6.361E12 (0.0470)	4.588E13 (0.0331)	1.717E16 (0.0351)
N	6.469E10 (0.2000)	3.722E12 (0.0884)	7.016E12 (0.0470)	6.493E13 (0.0306)	2.236E16 (0.0367)

All reactions rates are infinitely dilute, and are averaged over the length of the core (3 ft). The reaction units are reactions/cm³.

* Uncertainty estimates are included below in parenthesis.
Read as 3.376E11 ± 10.70%

TABLE 4.18						
Nd ₂ O ₃ Filter Pins Hard Spectrum Reaction Rates						
Test Assembly in Row 6 (Position 1610)						
POS	Zn-67 (n,p)	S-32 (n,p)	S-33 (n,p)	N-14 (n,p)	B-10 (n,α)	U-235 (n,fp)
G	5.083E11 (0.1231)	2.655E13 (0.0465)	3.315E13 (0.0366)	7.720E13 (0.0238)	6.727E16 (0.0374)	1.726E16 (0.0272)
H	4.224E11 (0.0871)	2.352E13 (0.0481)	3.002E13 (0.0371)	1.009E14 (0.0276)	1.299E17 (0.0329)	2.773E13 (0.0304)
I	4.123E11 (0.0899)	2.395E13 (0.0363)	3.000E13 (0.0292)	7.413E13 (0.0204)	7.120E16 (0.0296)	1.807E16 (0.0243)
J	2.703E11 (0.1053)	2.100E13 (0.0383)	2.707E13 (0.0301)	9.749E13 (0.0204)	1.307E17 (0.0265)	2.709E16 (0.0239)
K	5.298E11 (0.1009)	1.482E13 (0.0633)	2.005E13 (0.0328)	6.671E13 (0.0218)	8.126E16 (0.0294)	1.961E16 (0.0252)
L	1.370E11 (0.1009)	1.386E13 (0.0426)	1.925E13 (0.0310)	9.536E13 (0.0217)	1.454E17 (0.0265)	2.913E16 (0.0235)
M	1.370E11 (0.1608)	8.060E12 (0.0637)	1.313E13 (0.0402)	6.527E13 (0.0217)	9.180E16 (0.0363)	2.234E16 (0.0363)
N	1.273E11 (0.1507)	9.236E12 (0.0631)	1.442E13 (0.0404)	9.195E13 (0.0265)	1.470E17 (0.0321)	3.023E16 (0.0296)

All reactions rates are infinitely dilute, and are averaged over the length of the core (3 ft). The reaction units are reactions/cm³.

* Uncertainty estimates are included below in parenthesis. Read as 3.376E11 + 10.70%

TABLE 4.19 Nd ₂ O ₃ Effect on Hard Spectrum Reaction Rates Row 6 Test Assembly Position			
REACTION	SS FILTER PINS	Nd ₂ O ₃ FILTER PINS	Nd ₂ O ₃ /SS
Zn-67 (n,p)	2.782E11	3.534E11	1.270
S-32 (n,p)	9.888E12	1.762E13	1.782
S-33 (n,p)	1.393E13	2.339E13	1.679
N-14 (n,p)	6.130E13	8.363E13	1.364
U-235 (n,fp)	4.172E16	2.393E16	0.574
B-10 (n,α)	2.353E17	1.081E17	0.459

Reaction rates are in units of reactions/cm³-s
All uncertainties are under 8.0%

TABLE 4.20 Row 6 and 7 Reaction Rate Comparison			
Reaction	Row 6	Row 7	Row 7 / Row 6
N-14 (n,p)	3.172E14	2.245E14	0.708
S-32 (n,p)	1.314E13	7.032E12	0.535
S-33 (n,p)	1.957E13	1.164E13	0.595
S-34 (n,γ)	7.860E13	5.795E13	0.737
Fe-54 (n,γ)	8.392E14	63937E14	0.827
Ni-62 (n,γ)	2.351E15	1.686E15	0.717
Se-74 (n,γ)	7.241E16	4.603E16	0.636
Mo-98 (n,γ)	1.029E15	7.493E14	0.728
Mo-99 (n,γ)	3.549E15	2.560E15	0.721
Tc-99 (n,γ)	3.590E16	2.720E16	0.758
Ag-107 (n,γ)	1.767E16	1.319E16	0.746
Ag-108 (n,γ)	2.156E16	1.587E16	0.736
Sm-144 (n,γ)	5.023E15	3.507E15	0.698
Sm-149 (n,γ)	9.388E18	7.528E18	0.802
Eu-151 (n,γ)	1.432E18	1.041E18	0.727
Eu-152 (n,γ)	4.946E17	3.387E17	0.685
Eu-154 (n,γ)	3.333E17	2.330E17	0.699
Gd-152 (n,γ)	4.718E16	3.737E16	0.792
Re-185 (n,γ)	1.453E17	1.384E17	0.953
W-186 (n,γ)	6.029E16	4.362E16	0.724
W-187 (n,γ)	2.320E17	1.695E17	0.731
W-188 (n,γ)	4.516E16	±0)±0)pBE108649)z 2c K6.793E16	0.699
U-235 (n,fp)	9.713E16		0.699

All uncertainties are less than 7.0%

TABLE 4.21 ¹⁴⁶ Nd (n,γ) Reaction Rates Radio-isotope Production in the Nd ₂ O ₃ Filter Pins		
POSITION	RATE	ERROR
O	3.516E14	0.0254
P	3.973E14	0.0381
Q	3.262E14	0.0245
R	3.090E14	0.0262
S	3.523E14	0.0401
T	3.103E14	0.0390

Reactions are in units of reactions/cm³-s.

4.4.5 Macrocell Run Accuracy Check

Unrelated to the results of the MIP-II test, but important to the calculational process involved in both the MIP-II and MOTA tests, a check of the accuracy of using a macrocell for the calculations was performed. This was done with heating tallies. When the long run was performed which recorded incident neutron current upon the macrocell, heating tallies were made on the fuel pins in assembly 1609 and 1610. These are the same fuel pins that were analyzed in the row 7 test assembly problem. The results of the tallies were compared to the heating tallies performed in the row 7 test assembly calculations. The results of the comparison are summarized in Table 4.22. The table shows that the accuracy of the heating tallies is very good in assembly 1610, with the difference between the two calculations ranging from 0.1 to 4.2 percent. The difference is greater in assembly 1609, where because of its closer proximity to the reflector, the impact of that reflector is stronger in the whole core model. The difference ranges from 2.2 to 10.4 percent.

TABLE 4.22 Comparison of Macrocell Run - Accuracy Test Peak Heating in Fuel Assemblies 1609 and 1610 Test Assembly in Position 1712					
ASSEMBLY 1609					
POS	CORE PIN HEAT.	UNCERT.	MACROCELL PIN HEAT.	UNCERT.	DIFF.
A	11.305	0.043	11.053	0.041	-0.022
B	10.712	0.039	11.829	0.040	0.104
C	10.442	0.039	11.175	0.041	0.070
D	8.296	0.040	8.855	0.031	0.067
E	8.486	0.029	8.999	0.035	0.060
F	8.684	0.027	8.928	0.028	0.028
ASSEMBLY 1610					
POS	CORE PIN HEAT.	UNCERT.	CELL PIN HEAT.	UNCERT.	DIFF.
A	10.014	0.036	10.439	0.040	0.042
B	10.843	0.038	10.835	0.046	-0.001
C	10.080	0.041	9.981	0.039	-0.010
D	8.377	0.027	8.285	0.030	-0.011
E	8.338	0.028	8.306	0.029	-0.004
F	8.318	0.027	8.477	0.030	0.019

Although the 10.4 percent difference is disconcerting, it appears to be an anomaly when compared to the other differences. All other differences are below the relative uncertainty in the tally results themselves. Because all macrocell calculations for each test assembly location were made using the same neutron current, the macrocell offers a solid and accurate basis for comparison.

4.5.0 CONCLUSIONS

These MCNP calculations produced a huge quantity of data that could

be compared and analyzed in many different ways. Most of this data and key comparisons have been summarized in the tables.

4.5.1 Discussion of Results

Despite the bulk and voluminous nature of the data, a number of pertinent conclusions are supported by comparing the results of the calculations. This is not, in any way, an exhaustive list, but serves as an example of the functional power of Monte Carlo calculations in design applications.

1. Row 7 provides 5 to 50 percent lower reaction rates in target pins than row 6. The average decrease was 28 percent.
2. The Nd_2O_3 filter pins reduced reaction rates in target pins by an average of 18 percent in both row 6 and row 7 locations.
3. Most reaction rates in target pins were not very dependent on pin location. No significant radial gradient in reaction rates was observed except for high energy threshold reactions, which decreased by about a factor of two across the target pin locations and by about a factor of five across the assembly.
4. Adjacent row 6 fuel pin radial power peaking factors with the test assembly in row 7 were approximately 1.5 with stainless steel filter pins and 1.3 with Nd_2O_3 filter pins.
5. Adjacent row 6 peak pin linear powers with the test assembly in row 7 were generally low enough for test irradiation even with stainless steel filter pins.
6. Adjacent row 6 fuel pin radial power peaking factors with the test assembly in row 6 were approximately 1.5 to 1.7 with steel filter pins and 1.4 to 1.6 with Nd_2O_3 filter pins.

7. Adjacent row 5 fuel pin radial power peaking factors with the test in row 6 were approximately 1.4 to 1.5 with stainless steel filter pins and 1.2 to 1.3 with Nd_2O_3 filter pins.
8. The adjacent row 6 peak pin linear powers with the test assembly in row 6 were generally low enough for test irradiation even with stainless steel filter pins.
9. The adjacent row 5 peak pin linear powers with the test assembly in row 6 were generally low enough to allow test irradiation even with stainless steel filter pins.
10. Acceptable fuel performance with these radial power distributions and peak linear powers needs to be evaluated separately.
11. Alternate filter materials or assembly designs should be evaluated to reduce power peaking in adjacent fuel.

4.5.2 MIP-II Calculations Application

At the time of this publication, the MIP-II test assembly had not been irradiated in the FFTF.

CHAPTER 5

NEUTRON MODERATION IN A MOTA CANISTER

5.1.0 INTRODUCTION

5.1.1 The Materials Open Test Assembly Canister

The MOTA¹ is a highly instrumented facility in the FFTF, which allows for more in-depth analysis and quicker retrieval of test materials than other FFTF irradiation facilities. It is a full assembly that occupies assembly 2406 in Figure 4.2. While providing high resolution temperature control and measurement, the MOTA also records density and dimensional measurements. This feature makes it an invaluable facility in the investigation of irradiation impact upon advanced materials. The MOTA is composed of six test canisters, which allows for 48 specimen capsules, 30 of which have independent temperature control. The MOTA was designed to accommodate 2500 cm³ of nonfissioning test materials within the capsules. The MOTA can be removed entirely from the reactor at the end of an operating cycle. This permits the test capsules to be retrieved and examined almost immediately after shutdown. New experiments can be loaded just as quickly and be in the reactor by the start of the next operating cycle.

5.1.2 MOTA Computational Objectives

Based on the demand for radionuclides described in Section 4.1.1 and the availability and features of the MOTA, described above, design calculations were performed to investigate the feasibility of radioisotope production in the MOTA canisters. This chapter summarizes the neutronic calculations that were made for that test.

The test utilized one of the six canisters in the MOTA-2B assembly in location 2406 of Figure 4.2. In an effort to tailor the neutron flux incident on the target material, an annulus of yttrium-hydride ($\text{YH}_{1.8}$) was designed to surround the target within the MOTA canister. Figure 5.1 shows the canister of interest with the concentric cylinders. The $\text{YH}_{1.8}$ annulus is labeled F in the figure. The geometry and material composition of the MOTA test canister will be discussed in detail in Section 5.2.1. Six detailed neutronic calculations were made for this test by varying the size and composition of the $\text{YH}_{1.8}$ annulus in the canister.

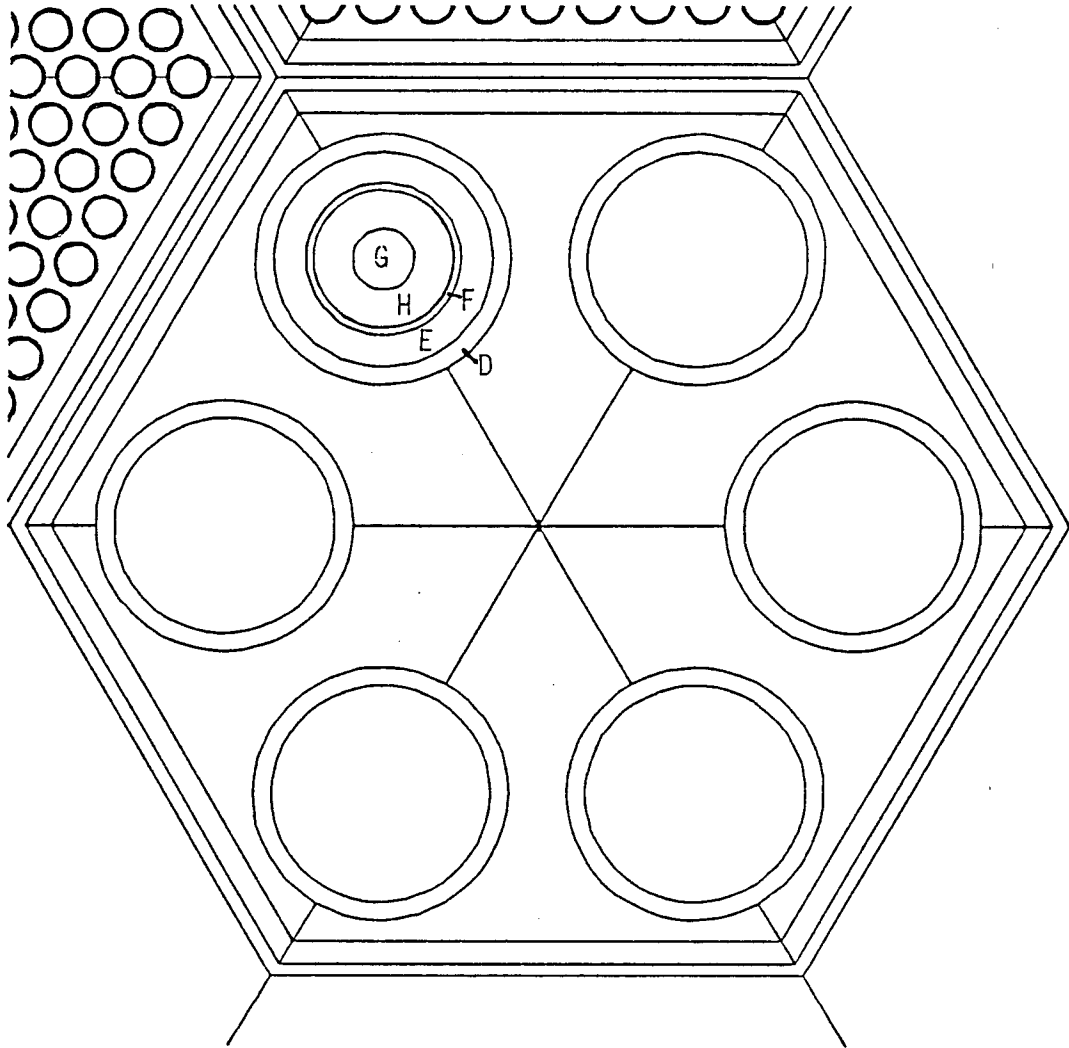
The emphasis of these calculations was threefold:

- 1) To determine reaction rates in the target area as a function of the amount of $\text{YH}_{1.8}$ for a variety of nuclides. Infinitely dilute reaction rates were calculated for 14 nuclides inside the target area.

- 2) To determine heating in adjacent fuel pins increased by the thermalized neutrons returning from the $\text{YH}_{1.8}$ moderator. Linear heating factors in rows 1 through 5 are generally between 8 and 12 kW/ft. It was necessary to demonstrate that the extra moderator would not drive pin heating radically over the normal operating condition radial peaking factors and linear peaking factors in the rows of fuel pins nearest the test canister.

- 3) To determine the impact that the proposed test configuration would have on other experiments also utilizing the MOTA. Concurrent with the planned isotope production test were a number of tritium production tests utilizing other canisters in the MOTA assembly. It

FIGURE 5.1
PLAN VIEW OF MOTA TEST ASSEMBLY



was necessary to find a location within the MOTA canister for the isotope production test that would yield useful results while not perturbing the flux in such a way that would impede the tritium tests.

5.2.0 MCNP CALCULATIONAL MODEL

5.2.1 Geometry and Materials

The full core hexagonal matrix model with nine rows and five axial zones that was described in Section 4.2.1 for the MIP-II test was also used for the MOTA calculations. Each fuel assembly in the core had individual isotopic compositions based on enrichment and burn time. A cross sectional view of the reactor matrix is shown in Figure 4.2. As in the MIP-II calculations, a seven cell macrocell was utilized. The MOTA is located in assembly 2406. The macrocell also included fuel assemblies 2304, 2405, 2508, 3301, 3401, and 3501. Assemblies 2406, 2304, and 3301 were heterogeneously modeled while all other assemblies were individually homogenized. As with the MIP-II test, a long calculation was performed for the full core model, with the neutron current on the outer surface of the macrocell recorded for the design iterations. The calculations are detailed in Section 5.3.1.

Figure 5.1 shows the MOTA with the model of the canisters detailed. There are six canisters in the model. The test was to be run in Canister 4-C in the upper left of the figure. The canisters are stainless steel cylinders with inner radii of 1.44272 cm and a thicknesses of 0.2413 cm. Within the heterogeneous model of the MOTA-2B assembly, only Canister 4-C was modeled in detail. Canister 4-C consisted of the outer cylinder, labeled as cylinder D in Figure 5.1,

a sodium flow channel with inner radius 1.02235 cm and thickness 0.42037 cm (Cell E), a stainless steel sleeve of inner radius 0.92525 cm and thickness 0.0971 cm (Cell F), a void gap just inside Cell F of thickness 0.0045 cm, the yttrium hydride moderator cylinder of inner radius 0.4064 cm and thickness 0.51435 cm (Cell H) and the central target area with a radius of 0.4064 cm. The other five canisters were modeled with the outer steel canister and void experiment region.

It is important to note that Cell G and the interiors of the other five canisters were represented as being void of material. Therefore, when nuclide reaction rates in Cell G and lithium reaction rates in Cells A, B, and C are calculated, they are infinitely dilute, with no self shielding accounted for within the target regions.

Fuel assemblies 2304 and 3301, which were modeled in heterogeneous detail, were given fuel compositions based on an early Cycle 11C fuel loading. The fuel pin description can be found in Section 4.2.1. Figure 5.2 shows the heterogeneous detail given to the macrocell.

5.2.2 Biasing

Figure 5.3 shows the details of the full core biasing scheme utilized in the long run to establish the neutron and photon current SRCTP file. It is much the same as was described in Section 4.2.2 for the MIP-II test assembly. Assembly 2406 and the six fuel cells surrounding it were given a neutron weight of 0.024. The weights of each assembly increased by a factor of approximately four every other assembly radially outward from the MOTA. The weight reached a maximum of 3.112 in the assemblies furthest from the MOTA.

FIGURE 5.2
PLAN VIEW OF MOTA COMPUTATIONAL MACROCELL

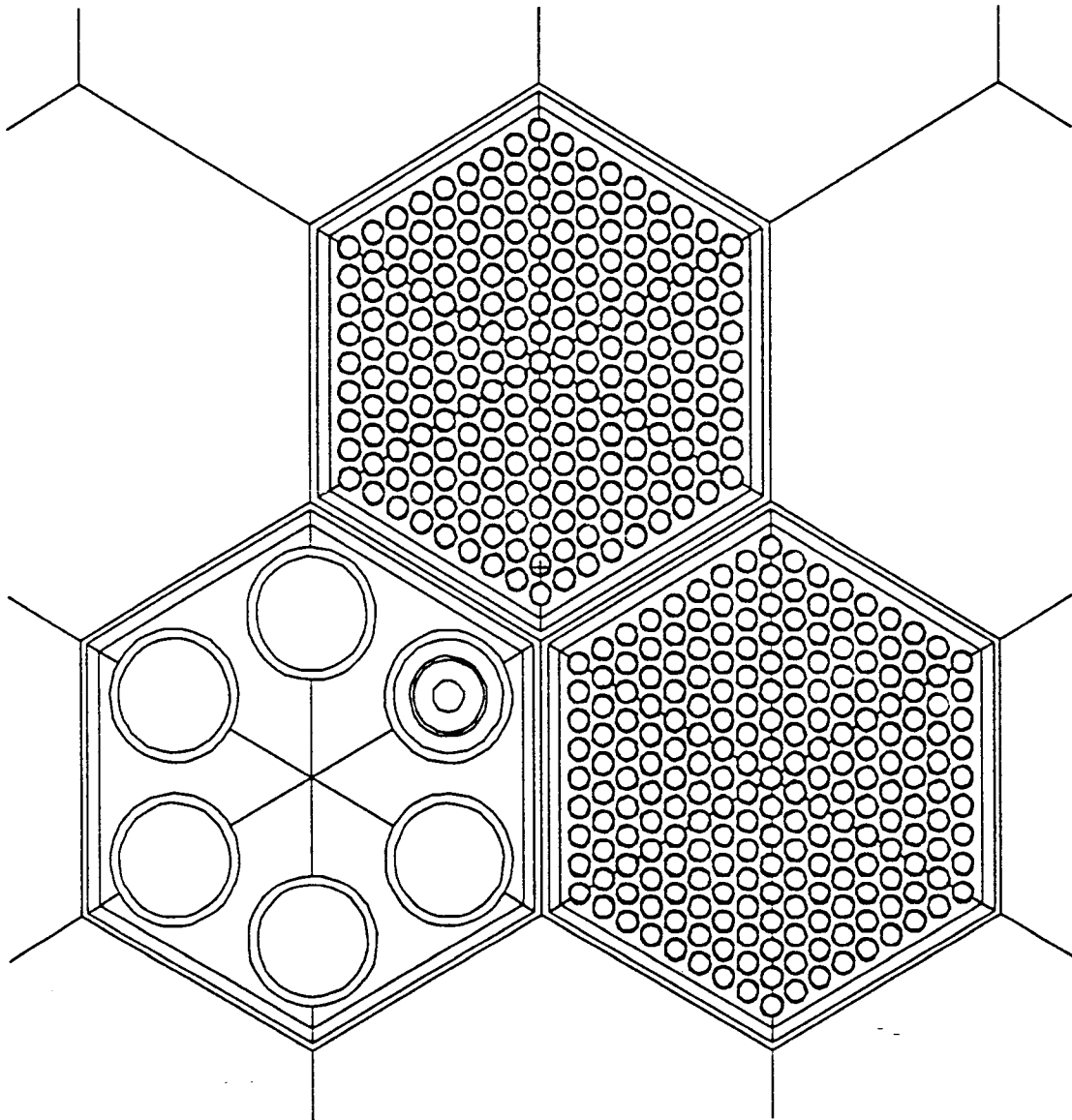
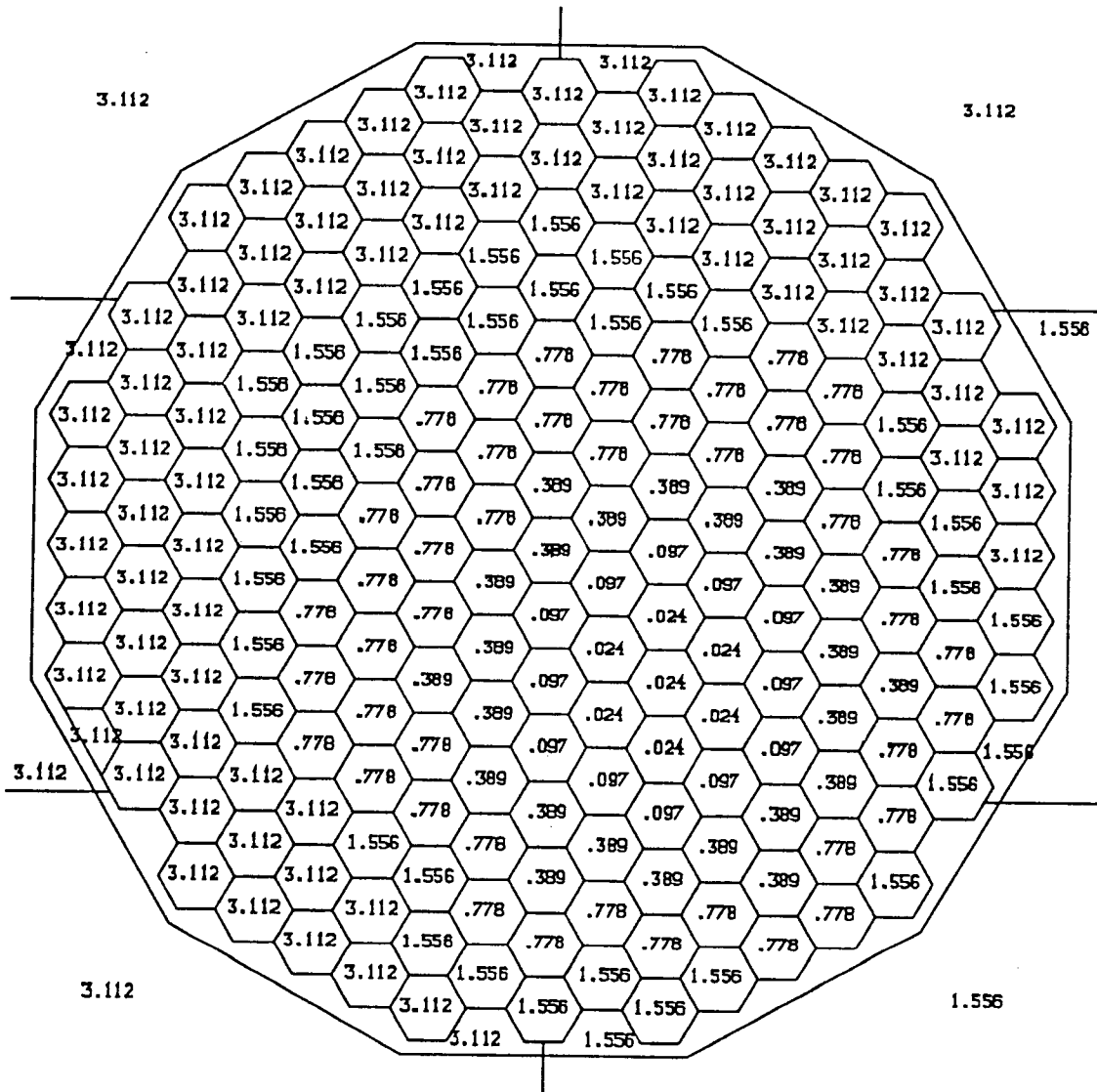


FIGURE 5.3
 LOWER BOUNDS OF NEUTRON WEIGHT WINDOWS IN FULL CORE MODEL



Due to the nature of the MOTA, with only one canister of interest in the corner of the assembly, biasing was employed within the heterogeneous macrocell as well. Within the MOTA, all the space outside the test canister 4-C was given a weight of 0.036. This includes the other five canisters, their cladding, and the stainless steel walls of the MOTA. The stainless steel outer annulus (Cell D in Figure 5.1), the sodium flow region (Cell E), the stainless steel sleeve (Cell F), and the void gap inside Cell F were also given a weight of 0.036. The yttrium hydride moderator annulus (Cell H) and the target region (Cell G) were assigned a weight of 0.018. This is not a large biasing strategy, but it does have the effect of spending more of the calculational time in the target and moderator region.

In the fuel pin assemblies, neutrons were biased toward the two rows of fuel pins on which the heating tallies were performed. These two rows of pins, labeled in Figures 5.4 and 5.5 with letters, along with the other pins that are in the two triangular "pie" slices in which the first two rows fell, were assigned a weight of 0.036. The pins in the other four triangular slices of the fuel assemblies were assigned a weight of 0.146. The purpose of this weighting was twofold. First, within the fuel assemblies, it was desired to spend the majority of the random walk sampling in the two rows where the tallies of interest were being compiled. Second, biasing in such a fashion pushed the neutrons into the triangular slices nearest the MOTA 4-C test canister. This caused the majority of the random walk calculations to be performed in the region of interest.

FIGURE 5.4
ADJACENT FUEL PIN LOCATIONS FOR FUEL ASSEMBLY 2304

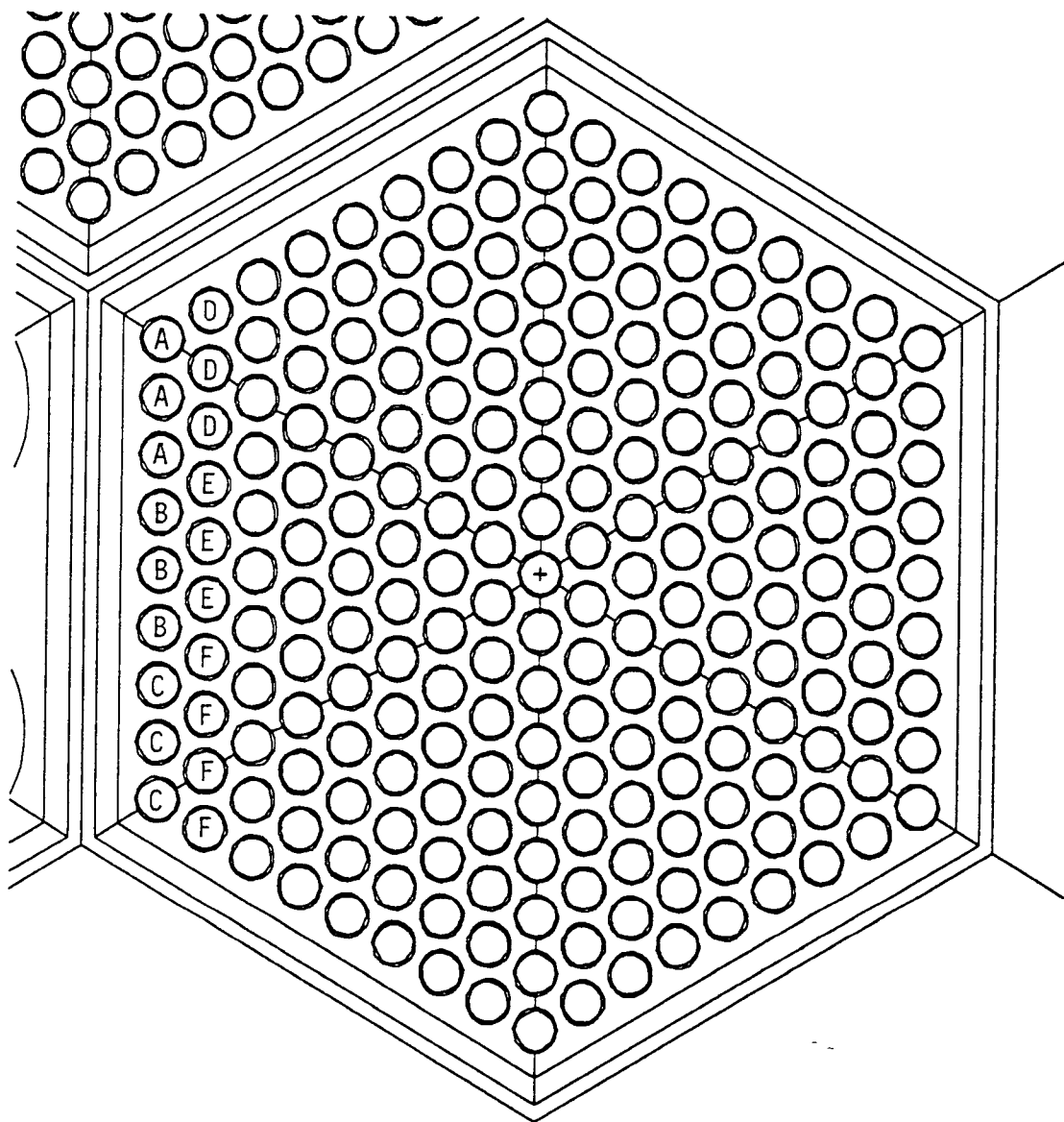
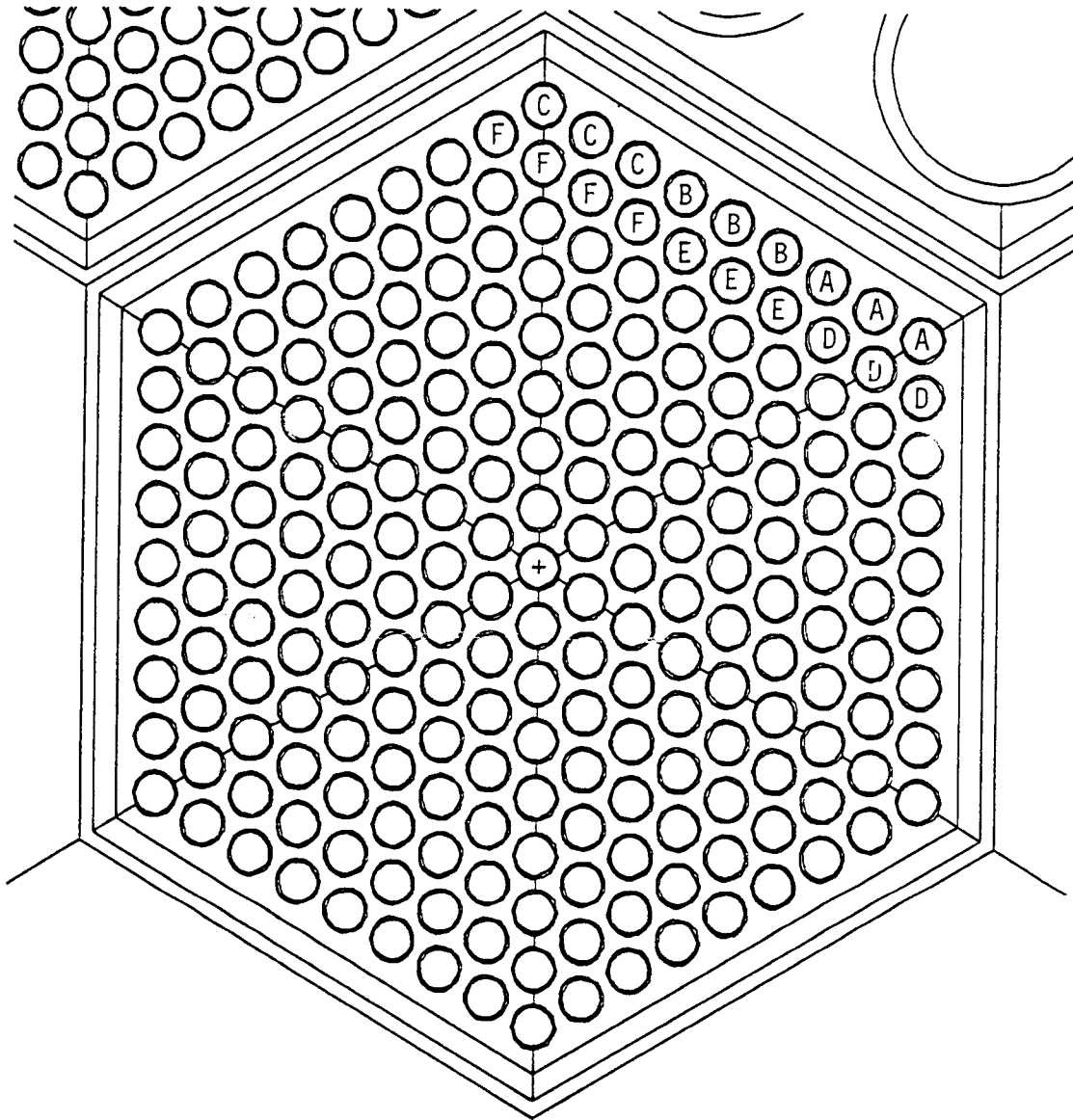


FIGURE 5.5
ADJACENT FUEL PIN LOCATIONS FOR FUEL ASSEMBLY 3301



5.3.0 CALCULATIONAL SUMMARY

5.3.1 Summary of Runs

The philosophy behind the logistics of the calculational runs for the MOTA test was quite different than that for the MIP-II test. In contrast to the MIP-II calculations, which could have been run concurrently to determine which location would optimize special nuclide production, the MOTA test calculations were more iterative in nature. The location of the test was already determined. It was necessary to determine which thickness of $YH_{1.8}$ would produce the optimum results and minimize the impact on the surrounding tests. In light of this, a series of Monte Carlo calculations were performed consecutively, each one problem designed in response to the results of the prior run. There were seven different calculations performed which are described below. These each compared a different material or geometric configuration.

BASE CASE. The base case, that to which all subsequent calculations were compared, consisted of the macrocell described in Section 5.2.1 with the exception that rather than filling Cell H with yttrium hydride, it was replaced by a void. In choosing this as the base case, all subsequent cases would be compared to a problem where there was no moderating material used. Thus, the effects of the different yttrium hydride configurations and densities could be more clearly observed. Other reasons for using a base case were detailed in Chapter III. A total of 340,252 neutrons were run in the problem generating a total of 53,827 neutrons recorded on the WSSA file to be run in the subsequent calculations.

CASE I. The Case I geometry and material configuration was identical to that utilized in the base case. The purpose behind Case I was to allow comparison between the test assembly with yttrium hydride and without yttrium hydride. It was run separately, rather than just tallying during the running of the base case, so that the tallies that the problem generated would be the result of the same neutron current source upon the macrocell that the other five cases used. In this way, Monte Carlo comparisons between the cases would be more valid.

CASE II. This case was identical to the macrocell described in Section 5.2.1, with yttrium hydride material filling Cell H. The Case II calculation was the first model with the yttrium hydride moderator. Although the test canister is only about 4 inches in length, in the interest of obtaining better statistics, all materials in the MOTA-2B assembly ran the full 36 inch length of the core. Heating tallies in the MOTA and adjacent fuel pin rows, reaction rate tallies in the target region for a variety of nuclides, and ${}^6\text{Li}$ reaction rate tallies in the other five MOTA canisters were performed. Tallies were made along the entire length of the core as well.

CASE III. Case III differed from Case II only in that the thickness of the canister sleeve (Cell D in Figure 5.1) was increased from 0.241 cm to 0.535 cm. This calculation was performed in response to observations that the effect of the yttrium hydride was driving up the ${}^6\text{Li}$ reaction rate in the other canisters. It was necessary to find out exactly what the effect would be of increasing the sleeve thickness in the hope that it would stop enough of the thermal

neutrons leaving the test canister that the adjacent tests would not be affected. Running this case also allowed for closer observation of the effect of the yttrium hydride on the neutron flux within the target region.

CASE IV. In Case IV, the heterogeneous detail of the MOTA-2B assembly was reduced from the full length of the core to a 6 inch model centered in the space occupied by Canister 4-C. This calculation was performed to determine the difference between tallying along the full length of the core and tallying only in the smaller space representative of the actual test target. This Monte Carlo problem showed the effect of a smaller yttrium hydride moderator volume, not only on the test nuclide reaction rates, but also the impact upon the tritium tests adjacent to the 4-C canister. As was stated above, the reason for running the materials and tallies the full length of the core was to obtain better statistics to the tallies given. Regions above and below the 6 inch test region were modeled homogeneously.

CASE V. Case V was identical to Case III except, as in Case IV, only the 6 inches representing Canister 4-C were modeled heterogeneously, and tallies were made only in that region. The purpose of running this case was the same as for Case IV.

CASE VI. Case VI utilized the same geometry as Case IV, except the yttrium hydride density in Cell H was reduced by a factor of two, although the dimensions of the annuli remained the same. This, in effect, modeled a case where there was only one-half the yttrium hydride moderator present. The purpose of this calculation was to

determine the impact of reducing the density of the moderator rather than the volume upon the special nuclide production tests.

These six cases are summarized in Table 5.1.

TABLE 5.1 Summary of Cases	
Case I	The base case, without $YH_{1.8}$, full length
Case II	With $YH_{1.8}$, full length
Case III	With $YH_{1.8}$, full length, thick canister wall
Case IV	With $YH_{1.8}$, 6 inch model
Case V	With $YH_{1.8}$, 6 inch model, thick canister wall
Case VI	With $YH_{1.8}$, 6 inch model, reduced $YH_{1.8}$ density

5.3.2 Calculational Techniques

5.3.2.1 Heating Tallies

As in the MIP-II calculations, the fuel pin heating calculations were performed with the use of the F6 tally card. The theory behind and utilization of the F6 tally card were discussed in Section 2.3.3 and Section 4.3.2.1. The tally multiplier card for the MOTA experiment was the same as was calculated in Section 4.3.2.1 for the MIP-II test. Heating tallies were also performed on the stainless steel walls of the MOTA as well as regions of the seven macrocell assemblies directly above and below the target and fuel region (Regions 1, 2, 4, and 5 of Figure 3.2).

5.3.2.2 Reaction Rate Tallies

Reaction rates within the target region and other test canisters were performed with the F4 tally card, just as with the MIP-II test. The F4 tally is described in Section 2.3.3. The multiplicative constants were the same as for the MIP-II test (see Section 4.3.2.2 for calculations). The calculations yielded infinitely dilute reaction rates.

5.4.0 RESULTS

The preliminary physics calculations for the MOTA isotope production test had a three-fold purpose. First, the yttrium hydride annulus within the MOTA test configuration would introduce extra moderating power into the assembly. The effect of the moderator would be to drive the fission rate up in the fuel pins nearest the test assembly when neutrons returning from the yttrium hydride impinge upon the fuel. It was necessary to determine the proper material configuration and concentrations which would keep the test assembly heating impact to a minimum, while maximizing special isotope production.

Second, 14 candidate nuclides were selected for production calculations within the MOTA Canister 4-C target region. Infinitely dilute reaction rates were calculated for each of the nuclides to determine which of the candidate targets would yield the best results within the test.

Third, because of the increased moderation within the MOTA, tests running adjacent to the Canister 4C test could be affected. In particular, tritium production tests, scheduled to run concurrently, could be impacted by the thermal flux increase within the MOTA.

5.4.1 Isotope Reaction Rates in the Target Area

The reaction rates for all six cases are listed in Table 5.2. Because of the iterative nature of the calculations, the results reported in the table are normalized to Case I. Therefore, an absolute reaction rate in units of captures/cm³-s is given only for Case I. For the remaining five cases, a reaction rate relative to Case I is given. Case I modeled the test canister without the yttrium hydride moderator. By normalizing the remaining cases, the effect of the yttrium hydride can be seen directly.

Below each reaction an uncertainty is listed which gives some indication as to whether or not the tally is reliable. Any tally with an uncertainty less than 5 or 10 percent can be considered reliable. Note that the tables list only infinitely dilute reaction rates within the Canister 4C target region (Cell G in Figure 5.1) and not production rates of the target nuclide.

The hard spectrum reaction rates, such as Zn-67(n,p), were reduced with addition of the yttrium hydride, as would be expected. The magnitude of the reduction, however, was generally small, on the order of 10 percent or less. This becomes apparent from Figure 5.6, where the epithermal and higher energy group fluxes are largely unchanged compared to the thermal flux.

TABLE 5.2 Isotope Reaction Rates in MOTA Target Area						
REACTION	I	II	III	IV	V	VI
Zn-67 (n,p) (12%)	4.036E11	0.91	0.96	0.65	0.97	0.57
Re-185 (n, γ) (8%)	4.921E15	6.80	8.88	10.09	8.24	3.08
W-186 (n, γ) (15%)	1.016E15	15.11	13.50	15.97	17.61	5.21
W-187 (n, γ) (5%)	3.953E15	15.97	17.89	13.97	16.38	4.33
W-188 (n, γ) (5%)	7.888E14	15.72	17.52	12.58	15.94	8.20
Mo-98 (n, γ) (8%)	3.977E14	1.93	2.07	1.57	1.31	1.52
Mo-99 (n, γ) (2%)	1.686E15	1.91	1.91	1.98	1.84	1.40
Gd-152 (n, γ) (7%)	2.870E15	6.45	6.58	6.71	5.45	2.72
Fe-54 (n, γ) (5%)	7.078E13	2.69	3.00	2.52	2.78	1.55
Ag-107 (n, γ) (5%)	2.345E15	2.82	2.96	2.42	2.73	1.43
Ag-108 (n, γ) (2%)	2.951E15	2.69	2.85	2.53	2.68	1.53
Se-74 (n, γ) (10%)	4.649E15	4.47	4.12	3.74	4.19	0.59
U-235 (n,fp) (2%)	7.180E15	2.50	2.70	2.37	2.52	1.37
Cd-108 (n, γ) (2%)	7.184E14	1.30	1.29	1.35	1.30	1.13

Reaction rates for Cases II to VI are normalized to Case I.
See Table 5.1 for case description.
Target area is Cell G on Figure 5.1
Uncertainties under the reactions are typical for Cases I, II, and III.

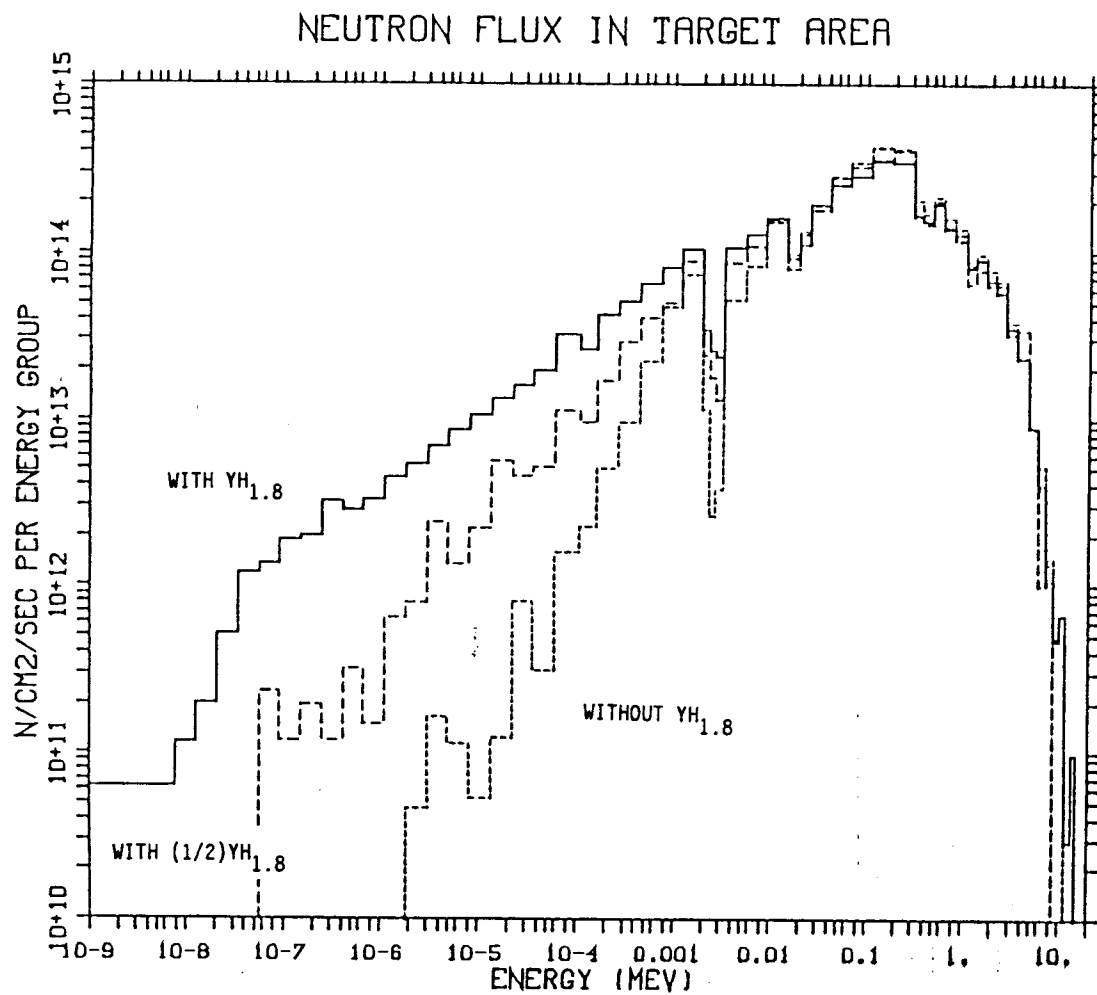
The lower energy reaction rates, especially those involving tungsten, increased by well over an order of magnitude. In the 6 inch model, the W-186(n, γ) reaction rate is a factor of 17.61 greater with the yttrium hydride moderator and thick canister wall. However, by reducing the density of the yttrium hydride by a factor of two, the

reaction rates for many of the radionuclides dropped by factors of three and four. This is again apparent from the flux shapes shown in Figure 5.6. The thermal flux in the target area drops considerably when the yttrium hydride density is reduced. All other reaction rates calculated, which do not depend on the low-energy flux that tungsten does, generally increased by factors of two to six with the addition of yttrium hydride. The ^{152}Gd capture rate, essential in medical diagnostics (see Section 5.5.2), did increase by a factor of over six with the moderator. The ^{98}Mo and ^{99}Mo (n,γ) reaction rates, which are important in the production of the highly valuable medical isotope $^{99\text{m}}\text{Tc}$, increased by a factor of less than two with the yttrium hydride moderator.

Increasing the thickness of the sleeve had little effect on the reaction rates. The most marked difference was in the ^{185}Re (n,γ) reaction where increasing the thickness of the sleeve drove the reaction rate up around 30 percent. For the most part, any differences in the magnitude of the numbers in Table 5.1 are probably lost in the uncertainties.

Case II differs very little from Case IV. This shows that the full-length core modeling does provide a reasonably accurate representation of the problem, allowing for more statistically reliable numbers. Generally, shortening the model length causes a small decrease in the reaction rates, but this difference is not statistically relevant when the uncertainties are included in the analysis.

FIGURE 5.6
NEUTRON FLUX IN CANISTER 4-C TARGET AREA



5.4.2 Effect of $YH_{1.8}$ on Li-6 Experiments

Tritium production experiments were scheduled to run in the MOTA-2B assembly concurrent with the proposed isotope production test. To determine the impact of the yttrium hydride on these experiments, infinitely dilute reaction rates were calculated for all six cases in Cells A, B, and C of Figure 5.1. Symmetry allowed two cells to be combined for the Cell A and B calculations, as indicated on the figure. Combining the two doubled the number of neutrons incident on the "target" and improved the statistics of the tally. The results of the six cases are listed in Table 5.3. As in Table 5.2, the results

TABLE 5.3 Effect of $YH_{1.8}$ on Tritium Production Experiments in Adjacent Canisters						
Li-6						
POSITION	I	II	III	IV	V	VI
A	3.906E15	1.547	1.547	1.338	1.385	1.048
B	3.795E15	1.292	1.310	1.152	1.213	0.996
C	3.750E15	1.269	1.272	1.087	1.115	0.960
Uncertainties are all under 6.3%						
Li-7						
POSITION	I	II	III	IV	V	VI
A	7.057E12	1.087	1.080	0.962	1.084	1.077
B	6.266E12	1.107	1.126	1.141	1.038	1.130
C	6.260E12	1.117	1.186	1.096	1.067	1.216
Uncertainties are all under 6.3% except for Case VI which are over 11%. Case descriptions in Table 5.1. Target positions labeled in Figure 5.1.						

are all normalized to Case I, so that the impact of the different yttrium hydride configurations can be more easily seen.

The effects of the yttrium hydride are dramatic in the canisters closest to Canister 4-C. These effects diminish as distance from the moderator is increased. The ${}^6\text{Li}$ tritium production reaction rates in the A canisters are about a factor of 1.2 higher than in the B canisters and a factor of approximately 1.23 higher than the C canisters. The impact of the yttrium hydride upon ${}^7\text{Li}$ tritium production reactions is negligible and the reaction rates seem to actually increase as distance from the target increases. This is probably due to the shielding of the fast neutrons from the fuel by the yttrium hydride. The fast neutron flux incident upon the B and C canisters is largely unaffected by the moderator in the test assembly.

Increasing the thickness of the sleeve surrounding the yttrium hydride had little effect on the ${}^6\text{Li}$ reaction rates. Any differences in the values in Table 5.3 is lost in the uncertainties. The impact of the thicker sleeve seems to increase with distance from the yttrium hydride; however, this difference is not statistically relevant.

Reducing the yttrium hydride density by a factor of two removed any impact that the moderator had on the ${}^6\text{Li}$ reactions. The thermal neutron spectrum in Cells A, B, and C was the same as in the case where no yttrium hydride was used.

The 6 inch model shows that the yttrium hydride impact on adjacent ${}^6\text{Li}$ tests would result in an increase in reaction rates of about 10 percent, if the distance between the two is maximized (see the ${}^6\text{Li}$ reaction rates for Case V in position C). These calculations are all infinitely dilute and the magnitude of the reaction rate increase will probably be reduced when self-shielding is considered.

5.4.3 Effect of $\text{YH}_{1.8}$ on Total and Fast Neutron Flux

Table 5.4 shows the impact of the yttrium hydride annulus on the total neutron flux and the fast (>0.11 MeV) neutron flux in the adjacent capsules and in the interior of the yttrium hydride annulus. Compared to the base case, the total flux and the fast flux in the adjacent capsules remained unchanged. Inside the yttrium hydride annulus, the total flux was increased by about 5 percent, while the fast flux was decreased by about 13 percent. Figure 5.5 shows the effect of yttrium hydride on the neutron spectrum in the MOTA canister.

5.4.4 Heat Deposition Rates in Adjacent Fuel

The heat deposition rates are summarized in Tables 5.5 and 5.6. This is the peak heating that takes place in the individual fuel pins in the first two rows adjacent to the MOTA. The peak heating shows the hot spot in the pin as a function of the axial temperature distribution. Prior calculations and experiments have shown that the peak heating is usually around 1.2 times greater than the average pin heating. A conservative number of 1.22 was used for these calculations. The conservative nature of this factor is demonstrated by a special calculation described later in the section. Table 5.5 shows the heating rates for individual pins in the first two rows of fuel assemblies 2304 and 3301 adjacent to the test assembly when the reactor is operating at a power level of 291 MW, which is the expected power level during the test irradiation. Figure 5.4 and Figure 5.5 show the location of the individual fuel pins specified in the

TABLE 5.4 Effect of $YH_{1.8}$ on Fast Flux and Total Flux in MOTA						
CASE ($YH_{1.8}$ length)	I		II 36 in.		IV 6 in.	
Location	Total	Fast	Total	Fast	Total	Fast
G	3.63E15	2.12E15	1.04	0.87	1.06	0.89
A	3.51E15	2.07E15	1.01	0.99	1.01	0.99
B	3.40E15	2.01E15	1.01	1.00	1.01	1.00
C	3.37E15	2.01E15	1.00	0.99	0.99	0.98

All values normalized to Case I.

TABLE 5.5 Fuel Pin Heating in Adjacent Fuel Assemblies Calculations for Power Level of 291 MW						
ASSEMBLY 2304						
POS	I	II	III	IV	V	VI
A	6.826	7.864	7.989	7.141	7.058	6.908
B	6.759	7.536	7.539	6.906	6.894	6.712
C	6.514	7.081	7.034	6.801	6.657	6.651
D	6.812	7.582	7.585	7.176	7.119	6.969
E	6.850	7.309	7.296	6.912	6.843	6.843
F	6.624	6.902	6.976	6.822	6.710	6.670
ASSEMBLY 3301						
POS	I	II	III	IV	V	VI
A	6.826	7.532	7.252	7.000	6.965	6.812
B	6.922	7.926	7.946	7.293	7.233	6.922
C	7.006	8.330	8.113	7.432	7.461	7.020
D	6.928	7.413	7.232	6.929	7.039	7.157
E	6.861	7.691	7.441	7.265	7.231	7.225
F	7.050	7.959	7.970	7.435	7.381	7.233

The numbers above have units of kW/ft and are the average of three pins (four for location F), with locations shown on Figures 5.4 and 5.5.

Case descriptions are found on Table 5.1.

tables. Each location is comprised of three to four pins, averaged in the interest of better statistics. Table 5.5 shows that the maximum linear pin heating during the test should never be too high to forbid

test irradiation. As would be expected, the peak power levels in the fuel pins are highest in the pins nearest the moderated test canister (the A group pins in assembly 2304 and the C group pins in assembly 3301).

Table 5.6 lists the radial peaking factor of each pin for Cases I through VI. This number is the ratio of the individual pin heating to the average pin heating for the entire assembly. Tables 5.7 and 5.8 show the linear peak heating and radial peaking factor for Cases I and II for each individual fuel pin. Tables 5.5 and 5.6 are a convenient summary of the details present in Tables 5.7 and 5.8.

TABLE 5.6						
Fuel Pin to Assembly Heating Ratio in Adjacent Fuel Assemblies Calculations for Power Level of 291 MW						
ASSEMBLY 2304						
POS	I	II	III	IV	V	VI
A	0.984	1.111	1.134	1.022	1.016	0.995
B	0.975	1.065	1.070	0.988	0.992	0.967
C	0.939	1.000	0.999	0.973	0.958	0.958
D	0.982	1.071	1.077	1.027	1.025	1.004
E	0.988	0.033	1.036	0.989	0.985	0.986
F	0.955	0.975	0.991	0.976	0.966	0.961
ASSEMBLY 3301						
POS	I	II	III	IV	V	VI
A	0.926	0.993	0.967	0.944	0.941	0.981
B	0.939	1.045	1.060	0.983	0.977	0.997
C	0.951	1.098	1.082	1.002	1.008	1.011
D	0.940	0.977	0.965	0.934	0.951	1.031
E	0.931	1.014	0.992	0.979	0.977	1.041
F	0.957	1.049	1.063	1.002	0.997	1.042
The numbers above are the average of three pins (four for location F), with locations shown on Figures 5.4 and 5.5. Case descriptions are found on Table 5.1.						

It can be seen from Table 5.4 that the peak linear power limit is not exceeded for any case, but that the impact of the yttrium hydride is noticeable. Pin heating rates increase by 15 percent for the full-length yttrium hydride and less than 5 percent for the 6 inch model and are far below the limit of 14.3 kW/ft. The effect of increasing the thickness of the stainless steel sleeve again appears to be negligible. As would be expected, the impact on the fuel pins was lowest in the cases where only 6 inches of the MOTA canister was modeled with yttrium hydride moderator. This effectively reduced the amount of moderator by a factor of six. In the Case IV test, the heating in the assembly 2304 A group pins only increased by 4.6 percent when the moderated test canister was added. However, tallies were made on 6 inch segments of the fuel pins for Cases IV and VI, and the heating in the segment nearest the yttrium hydride was less than the peak heating calculated for that pin. This would suggest that the multiplication factor of 1.22 yields conservative estimates of the linear peak heating.

Table 5.5 shows the impact of the yttrium hydride moderator on radial peaking factors. These calculations indicate that, at most, the radial peaking factors will be on the order of 1.05. Typical radial peaking factors for these same core locations are 1.04 to 1.06. Again, a thicker canister sleeve had insignificant impact on the radial peaking factor, and as would be expected, the peaking factor decreases in the 6 inch model.

For Case IV, the power deposited by the adjacent assembly over the 36 inch length was less than 1.0 percent higher than Case I with no

TABLE 5.7 Peak Heating in Individual Pins in Adjacent Fuel Assemblies Test Assembly in Position 2406 Without YH _{1,8}					
ASSEMBLY 2304					
POS	UNCERT	PIN HEAT (kW/ft)	PEAK HEAT (kW/ft)	PEAK HEAT (400 MW)	PIN/ASSEM. HEAT RATIO
1	0.015	5.643	6.884	9.463	0.993
2	0.017	5.651	6.894	9.477	0.994
3	0.024	5.750	7.015	9.643	1.011
4	0.015	5.544	6.764	9.297	0.975
5	0.015	5.406	6.595	9.066	0.951
6	0.014	5.455	6.655	9.148	0.960
7	0.016	5.308	6.476	8.902	0.934
8	0.017	5.382	6.566	9.026	0.947
9	0.015	5.217	6.365	8.749	0.918
10	0.014	5.816	7.096	9.754	1.023
11	0.014	5.680	6.930	9.526	0.999
12	0.014	5.635	6.875	9.450	0.991
13	0.014	5.499	6.709	9.222	0.967
14	0.014	5.523	6.738	9.263	0.972
15	0.015	5.501	6.711	9.226	0.968
16	0.016	5.44	6.640	9.128	0.958
17	0.016	5.556	6.783	9.325	0.978
18	0.017	5.470	6.673	9.174	0.962
19	0.021	5.291	6.455	8.874	0.931
ASSEMBLY 3301					
POS	UNCERT	PIN HEAT (kW/ft)	PEAK HEAT (kW/ft)	PEAK HEAT (400 MW)	PIN/ASSEM. HEAT RATIO
1	0.016	5.654	6.898	9.482	0.936
2	0.015	5.712	5.969	9.580	0.946
3	0.015	5.698	5.952	9.556	0.943
4	0.014	5.746	7.010	9.637	0.951
5	0.015	5.824	7.105	9.767	0.964
6	0.015	5.927	7.231	9.940	0.981
7	0.015	5.841	7.126	9.796	0.967
8	0.014	5.856	7.144	9.821	0.970
9	0.015	5.871	7.163	9.846	0.972
10	0.018	5.534	6.751	9.281	0.916
11	0.016	5.687	6.938	9.538	0.942
12	0.015	5.822	7.103	9.764	0.964
13	0.014	5.676	6.925	9.519	0.940
14	0.014	5.814	7.093	9.751	0.963
15	0.015	5.968	7.281	10.009	0.988
16	0.016	5.942	7.249	9.965	0.984
17	0.014	5.941	7.248	9.964	0.984
18	0.014	5.914	7.215	9.918	0.979
19	0.016	5.995	7.314	10.054	0.993
All calculations are at 291 MW unless specified otherwise.					

yttrium hydride moderator at all.

TABLE 5.8
Peak Heating in Individual Pins in Adjacent Fuel Assemblies
Test Assembly in Position 2406 With YH_{1,8}

ASSEMBLY 2304					
POS	UNCERT	PIN HEAT (kW/ft)	PEAK HEAT (kW/ft)	PEAK HEAT (400 MW)	PIN/ASSEM. HEAT RATIO
1	0.028	6.562	8.006	11.004	1.131
2	0.025	6.623	8.080	11.107	1.142
3	0.019	6.154	7.508	10.320	1.061
4	0.024	6.268	7.647	10.511	1.080
5	0.022	6.247	7.600	10.476	1.077
6	0.021	6.010	7.332	10.079	1.036
7	0.022	6.026	7.352	10.105	1.039
8	0.027	5.802	7.078	9.730	1.000
9	0.022	5.588	6.817	9.371	0.963
10	0.018	6.173	7.531	10.352	1.064
11	0.020	6.264	7.642	10.505	1.080
12	0.017	6.200	7.564	10.397	1.069
13	0.017	6.077	7.414	10.191	1.047
14	0.020	6.060	7.393	10.162	1.044
15	0.017	5.829	7.111	9.775	1.005
16	0.020	5.708	6.964	9.572	0.984
17	0.017	5.780	7.052	9.693	0.996
18	0.020	5.597	6.828	9.386	0.965
19	0.026	5.552	6.773	9.311	0.951
ASSEMBLY 3301					
POS	UNCERT	PIN HEAT (kW/ft)	PEAK HEAT (kW/ft)	PEAK HEAT (400 MW)	PIN/ASSEM. HEAT RATIO
1	0.019	6.047	7.377	10.141	0.973
2	0.025	6.159	7.514	10.328	0.991
3	0.030	6.316	7.706	10.592	1.016
4	0.021	6.449	7.868	10.815	1.037
5	0.019	6.370	7.771	10.682	1.025
6	0.023	6.671	8.139	11.187	1.073
7	0.025	6.698	8.172	11.232	1.077
8	0.027	6.672	7.140	11.189	1.073
9	0.033	7.121	8.688	11.942	1.145
10	0.019	6.003	7.324	10.067	0.966
11	0.020	6.015	7.338	10.087	0.968
12	0.018	6.203	7.568	10.402	0.998
13	0.025	6.295	7.680	10.557	1.013
14	0.018	6.307	7.685	10.577	1.014
15	0.017	6.318	7.708	10.595	1.016
16	0.019	6.490	7.918	10.884	1.044
17	0.025	6.618	8.074	11.098	1.065
18	0.016	6.448	7.867	10.813	1.037
19	0.020	6.545	7.985	10.976	1.053
All calculations are at 291 MW unless specified otherwise.					

5.5.0 CONCLUSIONS

The MCNP calculations for the proposed isotope production test within the MOTA canister produced a large quantity of data. Much of the data has been tabulated and summarized.

5.5.1 Discussion of Results

Preliminary results show that the effect of the yttrium hydride on isotope production is most prominent in the reaction rates involving ^{186}W , ^{187}W , and ^{188}W . The addition of the moderator resulted in an increase in the capture rate by a factor of approximately 15. The ^{152}Gd and ^{185}Re reaction rates increased by a factor of about seven. All other isotopic reaction rates increased by a factor of only two or three (see Table 5.1).

The calculations show that heating in adjacent fuel pins does occur but is not significantly greater than would be observed without the excess moderator. The fuel pin radial peaking factor increase would be 5 percent or less for a single yttrium hydride canister.

There is possibly a significant impact on surrounding tritium production experiments in adjacent MOTA canisters. It was calculated that at the proposed yttrium hydride annular thickness of 0.514 cm; the $^6\text{Li} (n,\alpha)$ reaction rate would increase almost 40 percent in the nearest canisters. This drops considerably as distance between the experiments increases -- down to only an 11 percent increase in the far canister (Canister C in Figure 5.1). The calculations show that the most effective means of reducing the impact on surrounding tritium experiments would be to reduce the yttrium hydride content. However,

doing so was shown to dramatically affect the reaction rates for nuclides of interest.

5.5.2 MOTA Calculations Application

The test assembly was irradiated in the MOTA facility during the spring of 1991. Enough ^{153}Gd was produced in the targets of the special test assembly to market.¹⁵ It was sold to Amersham International, a pharmaceutical firm based in England. Concurrent to this was an apparent worldwide shortage of this radioisotope which is used extensively in bone scanning imaging machines for the detection of osteoporosis. In June 1991, Amersham International received the first shipment of the ^{153}Gd which will operate the diagnostic machines for several years.

REFERENCES

1. Cabell, C. P., "A Summary Description of the Fast Flux Test Facility," Westinghouse Hanford Company report HEDL-400, December 1980.
2. Breismeister, J. F., Editor, "MCNP - A General Monte Carlo Code for Neutron and Photon Transport, Version 3A," LA-7369-M, Rev.2, Los Alamos National Laboratory, Los Alamos, New Mexico, 1986. [Changes to this documentation for Version 3B and 4 have also been issued.]
3. Metropolis, N., "The Beginning of the Monte Carlo Method," *Los Alamos Science - Special Issue*, 1987.
4. Carter, L. L. and Cashwell, E. D., "Particle Transport Simulation with the Monte Carlo Method," ERDA Critical Review Series, U.S. Energy Research and Development Administration, Technical Information Center, Oak Ridge, Tennessee, 1975.
5. Brissenden, R. J. and Garlick, A. R., "Biases in the Estimation of K_{eff} and Its Error by Monte Carlo Methods," *Annals of Nuclear Energy*, 13, No. 2, pp. 63-83, 1986.
6. Bowsher, H., Gelbard, E. M., Gemmel, P. and Pack, G., "Magnitude of Bias in Monte Carlo Eigenvalue Calculations," *Trans. Am. Nucl. Soc.*, Vol. 45, p. 324, 1983.
7. Gast, R. C. and Candelore, N. R., "Monte Carlo Eigenfunction Strategies and Uncertainties," ANL-75-2, Argonne National Laboratory, Argonne, Illinois, 1974.
8. Macmillan, D. B., "Monte Carlo Confidence Limits for Iterated - Source Calculations," *Nucl. Sci. Eng.*, Vol. 50, p. 219, 1973.
9. Ting, G., "Status of Radioisotope Production and Applications in Taiwan," *Trans. Am. Nucl. Soc. - 7th Pacific Basin Nucl. Conf.*, Vol. 61, pp. 398-406, 1990.
10. Schenter, R. E., "Comparison of Medical Isotope Production in Fast and Thermal Reactor Systems," Westinghouse Hanford Company report, WHC-SA-0956-FP, Nov., 1990.
11. Schenter, R. E. and Myjak, M. A., "Isotope Production in the FFTF by Neutron Transmutation," Westinghouse Hanford Company report, WHC-SA-0291, Dec., 1987.
12. "Oak Ridge National Laboratory Radioisotope Price List," Oak Ridge National Laboratory, March, 1989.

REFERENCES cont.

13. Schwarz, R. A., "Calculational Methods used in Determining Reaction Rates in the Multi-Isotope Production Assembly," M. S. Thesis, University of Washington, 1990.
14. Lamarsh, J. R., "Introduction to Nuclear Engineering," 2nd Edition, Addison-Wesley, Mass., 1983.
15. Druby, M., "FFTF Gadolinium for World Medicine," Hanford Reach, July 15, 1990.

APPENDIX A

APPENDIX A

DENOMAKUE Source Listing

```

c program denomakue
c A program to massage data from MCNP runs
c written by T. L. Miles
c July of 1989
c update: March of 1990
c update: July of 1990
c DENOMAKUE is a program to DEtermine the NOnconservative MAGnitude
c of Kcode Uncertainty Estimates.
c This program will determine the variation between cells located
c in congruent geometrical and material environments, to assess the
c bias involved in using a KCODE card as a neutron source. This
c is accomplished by calculating the percentage of cells in a
c variety of runs which differ from the expected "true" value by
c more than two standard deviations. The true values were found by
c running an MCNP problem for 200 SUN hours (20 CRAY hours) with the
c following parameters.
c importances of 1.0 in the fuel region
c 0.5 in the reflector region
c 0.0 in the universe (void)
c 5000 neutrons per generation
c This program has been updated a number of times to
c 1) Allow the skipping of cycles in the calculations to
c increase the number of neutrons in each "tally". This
c will increase the accuracy, but decrease the number of
c tallies contributing to the result.
c 2) Input a multiplier which will increase the given standard
c deviation. This will allow for the iterative determination
c of the factor by which the code underestimates the relative
c error.
c
c the dimensioning and declaring of variables
c integer t
c character acyc*7, acycl*13, atln*10, btln*10, todd*7
c character camille*1, u*1
c dimension acel(200,30), bcel(200,30), atal(200,30), atale(200,30)
c dimension btal(200,30), btale(200,30), bhtal(200,30)
c dimension bhtale(200,30), btal(200,30), btale(200,30)
c dimension bti(200,30), bto(200,30), btc(200,30), bhi(200,30)
c dimension bho(200,30), bhc(200,30), bli(200,30), blo(200,30)
c dimension blc(200,30), ai(200,30), ao(200,30), ac(200,30)
c dimension fs(200,30), dfda(200,30), fsd(200,30), dff(200,30)
c dimension dfdbl(200,30), fsbl(200,30), fsdbl(200,30)
c dimension dffbl(200,30), dfdbh(200,30), fsbh(200,30)
c dimension fsdbh(200,30), dffbh(200,30), dfdbt(200,30)
c dimension fsbt(200,30), fsdbt(200,30), dffbt(200,30)
c dimension dffc(200,30), dffblo(200,30), dffi(200,30)
c dimension dffbhc(200,30), dffbhi(200,30), dffbho(200,30)
c dimension dffbto(200,30), dffbtc(200,30), dffbti(200,30)
c dimension dfdac(200,30), dfdao(200,30), dfdai(200,30)
c dimension dfdblc(200,30), dfdblo(200,30), dfdbli(200,30)
c dimension dfdbhc(200,30), dfdbho(200,30), dfdbhi(200,30)
c dimension dfdbtc(200,30), dfdbto(200,30), dfdbti(200,30)
c dimension perac(200,30), perao(200,30), perai(200,30)
c dimension perblc(200,30), perblo(200,30), perbli(200,30)
c dimension perbhc(200,30), perbho(200,30), perbhi(200,30)
c dimension perbtc(200,30), perbto(200,30), perbti(200,30)
c implicit double precision (a-b,d,f)
c implicit double precision (t)
c the opening of the various files

```

```

c   open 31 for 'inp', open 32 for 'check', open 33 for mcnp output
   open(31,file='inp', form='formatted', access='sequential',
   lstatus='old')
   open(32,file='check', form='formatted', access='sequential',
   lstatus='old')
   open(33,file='mass', form='formatted', access='sequential',
   lstatus='new')
   l=0

c
   print *, "what is maximum number of intervals tallied over?"
   read *, talm
c   read the standard deviation multiplier
   print *, "enter standard deviation multiplier (1.0)"
   read *, standev
c   read output and locate the tally number
5  read(32,901) todd, acyc, camille
   if(acyc.eq."cycle =") then
   if(camille.eq."0") then
   ij=1
   else
   ij=0
   endif
   backspace 32
   read(32, 902) acycl
   goto 5
   elseif(acyc.eq."ate of") then
   goto 10
   elseif(acyc.eq."eation") then
   goto 10
c   elseif(todd.eq."endfile") then
c   goto 7
   else
   goto 5
   endif

c
c   read output and look for tally 34
10 if(ij.eq.0) then
   goto 37
   endif
   write(33,903) acycl
   l=l+1
15 read(32,900) atln
   if(atln.ne."tally 34") then
   goto 15
   endif
   write(33,904) atln

c
c   read output and locate cell and tally marks
   do 20 i = 1, 16
   read(32,905)
20  continue
   do 25 i = 1, 30
   read(32, 905) acel(1,i)
   read(32, 906)
   read(32, 906) atal(1,i), atale(1,i)
   read(32, 906)
25  continue
   do 30 i = 1, 30
   write(33,907) acel(1,i), atal(1,i), atale(1,i)
30  continue

c
c   look for and locate tally 67
40 read(32,900) btln
   if(btln.ne."tally 67") then
   goto 40

```

```

endif
write(33,904) btln
do 45 i = 1, 16
  read(32,908)
45 continue
c
c read and store tally 67 marks
do 50 i = 1, 30
  read(32, 905) bcel(1,i)
  read(32, 908)
  read(32, 908)
  read(32, 908) bltal(1,i), bltale(1,i)
  read(32, 908) bhthal(1,i), bhtale(1,i)
  read(32, 908) bttal(1,i), bttale(1,i)
  read(32, 908)
50 continue
do 36 i = 1, 30
  write(33, 928) bcel(1,i), bltal(1,i), bltale(1,i)
  write(33, 929) bcel(1,i), bhthal(1,i), bhtale(1,i)
  write(33, 930) bcel(1,i), bttal(1,i), bttale(1,i)
36 continue
do 22 i = 1, 30
  atale(1,i) = atale(1,i) * standev
  bltale(1,i) = bltale(1,i) * standev
  bhtale(1,i) = bhtale(1,i) * standev
  bttale(1,i) = bttale(1,i) * standev
22 continue
if(talm.eq.1) then
  goto 7
endif
37 goto 5
c
c routine to determine the intervals to be summed over
7 print *, "Which frequency of cycles read are to be summed over"
  read *, t
  print *, "Is there spatial or energy biasing? (y or n)"
  read *, u
c
c routine to calculate the standard deviation
c variable descriptions
c tca = tally cornercells a(34)
c toa = tally outercells
c tia = tally innercells
c tc1b = tally corners lowenergy (b67)
c to1b = tally outercells lowenergy
c ti1b = tally innercells lowenergy
c tchb = tally cornercells highenergy
c tctb = tally cornercells totalenergy
c v = average
38 write(33,909) l
do 121 i = 1, 30
  fs(t,i)=(atal(t,i)**2) * (t*50000*(atale(t,i)**2)+1)
  fsbl(t,i)=(bltal(t,i)**2) * (t*50000*(bltale(t,i)**2)+1)
  fsbh(t,i)=(bhthal(t,i)**2) * (t*50000*(bhtale(t,i)**2)+1)
  fsbt(t,i)=(bttal(t,i)**2) * (t*50000*(bttale(t,i)**2)+1)
  dfda(t,i)=atal(t,i)
  dfdbl(t,i)=bltal(t,i)
  dfdbh(t,i)=bhthal(t,i)
  dfdbt(t,i)=bttal(t,i)
  dff(t,i) = atal(t,i)*atale(t,i)
  dffbl(t,i) = bltal(t,i)*bltale(t,i)
  dffbh(t,i) = bhthal(t,i)*bhtale(t,i)
  dffbt(t,i) = bttal(t,i)*bttale(t,i)
121 continue
200 do 41 j = 2*t, 1, t

```

```

n=j*50000
  do 39 i = 1, 30
    p=t*50000
    dfda(j,i)=(atal(j,i)*j - atal(j-t,i)*(j-t))/t
    fs(j,i) = (atal(j,i)**2) * (n*(atale(j,i)**2)+1)
    fsd(j,i) =(abs(fs(j,i)*j - fs(j-t,i)*(j-t)))/t
    dff(j,i) = sqrt(fsd(j,i)-dfda(j,i)**2)/sqrt(p)
39  continue
41  continue
  do 42 j = t*2, 1, t
    n=j*50000
    do 43 i = 1, 30
      p = t*50000
      dfdbl(j,i) = (bltal(j,i)*j - bltal(j-t,i)*(j-t))/t
      fsbl(j,i) = (bltal(j,i)**2) * (n*(bltale(j,i)**2)+1)
      fsdbl(j,i) = (abs(fsbl(j,i)*j - fsbl(j-t,i)*(j-t)))/t
      dffbl(j,i) = sqrt(fsdbl(j,i) - dfdbl(j,i)**2)/sqrt(p)
43  continue
42  continue
  do 44 j = t*2, 1, t
    n=j*50000
    do 126 i = 1, 30
      p = t*50000
      dfdbh(j,i) = (bhtal(j,i)*j - bhtal(j-t,i)*(j-t))/t
      fsbh(j,i) = bhtal(j,i)**2 * (n*(bhtale(j,i)**2)+1)
      fsdbh(j,i) = (abs(fsbh(j,i)*j - fsbh(j-t,i)*(j-t)))/t
      dffbh(j,i) = sqrt(fsdbh(j,i) - dfdbh(j,i)**2)/sqrt(p)
126  continue
44  continue
  do 46 j = t*2, 1, t
    n=j*50000
    do 47 i = 1, 30
      p = t*50000
      dfdbt(j,i) = (bttal(j,i)*j - bttal(j-t,i)*(j-t))/t
      fsbt(j,i) = (bttal(j,i)**2)*(n*(bttale(j,i)**2)+1)
      fsdbt(j,i) = (abs(fsbt(j,i)*j - fsbt(j-t,i)*(j-t)))/t
      dffbt(j,i) = sqrt(fsdbt(j,i)-dfdbt(j,i)**2)/sqrt(p)
47  continue
46  continue
c
c  the storage of the "true value"
520  truac = 1.02079E-8
    truo = 1.21795E-8
    truai = 1.30317E-8
    trublc = 1.14203E-22
    trubhc = 1.11286E-25
    trubtc = 1.14836E-22
    trublo = 9.57571E-23
    trubho = 1.34845E-25
    trubto = 9.58917E-23
    trubli = 1.01729E-22
    trubhi = 1.43734E-25
    trubti = 1.01871E-22
c
c  normalize all array values to 1-12 rather than 1,5,6, etc
  if(u.eq."y") then
    goto 66
  endif
  do 65 i = 1, 1
    dffc(i,1) = dff(i,3)
    dffc(i,2) = dff(i,8)
    dffc(i,3) = dff(i,13)
    dffc(i,4) = dff(i,18)
    dffc(i,5) = dff(i,23)
    dffc(i,6) = dff(i,28)

```

```
dfdac(i,1) = dfda(i,3)
dfdac(i,2) = dfda(i,8)
dfdac(i,3) = dfda(i,13)
dfdac(i,4) = dfda(i,18)
dfdac(i,5) = dfda(i,23)
dfdac(i,6) = dfda(i,28)
dffblc(i,1) = dffbl(i,3)
dffblc(i,2) = dffbl(i,8)
dffblc(i,3) = dffbl(i,13)
dffblc(i,4) = dffbl(i,18)
dffblc(i,5) = dffbl(i,23)
dffblc(i,6) = dffbl(i,28)
dfdblc(i,1) = dfdbl(i,3)
dfdblc(i,2) = dfdbl(i,8)
dfdblc(i,3) = dfdbl(i,13)
dfdblc(i,4) = dfdbl(i,18)
dfdblc(i,5) = dfdbl(i,23)
dfdblc(i,6) = dfdbl(i,28)
dffbhc(i,1) = dffbh(i,3)
dffbhc(i,2) = dffbh(i,8)
dffbhc(i,3) = dffbh(i,13)
dffbhc(i,4) = dffbh(i,18)
dffbhc(i,5) = dffbh(i,23)
dffbhc(i,6) = dffbh(i,28)
dfdbhc(i,1) = dfdbh(i,3)
dfdbhc(i,2) = dfdbh(i,8)
dfdbhc(i,3) = dfdbh(i,13)
dfdbhc(i,4) = dfdbh(i,18)
dfdbhc(i,5) = dfdbh(i,23)
dfdbhc(i,6) = dfdbh(i,28)
dffbtc(i,1) = dffbt(i,3)
dffbtc(i,2) = dffbt(i,8)
dffbtc(i,3) = dffbt(i,13)
dffbtc(i,4) = dffbt(i,18)
dffbtc(i,5) = dffbt(i,23)
dffbtc(i,6) = dffbt(i,28)
dfdbtc(i,1) = dfdbt(i,3)
dfdbtc(i,2) = dfdbt(i,8)
dfdbtc(i,3) = dfdbt(i,13)
dfdbtc(i,4) = dfdbt(i,18)
dfdbtc(i,5) = dfdbt(i,23)
dfdbtc(i,6) = dfdbt(i,28)
dffo(i,1) = dff(i,2)
dffo(i,2) = dff(i,4)
dffo(i,3) = dff(i,7)
dffo(i,4) = dff(i,9)
dffo(i,5) = dff(i,12)
dffo(i,6) = dff(i,14)
dffo(i,7) = dff(i,17)
dffo(i,8) = dff(i,19)
dffo(i,9) = dff(i,22)
dffo(i,10) = dff(i,24)
dffo(i,11) = dff(i,27)
dffo(i,12) = dff(i,29)
dfdao(i,1) = dfda(i,2)
dfdao(i,2) = dfda(i,4)
dfdao(i,3) = dfda(i,7)
dfdao(i,4) = dfda(i,9)
dfdao(i,5) = dfda(i,12)
dfdao(i,6) = dfda(i,14)
dfdao(i,7) = dfda(i,17)
dfdao(i,8) = dfda(i,19)
dfdao(i,9) = dfda(i,22)
dfdao(i,10) = dfda(i,24)
dfdao(i,11) = dfda(i,27)
```

```

dfdao(i,12) = dfda(i,29)
dffblo(i,1) = dffbl(i,2)
dffblo(i,2) = dffbl(i,4)
dffblo(i,3) = dffbl(i,7)
dffblo(i,4) = dffbl(i,9)
dffblo(i,5) = dffbl(i,12)
dffblo(i,6) = dffbl(i,14)
dffblo(i,7) = dffbl(i,17)
dffblo(i,8) = dffbl(i,19)
dffblo(i,9) = dffbl(i,22)
dffblo(i,10) = dffbl(i,24)
dffblo(i,11) = dffbl(i,27)
dffblo(i,12) = dffbl(i,29)
dfdblo(i,1) = dfdbl(i,2)
dfdblo(i,2) = dfdbl(i,4)
dfdblo(i,3) = dfdbl(i,7)
dfdblo(i,4) = dfdbl(i,9)
dfdblo(i,5) = dfdbl(i,12)
dfdblo(i,6) = dfdbl(i,14)
dfdblo(i,7) = dfdbl(i,17)
dfdblo(i,8) = dfdbl(i,19)
dfdblo(i,9) = dfdbl(i,22)
dfdblo(i,10) = dfdbl(i,24)
dfdblo(i,11) = dfdbl(i,27)
dfdblo(i,12) = dfdbl(i,29)
dffbho(i,1) = dffbh(i,2)
dffbho(i,2) = dffbh(i,4)
dffbho(i,3) = dffbh(i,7)
dffbho(i,4) = dffbh(i,9)
dffbho(i,5) = dffbh(i,12)
dffbho(i,6) = dffbh(i,14)
dffbho(i,7) = dffbh(i,17)
dffbho(i,8) = dffbh(i,19)
dffbho(i,9) = dffbh(i,22)
dffbho(i,10) = dffbh(i,24)
dffbho(i,11) = dffbh(i,27)
dffbho(i,12) = dffbh(i,29)
dfdbho(i,1) = dfdbh(i,2)
dfdbho(i,2) = dfdbh(i,4)
dfdbho(i,3) = dfdbh(i,7)
dfdbho(i,4) = dfdbh(i,9)
dfdbho(i,5) = dfdbh(i,12)
dfdbho(i,6) = dfdbh(i,14)
dfdbho(i,7) = dfdbh(i,17)
dfdbho(i,8) = dfdbh(i,19)
dfdbho(i,9) = dfdbh(i,22)
dfdbho(i,10) = dfdbh(i,24)
dfdbho(i,11) = dfdbh(i,27)
dfdbho(i,12) = dfdbh(i,29)
dffbto(i,1) = dffbt(i,2)
dffbto(i,2) = dffbt(i,4)
dffbto(i,3) = dffbt(i,7)
dffbto(i,4) = dffbt(i,9)
dffbto(i,5) = dffbt(i,12)
dffbto(i,6) = dffbt(i,14)
dffbto(i,7) = dffbt(i,17)
dffbto(i,8) = dffbt(i,19)
dffbto(i,9) = dffbt(i,22)
dffbto(i,10) = dffbt(i,24)
dffbto(i,11) = dffbt(i,27)
dffbto(i,12) = dffbt(i,29)
dfdbto(i,1) = dfdbt(i,2)
dfdbto(i,2) = dfdbt(i,4)
dfdbto(i,3) = dfdbt(i,7)
dfdbto(i,4) = dfdbt(i,9)

```

```

dfdbto(i,5) = dfdbt(i,12)
dfdbto(i,6) = dfdbt(i,14)
dfdbto(i,7) = dfdbt(i,17)
dfdbto(i,8) = dfdbt(i,19)
dfdbto(i,9) = dfdbt(i,22)
dfdbto(i,10) = dfdbt(i,24)
dfdbto(i,11) = dfdbt(i,27)
dfdbto(i,12) = dfdbt(i,29)
dffi(i,1) = dff(i,1)
dffi(i,2) = dff(i,5)
dffi(i,3) = dff(i,6)
dffi(i,4) = dff(i,10)
dffi(i,5) = dff(i,11)
dffi(i,6) = dff(i,15)
dffi(i,7) = dff(i,16)
dffi(i,8) = dff(i,20)
dffi(i,9) = dff(i,21)
dffi(i,10) = dff(i,25)
dffi(i,11) = dff(i,26)
dffi(i,12) = dff(i,30)
dfdai(i,1) = dfda(i,1)
dfdai(i,2) = dfda(i,5)
dfdai(i,3) = dfda(i,6)
dfdai(i,4) = dfda(i,10)
dfdai(i,5) = dfda(i,11)
dfdai(i,6) = dfda(i,15)
dfdai(i,7) = dfda(i,16)
dfdai(i,8) = dfda(i,20)
dfdai(i,9) = dfda(i,21)
dfdai(i,10) = dfda(i,25)
dfdai(i,11) = dfda(i,26)
dfdai(i,12) = dfda(i,30)
dffbli(i,1) = dffbl(i,1)
dffbli(i,2) = dffbl(i,5)
dffbli(i,3) = dffbl(i,6)
dffbli(i,4) = dffbl(i,10)
dffbli(i,5) = dffbl(i,11)
dffbli(i,6) = dffbl(i,15)
dffbli(i,7) = dffbl(i,16)
dffbli(i,8) = dffbl(i,20)
dffbli(i,9) = dffbl(i,21)
dffbli(i,10) = dffbl(i,25)
dffbli(i,11) = dffbl(i,26)
dffbli(i,12) = dffbl(i,30)
dfdbli(i,1) = dfdbl(i,1)
dfdbli(i,2) = dfdbl(i,5)
dfdbli(i,3) = dfdbl(i,6)
dfdbli(i,4) = dfdbl(i,10)
dfdbli(i,5) = dfdbl(i,11)
dfdbli(i,6) = dfdbl(i,15)
dfdbli(i,7) = dfdbl(i,16)
dfdbli(i,8) = dfdbl(i,20)
dfdbli(i,9) = dfdbl(i,21)
dfdbli(i,10) = dfdbl(i,25)
dfdbli(i,11) = dfdbl(i,26)
dfdbli(i,12) = dfdbl(i,30)
dffbhi(i,1) = dffbh(i,1)
dffbhi(i,2) = dffbh(i,5)
dffbhi(i,3) = dffbh(i,6)
dffbhi(i,4) = dffbh(i,10)
dffbhi(i,5) = dffbh(i,11)
dffbhi(i,6) = dffbh(i,15)
dffbhi(i,7) = dffbh(i,16)
dffbhi(i,8) = dffbh(i,20)
dffbhi(i,9) = dffbh(i,21)

```

```

dffbhi(i,10) = dffbh(i,25)
dffbhi(i,11) = dffbh(i,26)
dffbhi(i,12) = dffbh(i,30)
dfdbhi(i,1) = dfdbh(i,1)
dfdbhi(i,2) = dfdbh(i,5)
dfdbhi(i,3) = dfdbh(i,6)
dfdbhi(i,4) = dfdbh(i,10)
dfdbhi(i,5) = dfdbh(i,11)
dfdbhi(i,6) = dfdbh(i,15)
dfdbhi(i,7) = dfdbh(i,16)
dfdbhi(i,8) = dfdbh(i,20)
dfdbhi(i,9) = dfdbh(i,21)
dfdbhi(i,10) = dfdbh(i,25)
dfdbhi(i,11) = dfdbh(i,26)
dfdbhi(i,12) = dfdbh(i,30)
dffbti(i,1) = dffbt(i,1)
dffbti(i,2) = dffbt(i,5)
dffbti(i,3) = dffbt(i,6)
dffbti(i,4) = dffbt(i,10)
dffbti(i,5) = dffbt(i,11)
dffbti(i,6) = dffbt(i,15)
dffbti(i,7) = dffbt(i,16)
dffbti(i,8) = dffbt(i,20)
dffbti(i,9) = dffbt(i,21)
dffbti(i,10) = dffbt(i,25)
dffbti(i,11) = dffbt(i,26)
dffbti(i,12) = dffbt(i,30)
dfdbti(i,1) = dfdbt(i,1)
dfdbti(i,2) = dfdbt(i,5)
dfdbti(i,3) = dfdbt(i,6)
dfdbti(i,4) = dfdbt(i,10)
dfdbti(i,5) = dfdbt(i,11)
dfdbti(i,6) = dfdbt(i,15)
dfdbti(i,7) = dfdbt(i,16)
dfdbti(i,8) = dfdbt(i,20)
dfdbti(i,9) = dfdbt(i,21)
dfdbti(i,10) = dfdbt(i,25)
dfdbti(i,11) = dfdbt(i,26)
dfdbti(i,12) = dfdbt(i,30)
65 continue
   goto 68
66 do 67 i = 1, 1
      dffc(i,1) = dff(i,13)
      dffc(i,2) = dff(i,18)
      dfdac(i,1) = dfda(i,13)
      dfdac(i,2) = dfda(i,18)
      dffblc(i,1) = dffbl(i,13)
      dffblc(i,2) = dffbl(i,18)
      dfdblc(i,1) = dfdbl(i,13)
      dfdblc(i,2) = dfdbl(i,18)
      dffbhc(i,1) = dffbh(i,13)
      dffbhc(i,2) = dffbh(i,18)
      dfdbhc(i,1) = dfdbh(i,13)
      dfdbhc(i,2) = dfdbh(i,18)
      dffbtc(i,1) = dffbt(i,13)
      dffbtc(i,2) = dffbt(i,18)
      dfdbtc(i,1) = dfdbt(i,13)
      dfdbtc(i,2) = dfdbt(i,18)
      dffo(i,1) = dff(i,14)
      dffo(i,2) = dff(i,17)
      dfdao(i,1) = dfda(i,14)
      dfdao(i,2) = dfda(i,17)
      dffblo(i,1) = dffbl(i,14)
      dffblo(i,2) = dffbl(i,17)
      dfdblo(i,1) = dfdbl(i,14)

```

```

dfdblo(i,2) = dfdbl(i,17)
dffbho(i,1) = dffbh(i,14)
dffbho(i,2) = dffbh(i,17)
dfdbho(i,1) = dfdbh(i,14)
dfdbho(i,2) = dfdbh(i,17)
dffbto(i,1) = dffbt(i,14)
dffbto(i,2) = dffbt(i,17)
dfdbto(i,1) = dfdbt(i,14)
dfdbto(i,2) = dfdbt(i,17)
dff(i,1) = dff(i,15)
dff(i,2) = dff(i,16)
fdai(i,1) = fdai(i,15)
fdai(i,2) = fdai(i,16)
dffbli(i,1) = dffbl(i,15)
dffbli(i,2) = dffbl(i,16)
dfdbli(i,1) = dfdbl(i,15)
dfdbli(i,2) = dfdbl(i,16)
dffbhi(i,1) = dffbh(i,15)
dffbhi(i,2) = dffbh(i,16)
dfdbhi(i,1) = dfdbh(i,15)
dfdbhi(i,2) = dfdbh(i,16)
dffbti(i,1) = dffbt(i,15)
dffbti(i,2) = dffbt(i,16)
dfdbti(i,1) = dfdbt(i,15)
dfdbti(i,2) = dfdbt(i,16)
67 continue
c
c the comparison of "true" values to problem values
68 ac1 = 0
ac2 = 0
ac3 = 0
ao1 = 0
ao2 = 0
ao3 = 0
ai1 = 0
ai2 = 0
ai3 = 0
blc1 = 0
blc2 = 0
blc3 = 0
blo1 = 0
blo2 = 0
blo3 = 0
bli1 = 0
bli2 = 0
bli3 = 0
bhc1 = 0
bhc2 = 0
bhc3 = 0
bho1 = 0
bho2 = 0
bho3 = 0
bhi1 = 0
bhi2 = 0
bhi3 = 0
btc1 = 0
btc2 = 0
btc3 = 0
bto1 = 0
bto2 = 0
bto3 = 0
bti1 = 0
bti2 = 0
bti3 = 0
pac1=0

```

pac2=0
pac3=0
pac4=0
pac5=0
pac6=0
pac7=0
pao1=0
pao2=0
pao3=0
pao4=0
pao5=0
pao6=0
pao7=0
pai1=0
pai2=0
pai3=0
pai4=0
pai5=0
pai6=0
pai7=0
pblc1=0
pblc2=0
pblc3=0
pblc4=0
pblc5=0
pblc6=0
pblc7=0
pblo1=0
pblo2=0
pblo3=0
pblo4=0
pblo5=0
pblo6=0
pblo7=0
pbli1=0
pbli2=0
pbli3=0
pbli4=0
pbli5=0
pbli6=0
pbli7=0
pbhc1=0
pbhc2=0
pbhc3=0
pbhc4=0
pbch5=0
pbhc6=0
pbhc7=0
pbho1=0
pbho2=0
pbho3=0
pbho4=0
pbho5=0
pbho6=0
pbho7=0
pbhi1=0
pbhi2=0
pbhi3=0
pbhi4=0
pbhi5=0
pbhi6=0
pbhi7=0
pbtc1=0
pbtc2=0
pbtc3=0

```

pbtc4=0
pbtc5=0
pbtc6=0
pbtc7=0
pbto1=0
pbto2=0
pbto3=0
pbto4=0
pbto5=0
pbto6=0
pbto7=0
pbti1=0
pbti2=0
pbti3=0
pbti4=0
pbti5=0
pbti6=0
pbti7=0
acm=0
aom=0
aim=0
blcm=0
blom=0
blim=0
bhcm=0
bhom=0
bhim=0
btcm=0
btom=0
btim=0
if(u.eq."y") then
  jc = 2
  jo = 2
  ji = 2
else
  jc = 6
  jo = 12
  ji = 12
endif
do 70 i = t, 1,t
  do 71 j = 1, jc
    if(dffc(i,j).eq.0) then
      goto 71
    endif
    ac(i,j)=abs(truac-dfdac(i,j))/dffc(i,j)
    if(ac(i,j).le.1.645) then
      ac1 = ac1 + 1
    elseif(ac(i,j).le.1.96) then
      ac2 = ac2 + 1
    elseif(ac(i,j).le.2.326) then
      ac3 = ac3+1
    elseif(ac(i,j).gt.2.326) then
      ac4 = ac4 + 1
    endif
71 continue
  do 72 j = 1,jo
    if(dffo(i,j).eq.0) then
      goto 72
    endif
    ao(i,j) = abs(truao-dfdao(i,j))/dffo(i,j)
    if(ao(i,j).le.1.645) then
      ao1 = ao1+1
    elseif(ao(i,j).le.1.96) then
      ao2 = ao2+1
    elseif(ao(i,j).le.2.326) then

```

```

    ao3 = ao3+1
    elseif(ao(i,j).gt.2.326) then
    ao4 = ao4+1
    endif
72 continue
do 73 j = 1,ji
    if(dffi(i,j).eq.0) then
    goto 73
    endif
    ai(i,j)=abs(truai-dfdai(i,j))/dffi(i,j)
    if(ai(i,j).le.1.645) then
    ai1=ai1+1
    elseif(ai(i,j).le.1.96) then
    ai2 = ai2+1
    elseif(ai(i,j).le.2.326) then
    ai3=ai3+1
    elseif(ai(i,j).gt.2.326) then
    ai4 = ai4+1
    endif
73 continue
do 74 j = 1,jc
    if(dffblc(i,j).eq.0) then
    go to 74
    endif
    blc(i,j)=abs(trubl-c-dfdblc(i,j))/dffblc(i,j)
    if(blc(i,j).le.1.645) then
    blc1 = blc1+1
    elseif(blc(i,j).le.1.96) then
    blc2 = blc2 + 1
    elseif(blc(i,j).le.2.326) then
    blc3 = blc3 + 1
    elseif(blc(i,j).gt.2.326) then
    blc4 = blc4 + 1
    endif
74 continue
do 75 j = 1, jo
    if(dffblo(i,j).eq.0) then
    write(33,940)
    goto 75
    endif
    blo(i,j)=abs(trublo-dfdblo(i,j))/dffblo(i,j)
    if(blo(i,j).le.1.645) then
    blo1 = blo1 + 1
    elseif(blo(i,j).le.1.96) then
    blo2 = blo2+1
    elseif(blo(i,j).le.2.326) then
    blo3 = blo3+1
    elseif(blo(i,j).gt.2.326) then
    blo4 = blo4+1
    endif
75 continue
do 76 j = 1, ji
    if(dffbli(i,j).eq.0) then
    goto 76
    endif
    bli(i,j) = abs(trubli-dfdbli(i,j))/dffbli(i,j)
    if(bli(i,j).le.1.645) then
    bli1 = bli1+1
    elseif(bli(i,j).le.1.96) then
    bli2 = bli2+1
    elseif(bli(i,j).le.2.326) then
    bli3 = bli3+1
    elseif(bli(i,j).gt.2.326) then
    bli4 = bli4+1
    endif

```

```

76 continue
  do 77 j = 1, jc
    if(dffbhc(i,j).eq.0) then
      goto 77
    endif
    bhc(i,j)=abs(trubhc-dfdbhc(i,j))/dffbhc(i,j)
    if(bhc(i,j).le.1.645) then
      bhc1=bhc1+1
    elseif(bhc(i,j).le.1.96) then
      bhc2=bhc2+1
    elseif(bhc(i,j).le.2.326) then
      bhc3=bhc3+1
    elseif(bhc(i,j).gt.2.326) then
      bhc4=bhc4+1
    endif
  77 continue
  do 78 j = 1, jo
    if(dffbho(i,j).eq.0) then
      goto 78
    endif
    bho(i,j)=abs(trubho-dfdbho(i,j))/dffbho(i,j)
    if(bho(i,j).le.1.645) then
      bho1=bho1+1
    elseif(bho(i,j).le.1.96) then
      bho2=bho2+1
    elseif(bho(i,j).le.2.326) then
      bho3=bho3+1
    elseif(bho(i,j).gt.2.326) then
      bho4=bho4+1
    endif
  78 continue
  do 79 j = 1, ji
    if(dffbhi(i,j).eq.0) then
      goto 79
    endif
    bhi(i,j) = abs(trubhi-dfdbhi(i,j))/dffbhi(i,j)
    if(bhi(i,j).le.1.645) then
      bhi1=bhi1+1
    elseif(bhi(i,j).le.1.96) then
      bhi2=bhi2+1
    elseif(bhi(i,j).le.2.326) then
      bhi3=bhi3+1
    elseif(bhi(i,j).gt.2.326) then
      bhi4=bhi4+1
    endif
  79 continue
  do 80 j = 1, jc
    if(dffbtc(i,j).eq.0) then
      goto 80
    endif
    btc(i,j)=abs(trubtc-dfdbtc(i,j))/dffbtc(i,j)
    if(btc(i,j).le.1.645) then
      btc1=btc1+1
    elseif(btc(i,j).le.1.96) then
      btc2=btc2+1
    elseif(btc(i,j).le.2.326) then
      btc3=btc3+1
    elseif(btc(i,j).gt.2.326) then
      btc4=btc4+1
    endif
  80 continue
  do 81 j = 1, jo
    if(dffbto(i,j).eq.0) then
      goto 81
    endif

```

```

      bto(i,j)=abs(trubto-dfdbto(i,j))/dffbto(i,j)
      if(bto(i,j).le.1.645) then
        bto1=bto1+1
      elseif(bto(i,j).le.1.96) then
        bto2=bto2+1
      elseif(bto(i,j).le.2.326) then
        bto3=bto3+1
      elseif(bto(i,j).gt.2.326) then
        bto4=bto4+1
      endif
81  continue
do 82 j = 1, ji
  if(dffbti(i,j).eq.0) then
    goto 82
  endif
  bti(i,j)=abs(trubti-dfdbti(i,j))/dffbti(i,j)
  if(bti(i,j).le.1.645) then
    bti1=bti1+1
  elseif(bti(i,j).le.1.96) then
    bti2=bti2+1
  elseif(bti(i,j).le.2.326) then
    bti3=bti3+1
  elseif(bti(i,j).gt.2.326) then
    bti4=bti4+1
  endif
82  continue
70  continue
c
c  the calculation of the percentages that cell output falls
c  within or above two standard deviations of the true values
act = ac1+ac2 + ac3 +ac4
ac1av = ac1/act
ac2av = (ac1+ac2)/act
ac3av = (ac4+ac3)/act
ac4av = ac4/act
aot = a01+a02+a03+a04
a01av=a01/aot
a02av=(a01+a02)/aot
a03av=(a03+a04)/aot
a04av=a04/aot
ait=ai1+ai2+ai3+ai4
ai1av=ai1/ait
ai2av=(ai1+ai2)/ait
ai3av=(ai3+ai4)/ait
ai4av=ai4/ait
alt=ac1+a01+ai1
a2t=ac2+a02+ai2
a3t=ac3+a03+ai3
a4t=ac4+a04+ai4
aav=alt/(alt+a2t+a3t+a4t)
aaav=(alt+a2t)/(alt+a2t+a3t+a4t)
aa3av=(a3t+a4t)/(alt+a2t+a3t+a4t)
aa4av=a4t/(alt+a2t+a3t+a4t)
blct=blc1+blc2+blc3+blc4
blc1av=blc1/blct
blc2av=(blc1+blc2)/blct
blc3av=(blc3+blc4)/blct
blc4av=blc4/blct
blot=blo1+blo2+blo3+blo4
blo1av=blo1/blot
blo2av=(blo1+blo2)/blot
blo3av=(blo3+blo4)/blot
blo4av=blo4/blot
blit=bli1+bli2+bli3+bli4
bli1av=bli1/blit

```

```

b1i2av=(b1i1+b1i2)/blit
b1i3av=(b1i3+b1i4)/blit
b1i4av=b1i4/blit
bl1t=b1c1+b1o1+b1i1
bl2t=b1c2+b1o2+b1i2
bl3t=b1c3+b1o3+b1i3
bl4t=b1c4+b1o4+b1i4
blav=bl1t/(bl1t+bl2t+bl3t+bl4t)
bb1av=(bl2t+bl1t)/(bl1t+bl2t+bl3t+bl4t)
bb13av=(bl3t+bl4t)/(bl1t+bl2t+bl3t+bl4t)
bb14av=bl4t/(bl1t+bl2t+bl3t+bl4t)
bhct=bhc1+bhc2+bhc3+bhc4
bhc1av=bhc1/bhct
bhc2av=(bhc1+bhc2)/bhct
bhc3av=(bhc3+bhc4)/bhct
bhc4av=bhc4/bhct
bhot=bho1+bho2+bho3+bho4
bho1av=bho1/bhot
bho2av=(bho1+bho2)/bhot
bho3av=(bho3+bho4)/bhot
bho4av=bho4/bhot
bhit=bhi1+bhi2+bhi3+bhi4
bhi1av=bhi1/bhit
bhi2av=(bhi1+bhi2)/bhit
bhi3av=(bhi3+bhi4)/bhit
bhi4av=bhi4/bhit
bh1t=bhc1+bho1+bhi1
bh2t=bhc2+bho2+bhi2
bh3t=bhc3+bho3+bhi3
bh4t=bhc4+bho4+bhi4
bhav=bh1t/(bh1t+bh2t+bh3t+bh4t)
bbhav=(bh1t+bh2t)/(bh1t+bh2t+bh3t+bh4t)
bbh3av=(bh3t+bh4t)/(bh1t+bh2t+bh3t+bh4t)
bbh4av=bh4t/(bh1t+bh2t+bh3t+bh4t)
btct=btcl+btcl+btcl+btcl
btclav=btcl/btct
btcl2av=(btcl+btcl)/btct
btcl3av=(btcl+btcl)/btct
btcl4av=btcl/btct
btot=btol+btol+btol+btol
btolav=btol/btot
btol2av=(btol+btol)/btot
btol3av=(btol+btol)/btot
btol4av=btol/btot
btit=bti1+bti2+bti3+bti4
bti1av=bti1/btit
bti2av=(bti1+bti2)/btit
bti3av=(bti3+bti4)/btit
bti4av=bti4/btit
bt1t=bti1+btol+btcl
bt2t=bti2+btol+btcl
bt3t=btcl+btol+bti3
bt4t=btcl+btol+bti4
btav=bt1t/(bt1t+bt2t+bt3t+bt4t)
bbtav=(bt1t+bt2t)/(bt1t+bt2t+bt3t+bt4t)
bbt3av=(bt3t+bt4t)/(bt1t+bt2t+bt3t+bt4t)
bbt4av=bt4t/(bt1t+bt2t+bt3t+bt4t)
do 89 i = t, l, t
  do 91 j = 1, jc
    perac(i,j) = dffc(i,j)/dfdac(i,j)
    perblc(i,j) = dffbhc(i,j)/dfdbhc(i,j)
    perbhc(i,j) = dffbhc(i,j)/dfdbhc(i,j)
    perbtc(i,j) = dffbtc(i,j)/dfdbtc(i,j)
  continue
do 92 j = 1, jo

```

```

    perao(i,j) = dffo(i,j)/dfdao(i,j)
    perai(i,j) = dffi(i,j)/dfdai(i,j)
    perblo(i,j) = dffblo(i,j)/dfdblo(i,j)
    perbli(i,j) = dffbli(i,j)/dfdbli(i,j)
    perbho(i,j) = dffbho(i,j)/dfdbho(i,j)
    perbhi(i,j) = dffbhi(i,j)/dfdbhi(i,j)
    perbto(i,j) = dffbto(i,j)/dfdbto(i,j)
    perbti(i,j) = dffbti(i,j)/dfdbti(i,j)
92   continue
    do 93 j = 1, ji
        perai(i,j) = dffi(i,j)/dfdai(i,j)
        perbli(i,j) = dffbli(i,j)/dfdbli(i,j)
        perbhi(i,j) = dffbhi(i,j)/dfdbhi(i,j)
        perbti(i,j) = dffbti(i,j)/dfdbti(i,j)
93   continue
89   continue
    do 320 i = t, 1, t
        do 325 j = 1, jc
            if(perac(i,j).le.0.05) then
                pac1 = pac1 + 1
            elseif(perac(i,j).le.0.1) then
                pac2 = pac2 + 1
            elseif(perac(i,j).le.0.2) then
                pac3 = pac3 + 1
            elseif(perac(i,j).le.0.3) then
                pac4 = pac4 + 1
            elseif(perac(i,j).le.0.5) then
                pac5 = pac5 + 1
            elseif(perac(i,j).le.1.0) then
                pac6 = pac6 + 1
            else
                pac7 = pac7 + 1
            endif
325   continue
        do 330 j = 1, jo
            if(perao(i,j).le.0.05) then
                pao1 = pao1+1
            elseif(perao(i,j).le.0.1) then
                pao2 = pao2 + 1
            elseif(perao(i,j).le.0.2) then
                pao3 = pao3 + 1
            elseif(perao(i,j).le.0.3) then
                pao4 = pao4+1
            elseif(perao(i,j).le.0.5) then
                pao5 = pao5 + 1
            elseif(perac(i,j).le.1.0) then
                pao6 = pao6 + 1
            else
                pao7 = pao7 + 1
            endif
330   continue
        do 335 j = 1, ji
            if(perai(i,j).le.0.05) then
                pai1 = pai1 + 1
            elseif(perai(i,j).le.0.1) then
                pai2 = pai2 + 1
            elseif(perai(i,j).le.0.2) then
                pai3 = pai3 + 1
            elseif(perai(i,j).le.0.3) then
                pai4 = pai4 + 1
            elseif(perai(i,j).le.0.5) then
                pai5 = pai5 + 1
            elseif(perai(i,j).le.1.0) then
                pai6 = pai6 + 1
            else

```

```

        pai7 = pai7 + 1
    endif
335  continue
    do 340 j = 1, jc
        if(perblc(i,j).le.0.05) then
            pblc1 = pblc1 + 1
        elseif(perblc(i,j).le.0.1) then
            pblc2 = pblc2 + 1
        elseif(perblc(i,j).le.0.2) then
            pblc3 = pblc3 + 1
        elseif(perblc(i,j).le.0.3) then
            pblc4 = pblc4 + 1
        elseif(perblc(i,j).le.0.5) then
            pblc5 = pblc5 + 1
        elseif(perblc(i,j).le.1.0) then
            pblc6 = pblc6 + 1
        else
            pblc7 = pblc7 + 1
        endif
340  continue
    do 345 j = 1, jo
        if(perblo(i,j).le.0.05) then
            pblo1 = pblo1 + 1
        elseif(perblo(i,j).le.0.1) then
            pblo2 = pblo2 + 1
        elseif(perblo(i,j).le.0.2) then
            pblo3 = pblo3 + 1
        elseif(perblo(i,j).le.0.3) then
            pblo4 = pblo4 + 1
        elseif(perblo(i,j).le.0.5) then
            pblo5 = pblo5 + 1
        elseif(perblo(i,j).le.1.0) then
            pblo6 = pblo6 + 1
        else
            pblo7 = pblo7 + 1
        endif
345  continue
    do 350 j = 1, ji
        if(perbli(i,j).le.0.05) then
            pbli1 = pbli1 + 1
        elseif(perbli(i,j).le.0.1) then
            pbli2 = pbli2 + 1
        elseif(perbli(i,j).le.0.2) then
            pbli3 = pbli3 + 1
        elseif(perbli(i,j).le.0.3) then
            pbli4 = pbli4 + 1
        elseif(perbli(i,j).le.0.5) then
            pbli5 = pbli5 + 1
        elseif(perbli(i,j).le.1.0) then
            pbli6 = pbli6 + 1
        else
            pbli7 = pbli7 + 1
        endif
350  continue
    do 355 j = 1, jc
        if(perbhc(i,j).le.0.05) then
            pbhc1=pbhc1+1
        elseif(perbhc(i,j).le.0.1) then
            pbhc2=pbhc2+1
        elseif(perbhc(i,j).le.0.2) then
            pbhc3=pbhc3+1
        elseif(perbhc(i,j).le.0.3) then
            pbhc4=pbhc4+1
        elseif(perbhc(i,j).le.0.5) then
            pbhc5=pbhc5+1
    
```

```

elseif(perbhc(i,j).le.1.0) then
  pbhc6=pbhc6+1
else
  pbhc7=pbhc7+1
endif
355 continue
do 360 j = 1,jo
  if(perbho(i,j).le.0.05) then
    pbho1=pbho1+1
  elseif(perbho(i,j).le.0.1) then
    pbho2=pbho2+1
  elseif(perbho(i,j).le.0.2) then
    pbho3=pbho3+1
  elseif(perbho(i,j).le.0.3) then
    pbho4=pbho4+1
  elseif(perbho(i,j).le.0.5) then
    pbho5=pbho5+1
  elseif(perbho(i,j).le.1.0) then
    pbho6=pbho6+1
  else
    pbho7=pbho7+1
  endif
360 continue
do 365 j = 1,ji
  if(perbhi(i,j).le.0.05) then
    pbhi1=pbhi1+1
  elseif(perbhi(i,j).le.0.1) then
    pbhi2=pbhi2+1
  elseif(perbhi(i,j).le.0.2) then
    pbhi3=pbhi3+1
  elseif(perbhi(i,j).le.0.3) then
    pbhi4=pbhi4+1
  elseif(perbhi(i,j).le.0.5) then
    pbhi5=pbhi5+1
  elseif(perbhi(i,j).le.1.0) then
    pbhi6=pbhi6+1
  else
    pbhi7=pbhi7+1
  endif
365 continue
do 370 j = 1, jc
  if(perbtc(i,j).le.0.05) then
    pbtc1=pbtc1+1
  elseif(perbtc(i,j).le.0.1) then
    pbtc2=pbtc2+1
  elseif(perbtc(i,j).le.0.2) then
    pbtc3=pbtc3+1
  elseif(perbtc(i,j).le.0.3) then
    pbtc4=pbtc4+1
  elseif(perbtc(i,j).le.0.5) then
    pbtc5=pbtc5+1
  elseif(perbtc(i,j).le.1.0) then
    pbtc6=pbtc6+1
  else
    pbtc7=pbtc7+1
  endif
370 continue
do 375 j = 1,jo
  if(perbto(i,j).le.0.05) then
    pbto1=pbto1+1
  elseif(perbto(i,j).le.0.1) then
    pbto2=pbto2+1
  elseif(perbto(i,j).le.0.2) then
    pbto3=pbto3+1
  elseif(perbto(i,j).le.0.3) then

```

```

        pbto4=pbto4+1
        elseif(perbto(i,j).le.0.5) then
            pbto5=pbto5+1
        elseif(perbto(i,j).le.1.0) then
            pbto6=pbto6+1
        else
            pbto7=pbto7+1
        endif
375    continue
        do 380 j = 1,ji
            if(perbti(i,j).le.0.05) then
                pbti1=pbti1+1
            elseif(perbti(i,j).le.0.1) then
                pbti2=pbti2+1
            elseif(perbti(i,j).le.0.2) then
                pbti3=pbti3+1
            elseif(perbti(i,j).le.0.3) then
                pbti4=pbti4+1
            elseif(perbti(i,j).le.0.5) then
                pbti5=pbti5+1
            elseif(perbti(i,j).le.1.0) then
                pbti6=pbti6+1
            else
                pbti7=pbti7+1
            endif
380    continue
320    continue
        pact=pac1+pac2+pac3+pac4+pac5+pac6+pac7
        pact1=pac1/pact
        pact2=pac2/pact +pact1
        pact3=pac3/pact +pact2
        pact4=pac4/pact +pact3
        pact5=pac5/pact +pact4
        pact6=pac6/pact +pact5
        pact7=pac7/pact
        paot=pao1+pao2+pao3+pao4+pao5+pao6+pao7
        paot1=pao1/paot
        paot2=pao2/paot +paot1
        paot3=pao3/paot +paot2
        paot4=pao4/paot +paot3
        paot5=pao5/paot +paot4
        paot6=pao6/paot +paot5
        paot7=pao7/paot
        pait=pai1+pai2+pai3+pai4+pai5+pai6+pai7
        pait1=pai1/pait
        pait2=pai2/pait +pait1
        pait3=pai3/pait +pait2
        pait4=pai4/pait +pait3
        pait5=pai5/pait +pait4
        pait6=pai6/pait +pait5
        pait7=pai7/pait
        pblct=pb1c1+pb1c2+pb1c3+pb1c4+pb1c5+pb1c6+pb1c7
        pblct1=pb1c1/pblct
        pblct2=pb1c2/pblct +pblct1
        pblct3=pb1c3/pblct +pblct2
        pblct4=pb1c4/pblct +pblct3
        pblct5=pb1c5/pblct +pblct4
        pblct6=pb1c6/pblct +pblct5
        pblct7=pb1c7/pblct
        pblot=pb1o1+pb1o2+pb1o3+pb1o4+pb1o5+pb1o6+pb1o7
        pblot1=pb1o1/pblot
        pblot2=pb1o2/pblot +pblot1
        pblot3=pb1o3/pblot +pblot2
        pblot4=pb1o4/pblot +pblot3
        pblot5=pb1o5/pblot +pblot4

```

```

pblot6=pblo6/pblot +pblot5
pblot7=pblo7/pblot
pblit=pbli1+pbli2+pbli3+pbli4+pbli5+pbli6+pbli7
pblit1=pbli1/pblit
pblit2=pbli2/pblit +pblit1
pblit3=pbli3/pblit +pblit2
pblit4=pbli4/pblit +pblit3
pblit5=pbli5/pblit +pblit4
pblit6=pbli6/pblit +pblit5
pblit7=pbli7/pblit
pbhct=pbhc1+pbhc2+pbhc3+pbhc4+pbhc5+pbhc6+pbhc7
pbhct1=pbhc1/pbhct
pbhct2=pbhc2/pbhct +pbhct1
pbhct3=pbhc3/pbhct +pbhct2
pbhct4=pbhc4/pbhct +pbhct3
pbhct5=pbhc5/pbhct +pbhct4
pbhct6=pbhc6/pbhct +pbhct5
pbhct7=pbhc7/pbhct
pbhot=pbho1+pbho2+pbho3+pbho4+pbho5+pbho6+pbho7
pbhot1=pbho1/pbhot
pbhot2=pbho2/pbhot +pbhot1
pbhot3=pbho3/pbhot +pbhot2
pbhot4=pbho4/pbhot +pbhot3
pbhot5=pbho5/pbhot +pbhot4
pbhot6=pbho6/pbhot +pbhot5
pbhot7=pbho7/pbhot
pbhit=pbhi1+pbhi2+pbhi3+pbhi4+pbhi5+pbhi6+pbhi7
pbhit1=pbhi1/pbhit
pbhit2=pbhi2/pbhit +pbhit1
pbhit3=pbhi3/pbhit +pbhit2
pbhit4=pbhi4/pbhit +pbhit3
pbhit5=pbhi5/pbhit +pbhit4
pbhit6=pbhi6/pbhit +pbhit5
pbhit7=pbhi7/pbhit
pbtct=pbtc1+pbtc2+pbtc3+pbtc4+pbtc5+pbtc6+pbtc7
pbtct1=pbtc1/pbtct
pbtct2=pbtc2/pbtct +pbtct1
pbtct3=pbtc3/pbtct +pbtct2
pbtct4=pbtc4/pbtct +pbtct3
pbtct5=pbtc5/pbtct +pbtct4
pbtct6=pbtc6/pbtct +pbtct5
pbtct7=pbtc7/pbtct
pbtot=pbto1+pbto2+pbto3+pbto4+pbto5+pbto6+pbto7
pbtot1=pbto1/pbtot
pbtot2=pbto2/pbtot +pbtot1
pbtot3=pbto3/pbtot +pbtot2
pbtot4=pbto4/pbtot +pbtot3
pbtot5=pbto5/pbtot +pbtot4
pbtot6=pbto6/pbtot +pbtot5
pbtot7=pbto7/pbtot
pbtit=pbti1+pbti2+pbti3+pbti4+pbti5+pbti6+pbti7
pbtit1=pbti1/pbtit
pbtit2=pbti2/pbtit +pbtit1
pbtit3=pbti3/pbtit +pbtit2
pbtit4=pbti4/pbtit +pbtit3
pbtit5=pbti5/pbtit +pbtit4
pbtit6=pbti6/pbtit +pbtit5
pbtit7=pbti7/pbtit
do 90 i = t, 1, t
  write(33,917)
  write(33,910)
  do 95 j = 1,jc
    write(33,911) i, j, ac(i,j),dfdac(i,j), dffc(i,j)/dfdac(i,j)
1,dffc(i,j)
    acm=max(acm,ac(i,j))

```

```

95   continue
      write(33,912)
      do 100 j = 1,jo
         write(33,911) i, j, ao(i,j),dfdao(i,j), dffo(i,j)/dfdao(i,j)
1,dffo(i,j)
         aom=max(aom,ao(i,j))
100   continue
      write(33,913)
      do 105 j = 1,ji
         write(33, 911) i, j, ai(i,j),dfdai(i,j),dffo(i,j)/dfdai(i,j)
1,dffo(i,j)
         aim=max(aim,ai(i,j))
105   continue
      write(33,914)
      write(33,910)
      do 110 j = 1, jc
         write(33,911)i,j,blc(i,j),dfdblc(i,j),dffblc(i,j)/dfdblc(i,j)
1,dffblc(i,j)
         blcm=max(blcm,blc(i,j))
110   continue
      write(33,912)
      do 115 j = 1,jo
         write(33,911)i,j,blo(i,j),dfdblo(i,j),dffblo(i,j)/dfdblo(i,j)
1,dffblo(i,j)
         blom=max(blom,blo(i,j))
115   continue
      write(33,913)
      do 120 j = 1,ji
         write(33,911)i,j,bli(i,j),dfdbli(i,j),dffbli(i,j)/dfdbli(i,j)
1,dffbli(i,j)
         blim=max(blim,bli(i,j))
120   continue
      write(33,915)
      write(33,910)
      do 125 j = 1,jc
         write(33,911)i,j,bhc(i,j),dfdbhc(i,j),dffbhc(i,j)/dfdbhc(i,j)
1,dffbhc(i,j)
         bhcm=max(bhcm,bhc(i,j))
125   continue
      write(33,912)
      do 130 j = 1,jo
         write(33,911)i,j,bho(i,j),dfdbho(i,j),dffbho(i,j)/dfdbho(i,j)
1,dffbho(i,j)
         bhom=max(bhom,bho(i,j))
130   continue
      write(33,913)
      do 135 j = 1, ji
         write(33,911)i,j,bhi(i,j),dfdbhi(i,j),dffbhi(i,j)/dfdbhi(i,j)
1,dffbhi(i,j)
         bhim=max(bhim,bhi(i,j))
135   continue
      write(33,916)
      write(33,910)
      do 140 j = 1, jc
         write(33,911)i,j,btc(i,j),dfdbtc(i,j),dffbtc(i,j)/dfdbtc(i,j)
1,dffbtc(i,j)
         btcm=max(btc,btc(i,j))
140   continue
      write(33,912)
      do 145 j = 1, jo
         write(33,911)i,j,bto(i,j),dfdbto(i,j),dffbto(i,j)/dfdbto(i,j)
1,dffbto(i,j)
         btom=max(btom,bto(i,j))
145   continue
      write(33,913)

```

```

        do 150 j = 1, ji
            write(33,911) i,j, bti(i,j), dfdbti(i,j), dffbti(i,j)/dfdbti(i,j)
1, dffbti(i,j)
            btim=max(btim, bti(i,j))
150        continue
90    continue
    write(33,918)
    write(33,919)
    write(33,920)
    write(33,921) ac1, ac2, ac3, ac4, ac1av, ac2av, ac3av, ac4av, acm
    write(33,922) ao1, ao2, ao3, ao4, ao1av, ao2av, ao3av, ao4av, aom
    write(33,923) ai1, ai2, ai3, ai4, ai1av, ai2av, ai3av, ai4av, aim
    write(33,927) alt, a2t, a3t, a4t, aav, aaav, aa3av, aa4av
    write(33,914)
    write(33,921) blc1, blc2, blc3, blc4, blc1av, blc2av, blc3av, blc4av, blcm
    write(33,922) blo1, blo2, blo3, blo4, blo1av, blo2av, blo3av, blo4av, blom
    write(33,923) bli1, bli2, bli3, bli4, bli1av, bli2av, bli3av, bli4av, blim
    write(33,927) bl1t, bl2t, bl3t, bl4t, blav, bblav, bbl3av, bbl4av
    write(33,915)
    write(33,921) bhc1, bhc2, bhc3, bhc4, bhc1av, bhc2av, bhc3av, bhc4av, bhcm
    write(33,922) bho1, bho2, bho3, bho4, bho1av, bho2av, bho3av, bho4av, bhom
    write(33,923) bhi1, bhi2, bhi3, bhi4, bhi1av, bhi2av, bhi3av, bhi4av, bhim
    write(33,927) bh1t, bh2t, bh3t, bh4t, bhav, bbhav, bbh3av, bbh4av
    write(33,916)
    write(33,921) btc1, btc2, btc3, btc4, btc1av, btc2av, btc3av, btc4av, btcm
    write(33,922) bto1, bto2, bto3, bto4, bto1av, bto2av, bto3av, bto4av, btom
    write(33,923) bti1, bti2, bti3, bti4, bti1av, bti2av, bti3av, bti4av, btim
    write(33,927) bt1t, bt2t, bt3t, bt4t, btav, bbtav, bbt3av, bbt4av
    write(33,935)
    write(33,936)
    write(33,920)
    write(33,932) pact1, pact2, pact3, pact4, pact5, pact6, pact7
    write(33,933) paot1, paot2, paot3, paot4, paot5, paot6, paot7
    write(33,934) pait1, pait2, pait3, pait4, pait5, pait6, pait7
    write(33,914)
    write(33,932) pblct1, pblct2, pblct3, pblct4, pblct5, pblct6, pblct7
    write(33,933) pblot1, pblot2, pblot3, pblot4, pblot5, pblot6, pblot7
    write(33,934) pblit1, pblit2, pblit3, pblit4, pblit5, pblit6, pblit7
    write(33,915)
    write(33,932) pbhct1, pbhct2, pbhct3, pbhct4, pbhct5, pbhct6, pbhct7
    write(33,933) pbhot1, pbhot2, pbhot3, pbhot4, pbhot5, pbhot6, pbhot7
    write(33,934) pbhit1, pbhit2, pbhit3, pbhit4, pbhit5, pbhit6, pbhit7
    write(33,916)
    write(33,932) pbtct1, pbtct2, pbtct3, pbtct4, pbtct5, pbtct6, pbtct7
    write(33,933) pbtot1, pbtot2, pbtot3, pbtot4, pbtot5, pbtot6, pbtot7
    write(33,934) pbtit1, pbtit2, pbtit3, pbtit4, pbtit5, pbtit6, pbtit7

c
c    the format statements
900 format(a10)
901 format(a7,46x,a7,5x,a1)
902 format(52x,a14)
903 format(a14)
904 format(5x,a10)
905 format(7x,i2)
906 format(17x,e11.5,1x,f6.4)
907 format(10x,"cell ",i2,4x,e11.5,1x,f6.4)
908 format(17x,e11.5,1x,f6.4)
909 format("A total of ",i2,"cycles")
910 format("corner cells")
911 format(5x,i2.0,5x,i2.0,5x,f8.5,5x,e11.5,5x,f8.5,5x,e11.5)
912 format("outer edge cells")
913 format("inner edge cells")
914 format("tally 67 - low energy")
915 format("tally 67 - high energy")

```

```
916 format("tally 67 - total energy")
917 format("tally 34")
918 format("totals")
919 format(24x,"<1.645SD",2x,"<1.96SD",2x,"<2.326SD",2x,">2.326SD",4x,
1"%<1.645",2x,"%<1.96",3x,"%>1.96",3x,"%>2.326",3x,"max SD")
920 format("tally 34")
921 format(2x,"corner",16x,f4.0,7x,f4.0,5x,f4.0,7x,f4.0,6x,f6.4,
14x,f6.4,3x,f6.4,3x,f6.4,3x,f9.4)
922 format(2x,"outer",17x,f5.0,6x,f4.0,5x,f4.0,7x,f4.0,6x,f6.4,
14x,f6.4,3x,f6.4,3x,f6.4,3x,f9.4)
923 format(2x,"inner",17x,f5.0,6x,f4.0,5x,f4.0,7x,f4.0,6x,f6.4,
14x,f6.4,3x,f6.4,3x,f6.4,3x,f9.4)
927 format("total",19x,f5.0,6x,f4.0,5x,f4.0,7x,f4.0,6x,f6.4,4x,
1f6.4,3x,f6.4,3x,f6.4)
928 format(10x,"cell ",i2,4x,"<7 MeV",4x,e11.5,1x,f6.4)
929 format(10x,"cell ",i2,4x,"<20 MeV",3x,e11.5,1x,f6.4)
930 format(10x,"cell ",i2,4x,"total ",4x,e11.5,1x,f6.4)
931 format(a7)
932 format(2x,"corner",16x,f6.4,3x,f6.4,3x,f6.4,3x,f6.4,3x,f6.4,3x,
1f6.4,3x,f6.4)
933 format(2x,"outer",17x,f6.4,3x,f6.4,3x,f6.4,3x,f6.4,3x,f6.4,3x,
1f6.4,3x,f6.4)
934 format(2x,"inner",17x,f6.4,3x,f6.4,3x,f6.4,3x,f6.4,3x,f6.4,3x,
1f6.4,3x,f6.4)
935 format("error totals")
936 format(24x,"<0.05",4x,"<0.10",4x,"<0.20",4x,"<0.30",4x,"<0.50",4x,
1,"<1.00",4x,">1.00")
940 format("this is the problem")
941 format(i6)
      stop
      end
```